CHALMERS

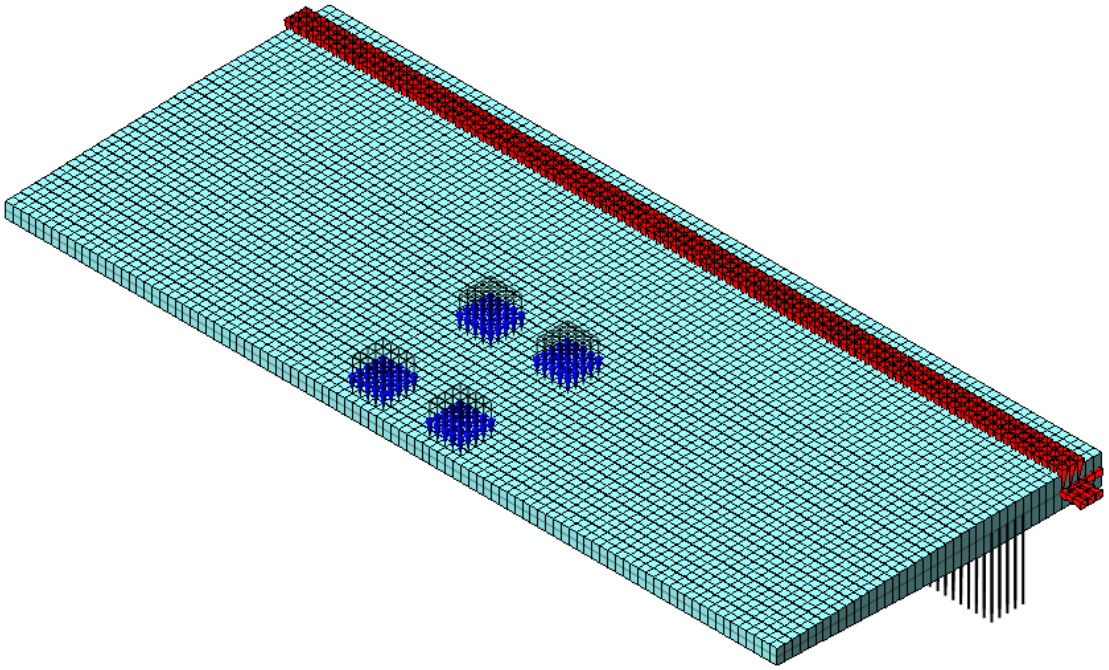

Distribution of Shear Force in Concrete Slabs

A study of how to distribute shear force from linear FE analyses in bridge decks

Master of Science Thesis in the Master's Programme Structural Engineering and Building Performance Design

POJA SHAMS HAKIMI

Department of Civil and Environmental Engineering
Division of Structural Engineering
Concrete Structures
CHALMERS UNIVERSITY OF TECHNOLOGY
Göteborg, Sweden 2012

Master's Thesis 2012:148

MASTER'S THESIS 2012:148

Distribution of Shear Force in Concrete Slabs

A study of how to distribute shear force from linear FE analyses in bridge decks

Master of Science Thesis in the Master's Programme Structural Engineering and Building Performance Design

POJA SHAMS HAKIMI

Department of Civil and Environmental Engineering
Division of Structural Engineering
Concrete Structures
CHALMERS UNIVERSITY OF TECHNOLOGY

Göteborg, Sweden 2012

Distribution of Shear Force in Concrete Slabs
A study of how to distribute shear force from linear FE analyses in bridge decks

Master of Science Thesis in the Master's Programme Structural Engineering and Building Performance Design

POJA SHAMS HAKIMI

Examensarbete / Institutionen för bygg- och miljöteknik,
Chalmers tekniska högskola 2012:148

Department of Civil and Environmental Engineering
Division of Structural Engineering
Concrete Structures
Chalmers University of Technology
SE-412 96 Göteborg
Sweden
Telephone: + 46 (0)31-772 1000

Cover:
Overview of the model designed with the pre-processor FX+.

Chalmers Reproservice Göteborg, Sweden 2012

Distribution of Shear Force in Concrete Slabs

A study of how to distribute shear force from linear FE analyses in bridge decks

Master of Science Thesis in the Master's Programme Structural Engineering and Building Performance Design

POJA SHAMS HAKIMI
Department of Civil and Environmental Engineering
Division of Structural Engineering
Concrete Structures
Chalmers University of Technology

ABSTRACT

During recent years the demand on using three-dimensional finite element (FE) analyses for bridge design has increased substantially. It has become a common practice to design such structures with the help of linear elastic FE analyses. The developments of design procedures for concrete slabs have come far regarding bending moment but when it comes to shear forces, there is no common resolution on how to proceed. This is mostly due to lack of knowledge about the behavior of shear and failures caused by shear in concrete slabs. To design such structures with linear elastic FE analysis, the concentrated shear forces gained must be distributed within larger parts of the structure. This is needed to describe the real behavior of the slab since occurrence of cracking leads to stress redistributions. The purpose of this master's thesis is to give recommendations on how to perform this distribution and also to investigate the influence of flexural cracking on the redistribution of shear forces. A literature study was made to get an overview of interesting research in this field and a non-linear analysis of a bridge deck cantilever was carried out to capture the behavior of shear redistributions.

The results show that the shear stress along the support of a cantilevering reinforce concrete slab becomes more evenly distributed when the non-linear flexural response is taken into account in the structural analysis. Sufficiently long cantilever decks have good capacity of plastic redistribution, which in the studied case gave a shear force reduction of about 20% compared to a linear analysis. The length within which the linear elastic shear forces could be distributed was calculated to between 3 and 3.15 meters.

Key words: concrete, design, shear force, distribution, punching shear, FE, finite element, bridge, slab, deck

Utjämning av tvärkraft i betongplattor
En studie om hur tvärkraft från linjär FE-analys bör utjämnas betongplattor
Examensarbete inom Structural Engineering and Building Performance Design
POJA SHAMS HAKIMI
Institutionen för bygg- och miljöteknik
Avdelningen för Konstruktionsteknik
Betongbyggnad
Chalmers tekniska högskola

SAMMANFATTNING

De senaste åren har kraven på dimensionering med tredimensionellt finita elementanalys (FE-analys) för brokonstruktioner ökat betydligt. Det har blivit en vanlig metod att utforma sådana konstruktioner med hjälp av linjärelastiska FE-analyser. Utvecklingen av dimensioneringsförfaranden för betongplattor har kommit långt när det gäller böjmoment, men för tvärkrafter finns ingen allmänt vedertagen uppfattning om hur man ska gå tillväga. Detta beror främst på bristande kunskap om tvärkraft och tvärkraftsbrott i betongplattor. För att utforma en sådan konstruktion med linjärelastisk FE-analys måste koncentrationer av tvärkrafter fördelas och utjämnas inom större delar av konstruktionen. Detta behövs för att beskriva det verkliga beteendet i plattan då uppkomsten av sprickor leder till omfördelning av spänningar. Syftet med detta mastersexamensarbete är att ge rekommendationer om hur man bör utföra denna fördelning och att undersöka påverkan av böjuppsprickning på omfördelning av tvärkrafter. En litteraturstudie har gjorts för att ge en översikt av intressant forskning inom området och en icke-linjär analys av en brobanekonsol har utförts för att fånga beteendet av tvärkraftens omfördelning.

Resultaten visar att tvärkraften längs stödet för en brobanekonsol i armerad betong blir mer jämnt fördelad när den olinjära böjuppsprickningen tas till hänsyn i analysen. Tillräckligt långa brobanekonsoler har bra kapacitet för plastisk omlagring, vilket i denna studie gav en reduktion av tvärkraft med ungefär 20%, jämfört med en linjär analys. Tvärkraften från linjär analys beräknades kunna fördelas inom en längd mellan 3 till 3.15 meter.

Nyckelord: betong, dimensionering, tvärkraft, utjämning, genomstansning, finita element, bro, platta, bjälklag.

Contents

ABSTRACT I
SAMMANFATTNING II
CONTENTS III
PREFACE V
NOTATIONS VI

1 INTRODUCTION 1
1.1 Background 1
1.2 Purpose and scope 1
1.3 Method 1

2 STRUCTURAL CONCRETE 2
2.1 Response of structural members subjected to bending 2
2.1.1 Behavior in service state 4
2.1.2 Behavior in ultimate state 5
2.2 Shear in concrete beams 6
2.2.1 Design without transverse reinforcement according to EC2 9
2.2.2 Design with transverse reinforcement according to EC2 11
2.3 Shear in concrete slabs 12
2.3.1 One- and two-way action 13
2.3.2 Failure in slabs due to shear 13
2.3.3 Design for punching shear according to EC2 14

3 LITERATURE REVIEW 15
3.1 Failure criteria 15
3.1.1 Shear failure 15
3.1.2 Punching shear failure 17
3.1.3 Intermediate shear failures 18
3.2 Laboratory testings 20
3.3 Swedish recommendations 24

4 NON-LINEAR FE ANALYSIS 26
4.1 General 26
4.1.1 Structural idealization 26
4.1.2 Computation process 30
4.1.3 Post-processing 35
4.2 Bridge deck cantilever 36
4.2.1 Finite Element model 36
4.2.2 Material models 42
4.2.3 Computation 43

5 RESULTS 44
5.1 Overall results 44
5.1.1 Critical events 48
5.1.2 Crack development 48
5.2 Shear distribution 57
5.2.1 Transversal shear force distribution in the slab 57
5.2.2 Transversal shear force distribution along the support 63
5.2.3 Observation of shear force fluctuations 67
5.2.4 Comparison to linear elastic results 69
6 DISCUSSION 71
7 CONCLUSIONS 72
8 FUTURE WORK 73
9 REFERENCES 74
APPENDIX A – SUPPORT MODELING 76
APPENDIX B – CONVERGENCE STUDY AND VERIFICATION 78
APPENDIX C – MEAN CRACK DISTANCE 81

Preface

On behalf of the Swedish Road Administration a handbook has to be developed to guide engineers in bridge design. This master's thesis is a part of the research work behind the handbook and concerns the shear force in concrete bridge decks. A literature study is carried out together with a non-linear finite element analysis of a bridge deck cantilever. The work on this thesis started October 2011 and ended July 2012.

The project is carried out as collaboration between the Department of Structural Engineering at Chalmers University of Technology and ELU Konsult AB. The work was mainly done from the office at ELU Konsult AB in Gothenburg. The software for finite element analysis was provided by Chalmers.

My supervisor Mario Plos is greatly appreciated for his genuine engagement in my work despite the lack of time. The guidance and help of Professor Rui Vaz Rodrigues is greatly valued. In addition he let me use significant amount of materials from his studies. I also want to thank Professor Costine Pacoste for sharing his expertise and Engineer Per Granström at ELU Konsult AB who always gladly answered my questions.

Notations

Roman upper case letters

A_{sw}	Contributing cross-sectional area of stirrups
$C_{Rd,c}$	National parameter for calculation of concrete shear capacity
EI	Bending stiffness
M_{cr}	Bending moment causing first crack
M_R	Bending moment resistance
M_y	Bending moment causing yielding in flexural reinforcement
M_{ult}	Maximum bending moment carried
Q_{Flex}	Theoretical flexural failure load
Q_R	Actual failure load from testing
V_d	Design shear load effect
$V_{Rd,c}$	Shear capacity of concrete
$V_{Rd,s}$	Shear capacity of stirrups
V_{test}	Maximum shear force from testing
V_{th}	Maximum shear force from theory

Roman lower case letters

b	Cross-sectional width of beam
b_0	Length of control section; control perimeter
$b_{0.elast}$	Modified length of control section
b_w	Smallest cross-sectional width in tensile zone in beam
d	Distance from compressed surface to center of tensile reinforcement
d_g	Maximum aggregate size
d_{g0}	Reference size (16mm)
dl	Infinitesimal change of length along beam
f_c	Concrete strength
f_{ck}	Characteristic concrete compressive strength

f_{cd}	Design concrete compressive strength
f_{ywd}	Design yield stress of stirrups
m_{xx}	Bending moment per unit length in x-direction
m_{yy}	Bending moment per unit length in y-direction
m_{xy}	Twisting moment or torsion
q	Distributed load
r	Radius of curvature
u	Length of control section; control perimeter
v	Poisson's ratio / Reduction factor for concrete compressive strength
v_1	Reduction factor for concrete compressive strength
v_0	Principal shear force per unit length
v_x	Shear force per unit length in x-direction
v_y	Shear force per unit length in y-direction
v_R	Nominal shear strength per unit length
w	Vertical deflection
x_{tp}	Distance from top surface to the level of cross-sectional center of mass

Greek letters

α	Angle between stirrups and main axis of beam
α_{cw}	Factor considering normal force in beam
β_o	Direction of principal shear force
ε	Normal strain in cross-section
κ	Curvature in beam
σ_c	Stress in concrete
τ_{max}	Maximum shear stress before cracking in beam
$d\theta$	Infinitesimal change of angle of curvature
θ	Angle between inclined compression strut and main axis of beam
ψ	Rotation of slab

1 Introduction

This report is part of a master's thesis carried out at the department of Civil- and Environmental Engineering at Chalmers University of Technology in collaboration with ELU Konsult AB. The ultimate goal of this project is to give recommendations on how to distribute shear force in concrete bridge decks with two-way action, based on linear finite element (FE) analysis.

1.1 Background

During recent years the demand on using three-dimensional FE analyses for bridge design has increased substantially. This has led to many questions, among them the interpretation of FE results for reinforced concrete. A common way to design reinforced concrete is by linear elastic FE analysis. This can give a good representation of concrete behavior as long as the structure remains un-cracked. Cracked reinforced concrete has a highly non-linear behavior and peaks of stresses that initiated the cracks will redistribute to other regions with higher stiffness. This stress redistribution is not simulated by a linear elastic FE analysis. Instead, stresses can become much larger than for the real structure, like stress concentrations at geometric- or static discontinuities. Hence, at some critical points the deviation of the FE results become too large compared to the real structural response and therefore one cannot directly use them for design purposes.

A way of taking into account the stress redistributions in design can be by smearing out the stress concentrations within larger parts of the structure and in this way get rid of the unrealistic peaks. By doing so, one could get better representation of the actual behavior and would not need to carry out demanding non-linear analyses for each design case. Therefore, recommendations are needed about how to perform this distribution.

1.2 Purpose and scope

The primary purpose of this project is to give recommendations on how to distribute shear force in a bridge deck with two-way action. The recommendations are of interest because they may help the design to become more accurate, avoiding over-conservatism. The purpose is also to gain better understanding about how concrete slabs behave with respect to shear and failures caused by shear. In this master's thesis, focus is put on specific cases with concentrations of shear force, for instance concentrated loads on bridge decks. The recommendations should however be general and applicable to all cases with concrete slabs.

1.3 Method

A large portion of this thesis consists of literature studies. It is of importance to get an overview of what research and experiments that have been carried out in this field. A compilation of relevant studies is made to clarify what things that may need further investigation. Existing methods that currently are being used for design are presented to give an insight to the problem. A non-linear FE analysis of a bridge deck cantilever is performed to investigate the effect of flexural cracking on the shear flow.

2 Structural concrete

In structural engineering, the design is always made with regard to two aspects; service state and ultimate state. In the service state, functionality of the structure during the expected service life is considered. Serviceability Limit State (SLS) is the load limit at which the criteria of functionality are no longer met. Examples of criteria concerning the functionality can be limitations of the vertical deflection of a bridge that spans over a trafficked road or the crack width in a member situated outdoors. Serviceability criteria make sure that the structure is usable, practical and durable. The second aspect of the design is the ultimate state and concerns the failure of the structure. At the Ultimate Limit State (ULS), the structure will not be able to cope with further load increase. The safety of the structure is an important factor that is taken into account in this state. This chapter is mainly based on the literature presented by Engström *et al.* (2008) and Engström (2011).

2.1 Response of structural members subjected to bending

The cracking of the concrete, the interaction between concrete and reinforcement and the amount of reinforcement provided are some factors that highly affect the structural behavior. A moment-curvature diagram over the sectional response in a concrete member gives a good representation of these factors. Terms like bond-slip, tension stiffening and brittle/ductile behavior describe some important properties of reinforced concrete structures that will be treated in this chapter. In Figure 1, a schematic picture illustrates a cracked member, the stresses in concrete affected by bond-slip and the definition of curvature in a cross-section.

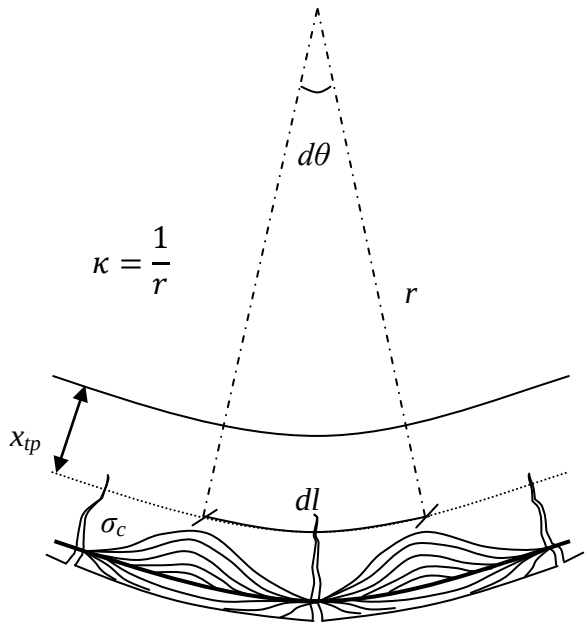

Figure 1. A cracked reinforced concrete member with the concrete stresses and the definition of curvature.

It is essential to understand the nature of reinforced concrete as a structure composed of two materials interacting with each other. When considering individual materials, stress-strain diagrams give good representations of the behavior and characteristics of the materials, see Figure 2. Both concrete in compression and reinforcement steel have linear-elastic relation between load and deformation in the service state. Yet, reinforced concrete is known to behave in a non-linear manner. This means that the stress distribution along a member does not remain the same when the load is changed.

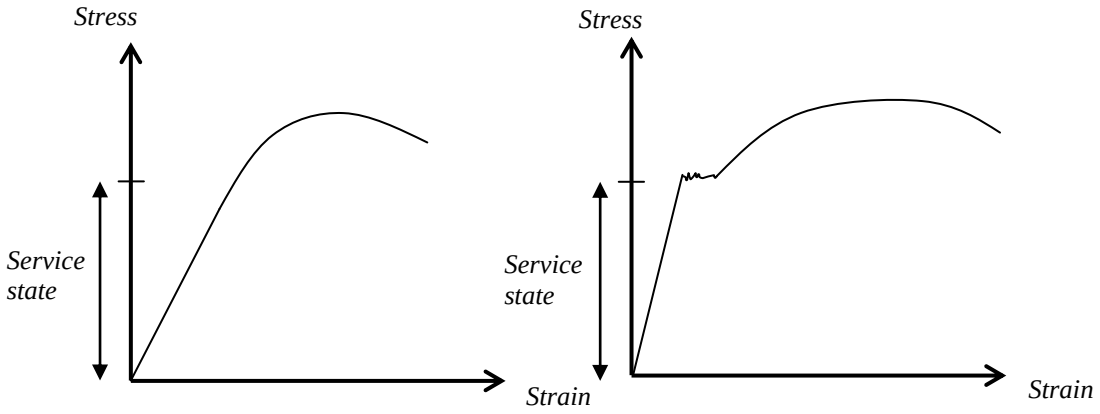

Figure 2. Stress-strain relations for concrete in compression (left) and steel (right).

The non-linearity refers to the reinforced concrete as an assembly rather than two independent materials, where cracking along with interaction between the two materials cause a non-linear performance. To illustrate this performance, the use of moment-curvature diagrams is advantageous, see Figure 3. The graph in Figure 3 represents the curvature of a small region of a member.

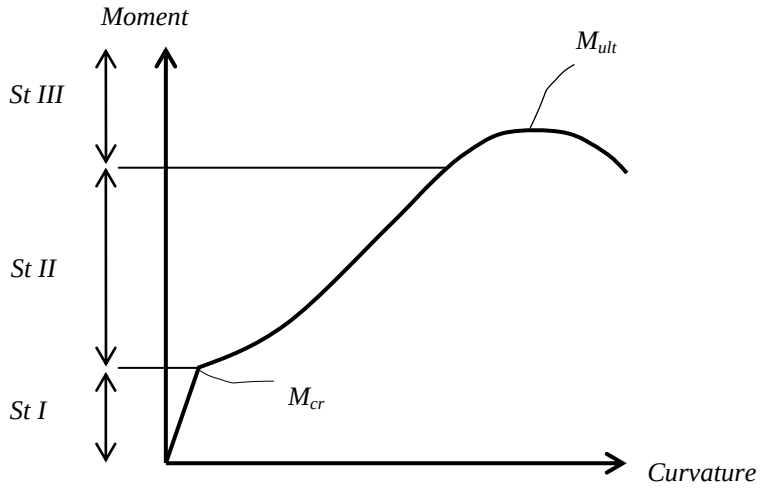

Figure 3. Moment-curvature relationship for a small reinforced concrete region. Adapted from Engström et al. (2008).

The status of a concrete member is commonly categorized into three different states, Engström *et al.* (2008). In state I, the concrete is un-cracked and both materials behave linearly. State II takes place at the point when the first crack occurs until one of the materials starts to yield or become non-linear. State III is also called the ultimate state and includes situations where the structural integrity undergoes significant changes. The member loses stiffness, a small load increase gives large deflections and the member approaches failure.

2.1.1 Behavior in service state

The behavior during service life basically resembles the moment-curvature relation of state I and II in Figure 3. The response is linear during the un-cracked state and the reinforcement has low influence on the performance. Compared to state II, the sections have high stiffness which is indicated by the slope of the graph. The first crack develops when the cracking moment, M_{cr}, is reached. This leads to a sudden loss of stiffness in the cracked section, which can be interpreted by the decreased inclination of the moment-curvature graph. The change of stiffness due to cracking along the member will give raise to stress redistributions, Engström (2011). Thus, load is transferred to stiffer un-cracked areas and the linearity is lost.

Looking closer into the process of cracking, it is realized that the stress in concrete in the tensile zone becomes zero in a cracked section. The strains that were built up before cracking have now been released in form of a crack opening and an increase of stress in the reinforcement. In order for this to happen, a slip must occur between the reinforcement and the surrounding concrete. This event is called bond-slip and the slip under development of bond stresses is the mechanism that makes the stress difference between concrete and reinforcement possible. When the load increases, tensile stresses in the un-cracked concrete will increase. As was shown in Figure 1, the largest concrete stresses emerge approximately midway between the cracks. This phenomenon is called tension stiffening and refers to the higher stiffness in concrete segments between the cracks compared to the cracked sections. Consequently, the

upcoming cracks will appear in the middle of these segments leading to further loss of stiffness in the structure. The effect of tension stiffening is gradually reduced until the crack distances are so small that the concrete stress cannot reach the tensile strength in between the cracks. From this moment on, the load increase will only lead to an increase of crack widths. The behavior of tension stiffening is described in Figure 4.

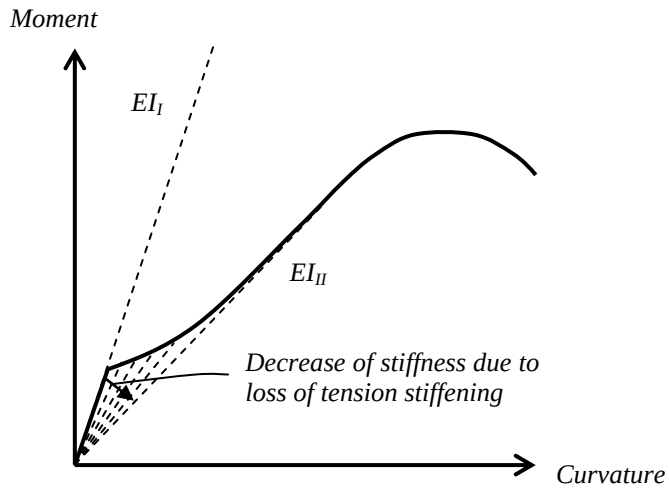

Figure 4. The loss of tension stiffening due to progressive cracking in a small region. Stiffness decreases from the high stiffness of state I to the low stiffness of state II.

As a simplified approach, the effect of tension stiffening is commonly disregarded when designing for service state. Instead it is assumed that the member is fully cracked, meaning that no further cracking can occur. Thus the low stiffness of state II is used. The stress distribution is in this case completely dependent on the amount of reinforcement provided since the reinforcement governs the stiffness distribution when the member is fully cracked.

2.1.2 Behavior in ultimate state

The ultimate state begins when one or both of the materials start to behave non-linearly. The illustration in Figure 5 shows that the ultimate state starts when the graph begins to deviate from the linear dotted line. In the sections where yielding takes place stiffness is lost significantly. A similar process of stress redistribution as in the service state takes place. Load is transferred from yielded sections to stiffer areas, mostly those with high reinforcement amount. This process is called plastic redistribution and requires that the member can withstand the deformations associated with it. These deformations are referred to as plastic- rotations or deformations.

In the ultimate state, behavioral differences can be observed between structures with high versus low reinforcement amounts. If the member is over-reinforced it will exhibit a brittle behavior, while an under-reinforced member shows high ductility. The same applies for sections within the same member with different reinforcement amounts. Brittle failures occur very sudden and sometimes in an explosion like manner and should therefore be avoided. On the contrary, ductile failures happen after

large amounts of deformation which is a desired property since the deformation act as a warning.

In an over-reinforced section, the concrete in compression will crush before any yielding starts in the flexural reinforcement. It is the crushing of the concrete that gives the brittle property. In an under-reinforced section, the flexural reinforcement will start to yield before the concretes compressive strength is reached. This gives the characteristic plateau in the right diagram in Figure 5. The length of the plateau describes the plastic rotation capacity.

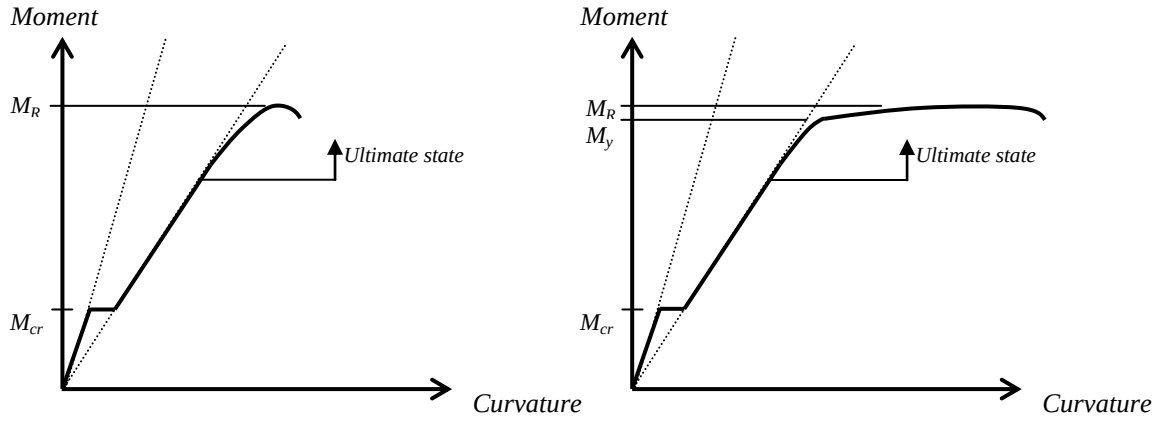

Figure 5. Sectional response of an over-reinforced section (brittle) to the left and under-reinforced section (ductile) to the right. Adapted from Engström et al. (2008).

2.2 Shear in concrete beams

The deformation of an elastic beam with constant stiffness along its length is commonly described by the differential equation according to Bernoulli's beam theory in equation (1). The bending stiffness EI, times the forth order derivative of the vertical deflection w, equals the distributed load q, see Figure 6. Based on this equation, the bending moment and shear force in a beam are generally expressed as in equations (2) and (3).

$$EI\frac{d^4w}{dx^4} = q \tag{1}$$

$$M = -EI\frac{d^2w}{dx^2},\ V = -EI\frac{d^3w}{dx^3} \tag{2), (3)}$$

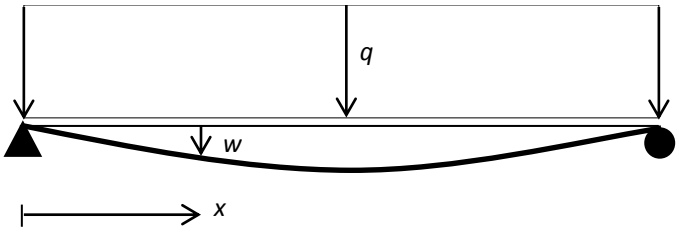

Figure 6. Deflected beam according to Bernoulli theory.

It can be noticed that the shear force is the first order derivative of the bending moment. In a case when a simply supported beam is subjected to a uniformly distributed load, the moment and shear force will vary according to Figure 7.

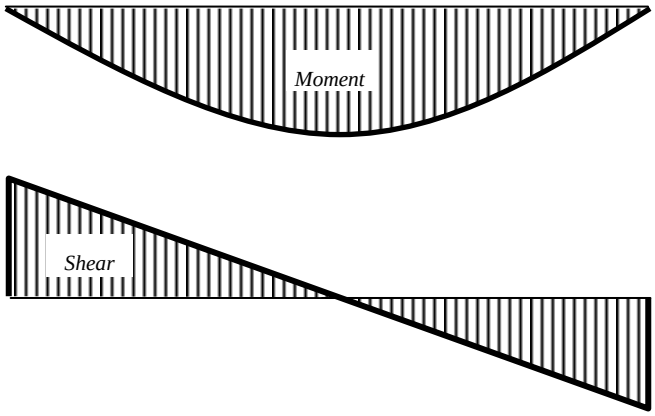

Figure 7. Bending moment and shear force in a simply supported beam subjected to distributed load.

The moment and shear distribution above cause a crack pattern in a reinforced concrete beam as illustrated in Figure 8. The cracks in mid-span are caused by the moment while the outer cracks are mostly influenced by the shear. The inclination of the cracks indicates that they are subjected to shear. This is because shear gives rise to rotation of principal stresses.

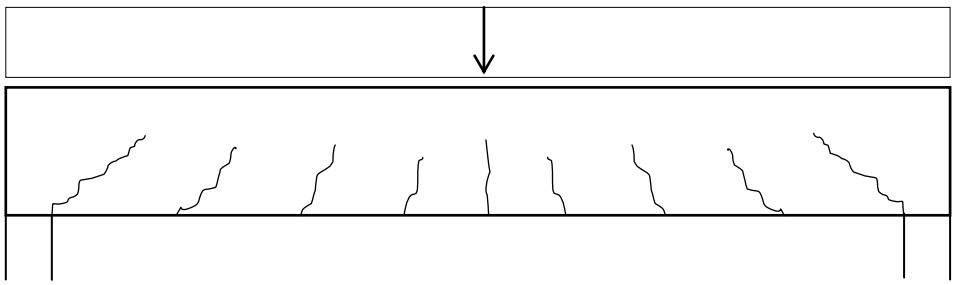

Figure 8. Cracking in a concrete beam due to moment and shear.

According to Engström *et al*. (2008), reinforced concrete beams have a certain shear-carrying capacity even when shear reinforcement is not provided. Shear reinforcement are also called stirrups or transverse reinforcement, and are usually placed in concrete members when the shear capacity of the concrete member without shear reinforcement is insufficient. The shear failure modes for beams without stirrups are

shear sliding in the crack or crushing of the concrete. Both of them are brittle types of failures. The capacity against sliding is built up by different mechanisms interacting with each other. Friction within the inclined cracks is one of the contributing factors and depends partly on the size of the aggregates and partly on how much the crack has opened, Muttoni and Fernández Ruiz (2008). Consequently, the tensile flexural reinforcement also contributes to the shear capacity by holding the cracks together. In addition, the flexural reinforcement has a small resistance against deformations perpendicular to its direction. This is called dowel-action and is often considered less significant compared to the resistance from friction, Engström *et al.* (2008). It is also known that the shear capacity increases in concrete subjected to compression. Hence the compression zone in the top of the cross-section has a positive influence. Although these mechanisms are well known, the interactions between them are complex and the shear capacity of beams without transverse reinforcement is still a subject for research, see Section 3.1.

To avoid shear sliding in the crack, transverse reinforcement can be used. This increases the shear capacity significantly, since shear sliding now requires the stirrups to yield. The increased shear capacity will raise the risk of crushing of the concrete. This is because the concrete segments between the inclined cracks are subjected to compression in order to keep equilibrium, and the stress within them will increase for larger vertical loading. The risk of crushing in the concrete constitutes an upper limit for the shear capacity, whether stirrups are provided or not.

The behavior of a reinforced concrete beam subjected to a distributed load can be explained with the truss model illustrated in Figure 9. The dashed lines are called struts and represent compression. The solid lines are called ties and represent tension. When cracking has started in the concrete, the provided reinforcement will take the role of the ties. The horizontal tie in the bottom represents flexural reinforcement and the vertical ties represent stirrups.

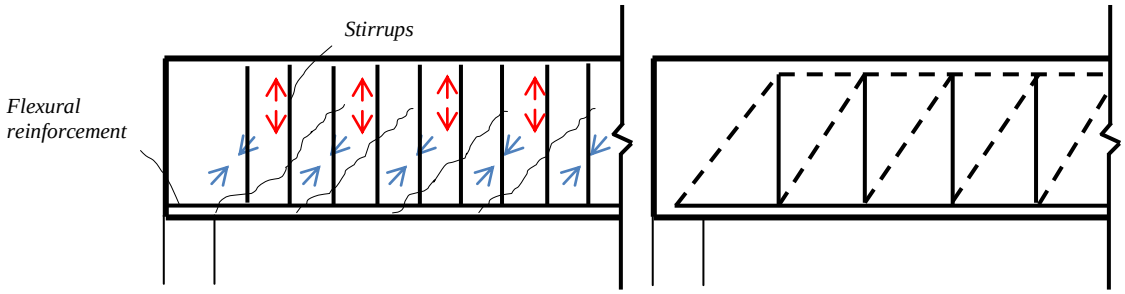

Figure 9. *The behavior of a reinforced concrete beam and representation with a truss model. Vertical arrows and solid lines are tension. Inclined arrows and dashed lines are compression.*

When the load is close to the support, some part of it is directly transferred to the support by an inclined strut while some part needs to be carried up by the truss, see Figure 10. The closer the load is to the support, the more of the load is carried directly by the inclined strut. Consequently, a smaller part of the load needs to be carried through friction or by the stirrups. This is a favorable effect that can be considered to make the design more effective.

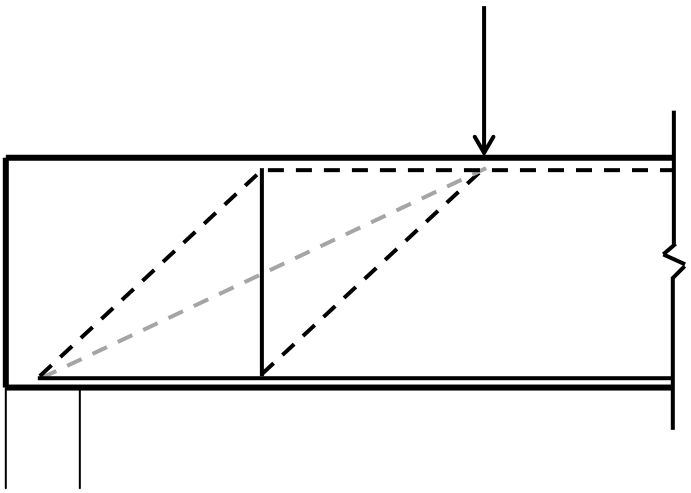

Figure 10. The effect of loading close to support. Adapted from Engström et al. (2008).

2.2.1 Design without transverse reinforcement according to EC2

Two criteria must be fulfilled in all cross-sections of the beam in order to carry the design shear load. As mentioned above, the criteria are related to the shear sliding and the crushing of the inclined strut. The capacity of the concrete against shear sliding in beams without any normal forces should according to Eurocode 2 (2008) be calculated with the empiric expression in equation (4).

$$V_{Rd,c} = C_{Rd,c} k (100 \rho_l f_{ck})^{1/3} \cdot b_w d \geq 0{,}035 k^{3/2} f_{ck}^{\ 1/2} \cdot b_w d \text{ , where} \quad (4)$$

$$C_{Rd,c} = 0{,}18 / \gamma_c \quad (\gamma_c = 1{,}5)$$
$$k = 1 + (200/d)^{1/2} \leq 2{,}0 \quad (d \text{ in mm})$$
$$\rho_l = A_{sl} / (b_w d) \leq 0{,}02$$

A_{sl} is the cross-sectional area of the fully anchored tensile reinforcement, f_{ck} is the concretes characteristic compressive strength, in MPa and b_w is the smallest cross-sectional width in the tensile zone. d is called effective depth and is the distance from the compressed surface to the center of the tensile reinforcement.

To be able to withstand the compression in the inclined strut, the stress within it should not exceed a reduced value of the compressive strength (vf_{cd}). The reduction is due to tensile stresses and cracking, that occur perpendicular to the compression direction. Concrete without transverse reinforcement has low capacities of plastic rotations in the ultimate state, Engström *et al.* (2008). It is therefore assumed that the angle of the inclined shear cracks will be influenced by the stress state before cracking. The angle of the largest tensile principal stress before cracking, in a section without any normal force, is 45 degrees in relation to the beams main axis. This stress arises in the mass center of the cross-section, see Figure 11. Thus, the cracking will occur orthogonal to the principal tensile stress before cracking. In Figure 12, an illustration is made of an inclined strut and the forces acting on it.

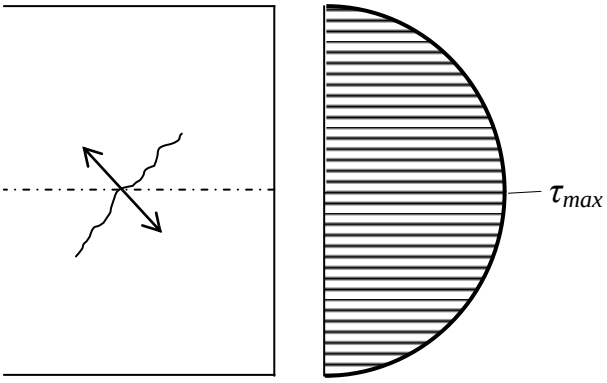

Figure 11. Shear stress variation along the height of a rectangular beam cross-section.

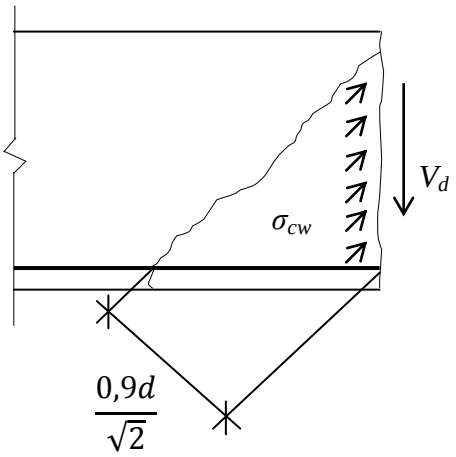

Figure 12. Forces in the inclined concrete strut. Adapted from Engstöm et al. (2008).

The force in the inclined strut is equal to

$$F_{cw} = \sigma_{cw} b_w \frac{0{,}9d}{\sqrt{2}}, \tag{5}$$

and since σ_{cw} should not exceed vf_{cd}

$$F_{cw} \leq v f_{cd} b_w \frac{0{,}9d}{\sqrt{2}}$$

The inclined strut should carry the shear force in its vertical component

$$F_{cw} = V_d \sqrt{2}$$

Thus, the criterion for crushing of the inclined strut becomes

$$V_{Ed} \le \frac{v f_{cd} b_w \frac{0{,}9d}{\sqrt{2}}}{\sqrt{2}} \approx 0{,}5 v f_{cd} b_w d \text{ , where} \quad (6)$$

$$v = 0{,}6(1 - f_{ck}/250) \ (f_{ck} \text{ in MPa}) \quad (7)$$

When designing flexural reinforcement, it is important to take into account that the horizontal contribution from the inclined strut needs to be carried by tension in the flexural reinforcement.

2.2.2 Design with transverse reinforcement according to EC2

When the concrete alone is not able to carry the shear force, transverse reinforcement must be provided. According to Eurocode 2 (2008), it is not allowed to take the contribution of the concrete into account when designing stirrups. Thus the provided reinforcement must be able to carry all shear force by itself. The designer is able to choose the inclination of the shear crack before it occurs. According to Engström *et al.* (2008), this is because the plastic redistribution is highly dependent on the stiffness provided by the stirrups. Consequently, a region with a dense content of stirrups will be able to lift the shear force by the stirrups within shorter distance, i.e. the crack angle becomes large and vice versa. The recommendation for choice of angle is given as an interval between 21,8 and 45,0 degrees, in EC2. Larger angles require more transverse reinforcement while on the other hand smaller angles require more longitudinal reinforcement and increase the compression in the inclined struts.

As mentioned earlier, shear sliding will cause the stirrups to yield. The capacity against this failure mode is dependent on the number of stirrups that help carrying the same crack. The most general expression, where inclination of stirrups can be considered is given in equation (8) according to EC2.

$$V_{Rd,s} = \frac{0{,}9d(\cot\theta + \cot\alpha)}{s} \cdot f_{ywd} \cdot A_{sw} \cdot \sin\alpha \quad (8)$$

Here, θ is the angle of the crack and α is the angle of the stirrups, both in relation to the main axis of the beam. s is the spacing between stirrups, f_{ywd} is the design yield stress of the stirrups and A_{sw} is the contributing area of the stirrups, usually twice the cross-sectional area.

For crushing of the inclined concrete struts in beams with transverse reinforcement, EC2 gives the expression in equation (9). Here, α_{cw} is a factor considering effects of possible normal forces and v_1 is the same as v in equation (7).

$$V_{Rd,max} = 0{,}9d \cdot \alpha_{cw} b_w v_1 f_{cd} \frac{\cot\theta + \cot\alpha}{1 + \cot^2\theta} \quad (9)$$

2.3 Shear in concrete slabs

When deriving the differential equation of plates, different assumptions are needed depending on the thickness of the plate and which application it is used for. According to Blaauwendraad (2010), normally slabs fall under the category of thin plates since the plate is used to carry out of plane loads and the span to thickness ratio is larger than 5,0. Thin plates are assumed not to have any shear deformations. The differential equation of linear elastic thin plates relates the vertical deflection w to the applied distributed load q as in equation (10).

$$\frac{\partial^4 w}{\partial x^4} + 2\frac{\partial^4 w}{\partial x^2 \partial y^2} + \frac{\partial^4 w}{\partial y^4} = \frac{q}{D} \tag{10}$$

The moments and shear forces can be derived from this differential equation. The results are presented in equations (11) to (15), where D is only the flexural stiffness since shear deformations are omitted, and v is Poisson's ratio. In addition, an important cross-sectional moment is introduced in plates. It is called twisting or torsional moment (m_{xy}) and must be taken into account in design of flexural reinforcement. Since the reinforcement bars do not always coincide with the principal direction of the bending moment, the presence of torsion will lead to an increased need of capacity in the reinforcement bars.

$$m_{xx} = -D\left(\frac{d^2 w}{dx^2} + v\frac{d^2 w}{dy^2}\right) \tag{11}$$

$$m_{yy} = -D\left(v\frac{d^2 w}{dx^2} + \frac{d^2 w}{dy^2}\right) \tag{12}$$

$$m_{xy} = -(1-v)D\frac{d^2 w}{dxdy} \tag{13}$$

$$v_x = -D\left(\frac{d^3 w}{dx^3} + \frac{d^3 w}{dxdy^2}\right) \tag{14}$$

$$v_y = -D\left(\frac{d^3 w}{dy^3} + \frac{d^3 w}{dx^2 dy}\right) \tag{15}$$

In oppose to bending moment which has two principal directions orthogonal to each other, shear has only one principal direction. One can imagine observing a plate from above, realizing that the flexural reinforcement is aligned in two directions, while the transverse reinforcement is presented in points.

Hence, it is possible to describe the maximum (principal) shear force with only a vector. The magnitude of the vector is calculated according to equation (16) and the direction of it with equation (17).

$$v_0 = \sqrt{{v_x}^2 + {v_y}^2} \tag{16}$$

$$\beta_0 = \arctan\left(\frac{v_y}{v_x}\right) \tag{17}$$

2.3.1 One- and two-way action

When it comes to concrete slabs it is necessary to distinguish between one- and two-way acting slabs, see Figure 13. This depends on the support conditions and refers to the direction that the forces and moments mainly are transferred in. Slabs with two-way action require bending reinforcement in two directions, while slabs with one-way action work similar to beams and need bending reinforcement in essentially one direction.

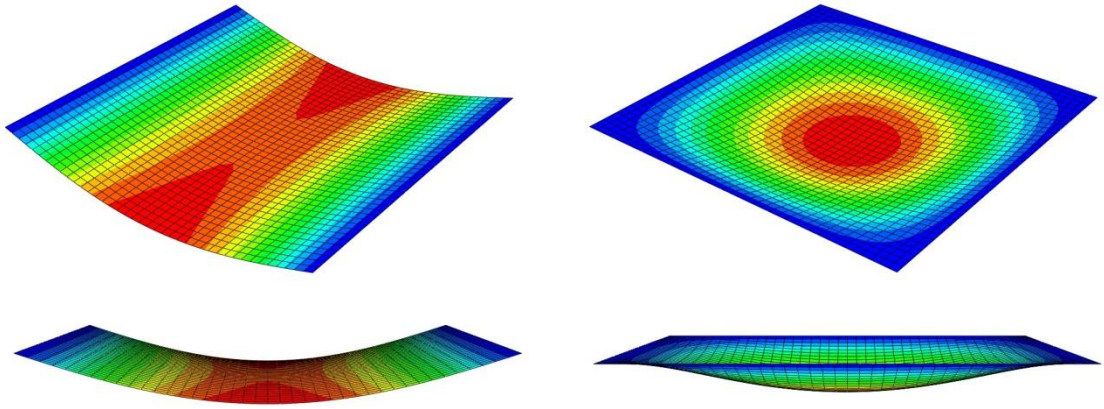

Figure 13. One-way action to the left and two-way action to the right. The contours indicate vertical deflection.

2.3.2 Failure in slabs due to shear

Traditionally, a failure mode caused by shear is categorized as one of the two following types. The first is simply called shear failure and the second is called punching shear failure. These two types of failure modes can be described by the cases in Figure 14. In case *a)*, the shear flow direction (β_0) is constant and is also referred to as one-way shear. This failure consists of a straight crack that will occur parallel to the direction of the support, i.e. a shear failure. In case *b)*, the shear flow direction is highly varying, called two-way shear. This causes the second type of failure mode, punching shear failure. It is characterized by a circular crack forming around a concentrated load.

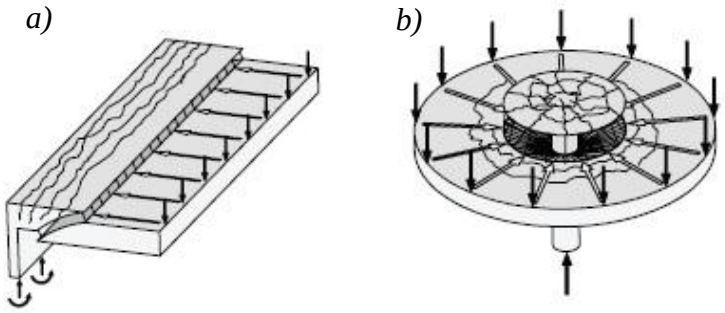

Figure 14. The modes of failure due to shear. a) Shear failure caused by one-way shear. b) Punching shear failure caused by two-way shear, Adapted from Vaz Rodrigues (2007).

Design codes usually separate these two modes from each other and give different ways of calculating the capacities. In Eurocode 2 (2008), no specific capacity is given for one-way shear in slabs. Instead, the slab is supposed to be designed in the same way as a beam. In reality the shape of the failure mode is case sensitive and may therefore become something in between a straight and a circular crack, resulting in a shear capacity that does not agree with the capacities from design codes.

Often when designing concrete slabs, the designer wishes to avoid transverse reinforcement. This is especially true when designing bride decks where the loads are in motion and the use of stirrups in the entire slab is unpractical. A common measure to increase the shear capacity and avoid stirrups is to increase the thickness of the slab.

2.3.3 Design for punching shear according to EC2

The nominal punching shear capacity of concrete without transverse reinforcement should according to EC2 be calculated as equation (18). This expression is based on evaluation of test results.

$$v_{Rd,c} = C_{Rd,c} k (100 \rho_l f_{ck})^{1/3} \geq 0{,}035 k^{3/2} f_{ck}^{1/2}, \text{ where} \quad (18)$$

$$\rho_l = (\rho_{ly} \cdot \rho_{lz}) / 2 \leq 0{,}02$$

ρ_{ly} , ρ_{lz} are the reinforcement ratio in y- and z-direction

The other parameters are the same as in equation (4). This capacity should be compared to the load effect at a control perimeter 2*d* from the load edge.

3 Literature review

The most relevant and interesting works that was found in the literature study is presented in this chapter. Focus is put on failures caused by shear that can occur in slabs and how to design for them. The purpose of this chapter is to assemble interesting research and give an overview of the extent of research in this field. The current Swedish recommendations and the background of them are also presented.

3.1 Failure criteria

A lot of research has been done for failures caused by shear in slabs during the years. The presented studies below are chosen mainly because they are recently performed and they discuss cases of intermediate shear failures and how to treat them with FEM. In the following sections, two failure criteria are presented for one-way and two-way shear failure and verified by comparison to test specimens that were loaded until failure.

3.1.1 Shear failure

Muttoni and Fernández Ruiz (2008) developed a failure criterion for one-way shear in concrete members without transverse reinforcement, as presented in equation (19). Values should be inserted with the units MPa and mm.

$$\frac{V_R}{bd\sqrt{f_c}} = \frac{1}{6} \cdot \frac{2}{1+120\left(\frac{\varepsilon d}{16+d_g}\right)} \tag{19}$$

V_R shear force capacity of the member
b width of the member
d effective depth
f_c concrete compressive strength
ε concrete compressive strain at a depth of 0,6d in the control section. The control section should be chosen to where the shear capacity equals the shear force.
d_g maximum aggregate size

The work of developing this expression is based on the critical shear crack theory which states that a crack will occur in the inclined strut and decrease the shear strength as in Figure 15a. The shear capacity is a function of the crack width, and the crack width is proportional to εd according to the authors. Muttoni and Fernández Ruiz (2008) state that experiments performed by Leonhardt and Walther show that cracking in the inclined strut and its effect will be strongly influenced by the ratio a/d, see Figure 15a. For small values of a/d, the crack will not develop inside the strut, allowing the flexural strength to be reached. For large values of a/d, the flexural strength will also govern the failure. Thus, only cases with intermediate ratios of a/d will get affected shear capacities.

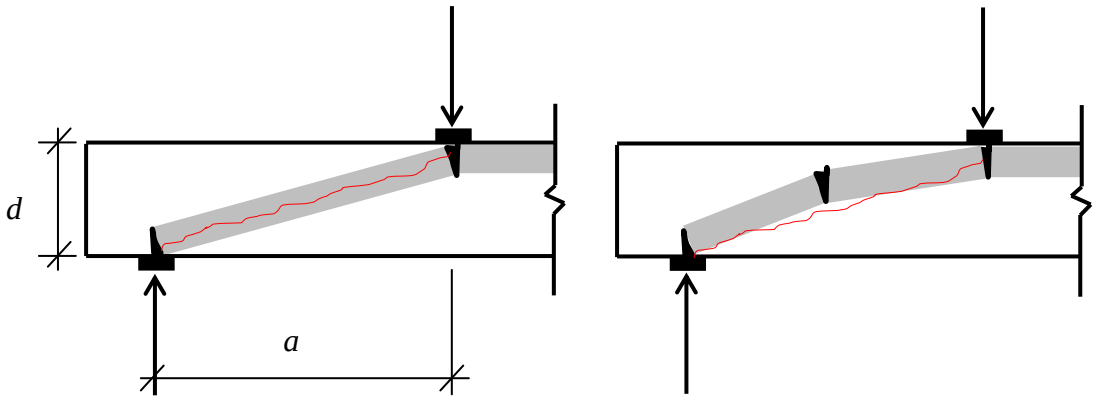

Figure 15. The compression struts in a simply supported beam loaded symmetrically. Alternative a), crack trough strut, alternative b), elbow-shaped arch. In alternative b), ties are needed to create equilibrium, but they are left out for the sake of simplicity. Adapted from Muttoni and Fernández Ruiz (2008).

It is mentioned that there are three shear-carrying mechanisms that act before the critical shear crack arises. They are called cantilever action, aggregate-interlock and dowel action and emerge when flexural cracks are present. They give rise to tensile stresses that will cause the propagation of existing flexural cracks, reducing the capacity of the mechanisms. The cantilever action mechanism is explained in Figure 16.

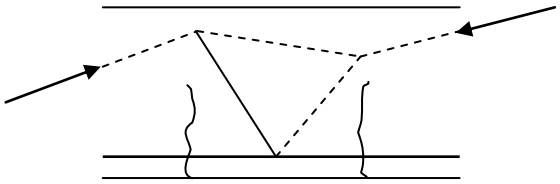

Figure 16. Cantilever action. Dashed lines are compression and solid lines tension.

There are two possible load-carrying states after the development of the crack. Either the compression strut remains straight and the compression is carried by aggregate-interlock through the crack (Figure 15a), or it tries to avoid the crack by creating an elbow-shaped arch as shown in Figure 15b. In order to maintain equilibrium, a tensile zone emerges above the elbow-shaped strut which is not shown in the figure. Experiments carried out by Muttoni and Thürlimann (1986) show that these two load-carrying states can interact. Hence an intermediate state can occur.

Comparison to 285 test results was made with the capacities calculated according to the presented criterion. The mean value of the ratio V_{test} / V_{th} (test result divided by result from criterion) became 0,99 with a coefficient of variation (scatter of results) of 0,1. Low values of coefficient of variation indicate that the individual comparisons do not deviate much from the mean value. This shows that the criterion is capable of predicting the shear capacity of concrete beams without transverse reinforcement. Moreover, it should be mentioned that the testings were made for members with rectangular cross-sections, including tensile and compressive axial forces, light-weight concrete, high-strength concrete, without pre-stressing or any skin reinforcement along side-faces.

3.1.2 Punching shear failure

The most commonly used expressions of punching shear strength for concrete slabs are often derived on the basis of test results, considering only the parts closest to the concentrated load. Muttoni (2008) presented a formulation for the punching shear failure criterion based on mechanical explanations, correlating the punching shear capacity to the slab rotation, see equation (20). In this formulation, effects of the size are taken into account. It is shown that the size effect concerns the span rather than the depth of the slab which was previously thought.

$$\frac{V_R}{b_0 d\sqrt{f_c}} = \frac{3/4}{1+15\left(\frac{\psi d}{d_{g0}+d_g}\right)} \tag{20}$$

b_0 control perimeter
ψ rotation of the slab
d_{g0} reference size (16 mm)

In general, a non-linear analysis is required to obtain the slab rotation for this method, but for an axisymmetric case an analytical expression is presented. The expression connects the slab rotation to the load but is too complex and out of the scope of this thesis to be presented. The load-rotation expression is based on the assumption that the critical shear crack emerges at a distance *d* from the face of the column and that the slab portion around the critical shear crack deforms following a conical shape, resulting in constant slab rotation around the whole crack. Furthermore, the expression is based on a quadrilinear moment-curvature relationship (Figure 17a) which is a simplification of the real behavior presented in Figure 3. It was shown that a simpler bilinear moment-curvature relationship also generated satisfactory results in general cases, see Figure 17b. The load-rotation curve in combination with a curve of the failure criterion presented above yields the punching shear capacity in the point where the two curves meet; the solution is achieved if the expression of rotation is substituted into equation (20).

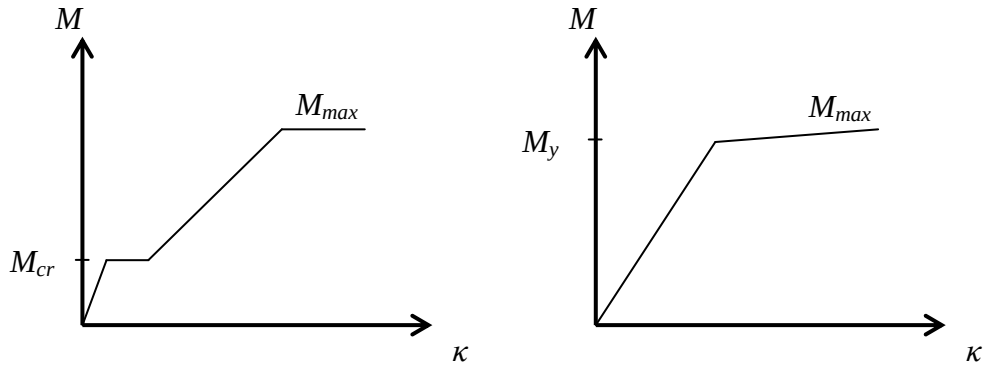

Figure 17. a) Quadrilinear moment-curvature relationship to the left. b) Bilinear moment-curvature relationship to the right.

The capacities of 87 different tests performed by other researchers were calculated with the method presented, and the statistics point toward satisfactory results. The ratio between the measured values from testing and the calculated value (V_{test} / V_{th}) had an average of 1,02 and a coefficient of variation of 0,08. The same comparison was made between test results and the capacities calculated according to EC2 and ACI 318-05. For EC2 an average of 1,14 and coefficient of variation of 0,12 was gained and for ACI an average of 1,37 with a coefficient of variation of 0,22. Important to note is that the test specimens in the comparisons all had the same bending reinforcement ratio in orthogonal directions.

3.1.3 Intermediate shear failures

The process of calculating the failure load with the criteria presented above is further discussed by Vaz Rodrigues (2007). For a concrete slab, it consists of a linear elastic analysis from which the location and mode of failure can be predicted by finding regions with large shear flow and distinguishing whether the flow is uni-directional or two-directional. In this way, the appropriate failure criterion can be chosen. Though in some cases, the mode of failure will not be either shear- or punching shear failure but something in between.

To investigate cases of intermediate failure, test results from two different testings were compared with calculated values of the failure loads based on Muttonis expressions. The first comparison was made with bridge deck cantilever tests performed by Vaz Rodrigues *et al.* (2006), presented in Section 3.2. The second comparison was carried out with the testing of Miller *et al.* (1994), where a 38-year old decommissioned concrete slab bridge was subjected to two concentrated loads. Both these testings resulted in shear failure, or an intermediate failure between shear- and punching shear failure. Calculations of the failure loads for these two testings were made with both of Muttonis criteria, and they corresponded well with the test results irrespective of which criterion that was used.

Vaz Rodrigues *et al*. (2008) further discuss the fact that concentrated loads on bridge deck cantilevers can cause intermediate types of failure. These types of failure are not covered by current design codes. A common formulation of the punching shear strength is $V_R = v_R \cdot b_0$, where v_R is the nominal shear strength per unit length and b_0, also referred to as the control perimeter, is the length of a control section which encircles the load at a certain distance from the load edge. The control perimeter according to Eurocode is illustrated in Figure 18.

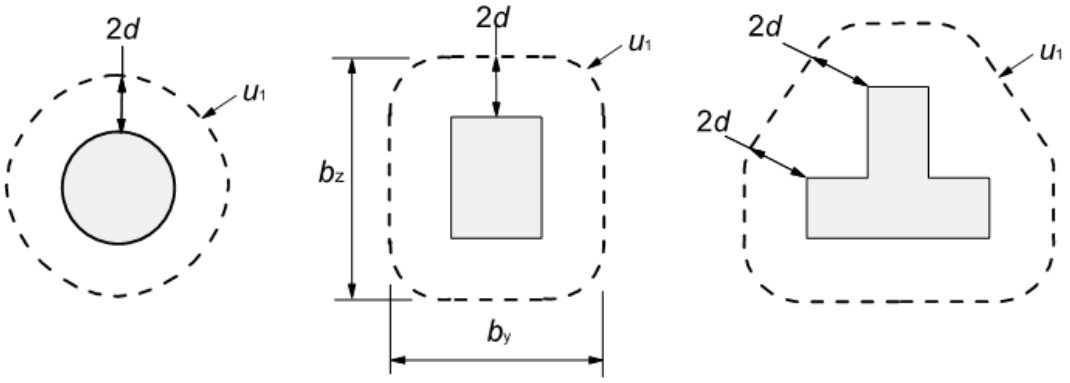

Figure 18. Control perimeter, u_1, defined by Eurocode for some different cases.

Vaz Rodrigues *et al*. (2008) strived to give recommendations on how to decide the control perimeter for intermediate cases. Usually the shear force perpendicular to the control perimeter is of interest since that is the actual force which needs to be transferred and carried by the concrete[1]. Vaz Rodrigues suggests the control perimeter to be calculated as $b_{0.elast} = V / v_{el.max}$. V is the total applied load within the perimeter and $v_{el.max}$ is the maximum shear force per unit length from a linear elastic FE analysis. This value is extracted along the control perimeter which is provided by Eurocode 2 (2008), and should be the component which is perpendicular to that control preimeter. This means that instead of using the actual shear force that varies greatly along b_0 (u_1 *in* Figure 18), one can use a constant shear force ($v_{el.max}$) along a reduced control perimeter ($b_{0.elast}$), to calculate the capacity of intermediate cases. This approach does not take into account effects of cracking or yielding, which would result in more effective load paths and lower magnitudes of shear needed to be transferred. Thus it gives a value of the shear strength that is conservative.

The control perimeter suggested is combined with the formulation of the nominal shear strength (v_R) according to both ACI 318-05 and EC2 2004, to get a value of the structures capacity. The results show good correspondence between the calculated values and the values gained from testings. The authors point out that it is of importance to take into account effects of possible edge beams which would significantly change the shear flow. Vaz Rodrigues (2007) showed that strong edge beams lead to diffusion of the shear forces in the slab, meaning that concentrations got spread out with the higher stiffness introduced by the edge beam. Considerations must also be taken regarding the global effect of longitudinal bending on the slab of a bridge, where tension give reduced nominal shear strength and compression has a positive influence.

[1] Mario Plos, Chalmers University of Technology, 2011.

3.2 Laboratory testings

In order to help improving the failure criteria presented by Muttoni and finding a relation between one-way shear and two-way shear, Vaz Rodrigues *et al*. (2006) carried out experiments on two 3/4 models of a full scale bridge deck cantilever. The goal was to assess the load carrying capacity when the structure is subjected to various compositions of concentrated traffic loads.

Structures that are designed on basis of the upper bound theorem of theory of plasticity, using e.g. the yield line theory, may actually fail for lower loads than designed for, mainly in brittle failures due to shear. This is because of the negative effect of plastic rotations that are required to reach the expected mechanism, on the shear strength of the cantilever. The experiment arrangements can be seen in Figure 19. The length of the cantilevers was 10.0 m. The loads were applied at different times and were considered not affecting each other. No shear reinforcement was provided in the test specimen. The two specimens were identical besides the reinforcement amounts, which were less in the top surface in transversal direction in specimen DR2.

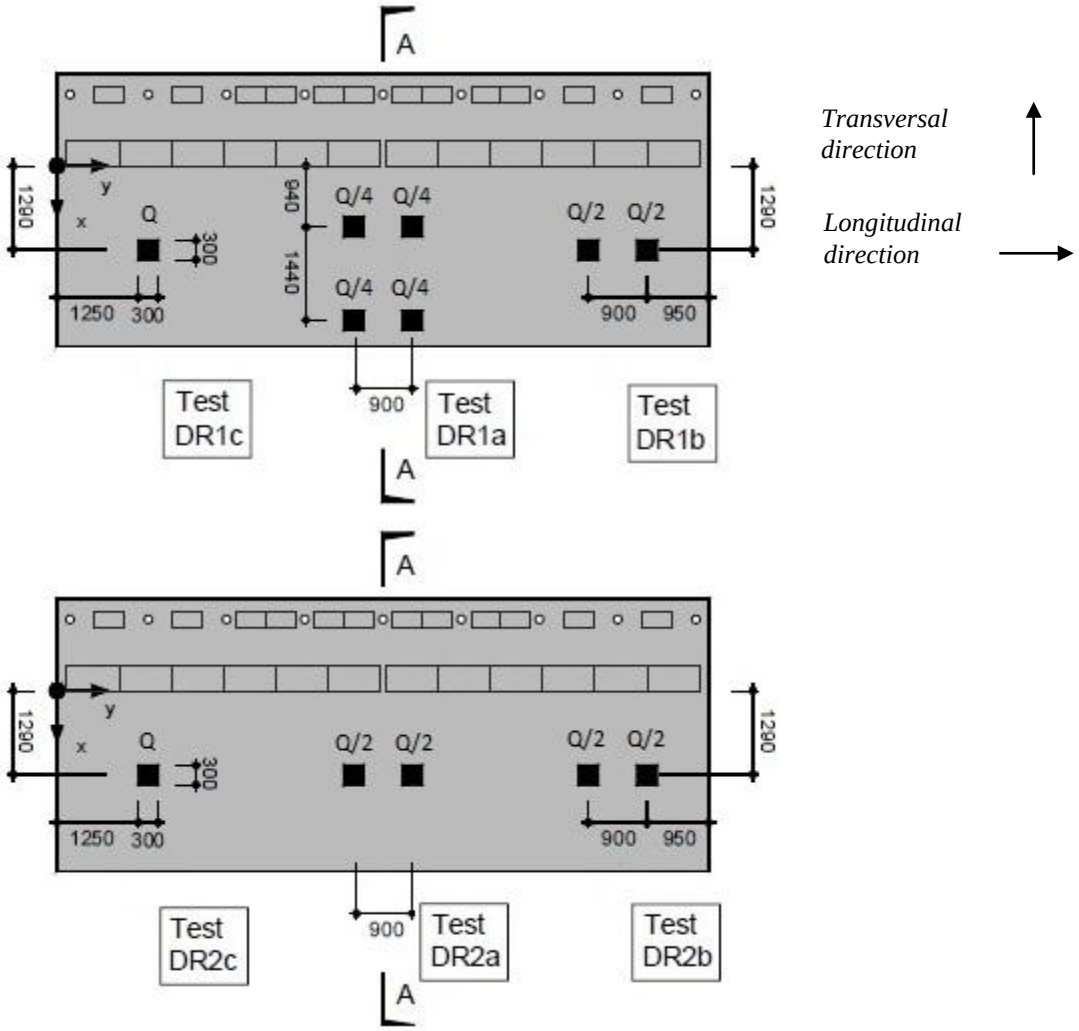

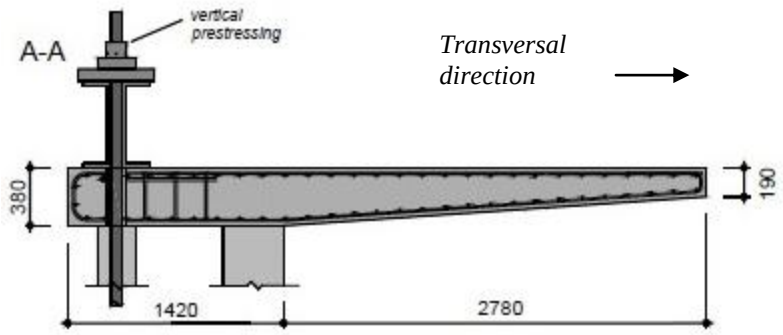

Figure 19. The experiment arrangements and the names of the tests. Adapted from Vaz Rodrigues (2006).

For all six loadings a brittle failure in shear was observed, and none of them did reach the design load calculated on the basis of the yield-line method. The load carrying capacities based on the yield-line method were also compared to a non-linear FE analysis which confirmed that they corresponded to the theoretical flexural capacity.

A linear elastic analysis was made of specimen DR1. It showed that the shear flow in test DR1a had large variation of direction in between the inner and outer load pairs, which led to the primary shear cracking shown in Figure 20a. The shear flow direction was almost constant between the clamped edge and the neighboring loads for all tests. The colored regions in Figure 20 had the highest strains and the most significant shear cracks appeared there.

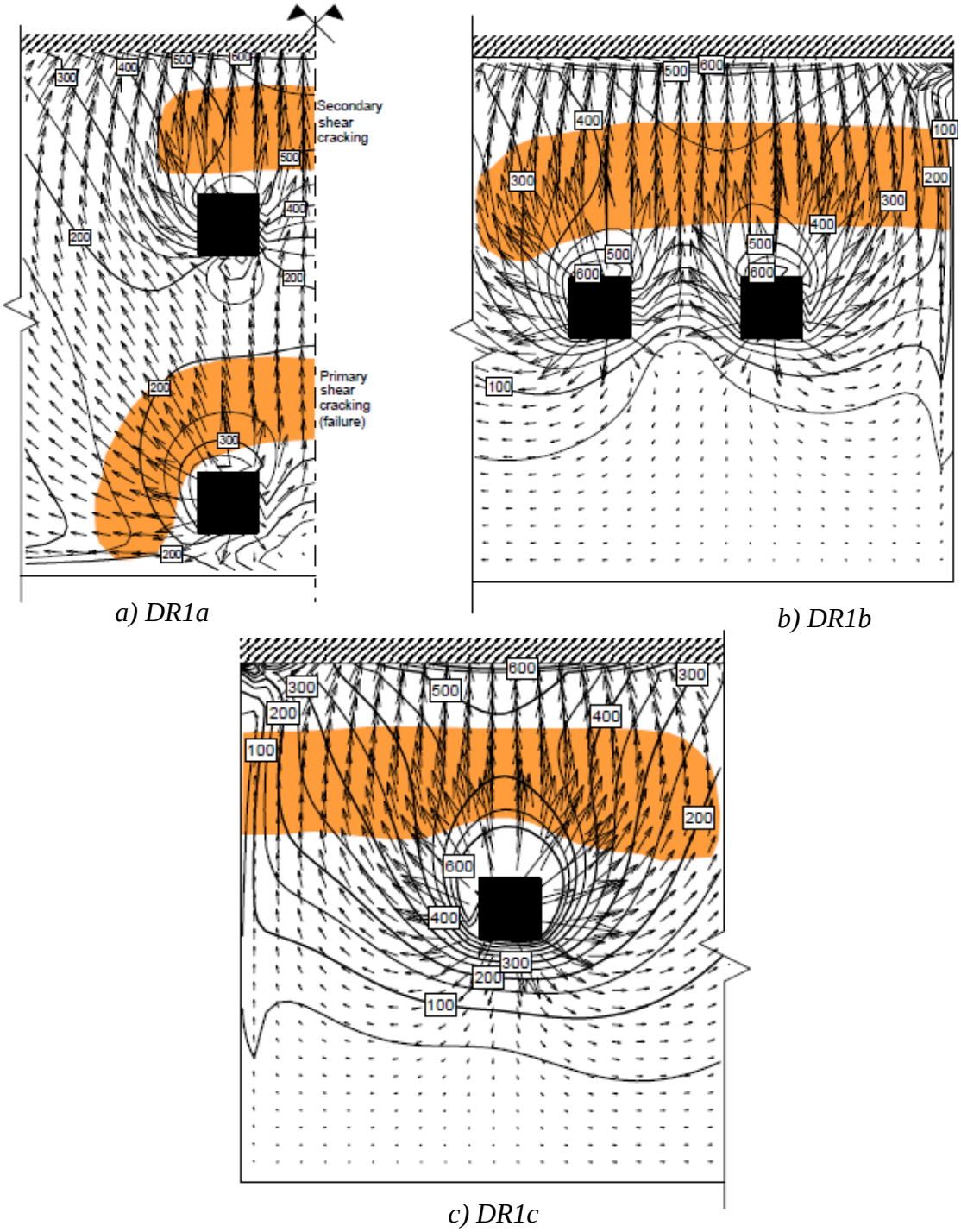

Figure 20. Shear flow directions and contour curves of v_0 [kN/m]. Vaz Rodrigues et al. (2006).

The failure in test DR1a came closest to the theoretical flexural failure load and the characteristics of it were somewhat different compared to the other two. For instance the flexural reinforcement in the top transversal direction and the bottom longitudinal direction (see Figure 19 for definition) started to yield before failure, which was not the case in DR1b and DR1c. In addition, a large shear crack was observed close to the clamped edge (secondary shear crack in Figure 20a) but the failure did not occur

there. Instead the failure took place in the primary shear crack around the outermost load pair. The authors explain this as a consequence of redistribution of the shear flow when the shear crack close to the clamped edge developed. The results of the tests can be seen in Table 1.

Table 1. Results from large scale bridge deck cantilever tests. Vaz Rodrigues (2006).

Test	Number of wheel loads	Failure Load Q_R [kN]	Q_{Flex} [kN]	Q_R/Q_{Flex} [-]	Failure location	Mode of failure
DR1a	4	1380	1600	0.86	Cantilever edge	Shear
DR1b	2	1025	1320	0.78	Fixed end	Shear
DR1c	1	937	1190	0.79	Fixed end	Shear
DR2a	2	961	1500	0.64	Fixed end	Shear
DR2b	2	856	1060	0.80	Fixed end	Shear
DR2c	1	725	960	0.75	Fixed end	Shear

Q_{Flex}: Theoretical flexural failure load

Some of the conclusions were that the failure loads can accurately be predicted by the criteria in Section 3.1 and when the failures in bridge deck cantilevers are of intermediate types, the capacities can be calculated with either criteria and still yield satisfactory results.

In addition to the cantilever tests, a set of reinforced concrete beams were also tested for shear failure. The beams were not reinforced with stirrups in the region where failure was expected to promote shear failure there, but stirrups were placed outside of that zone. The results from these tests point towards a relation between reduction of the shear capacity in regions of plastic hinges and the increase of with increasing plastic rotations.

3.3 Swedish recommendations

Davidson (2003) discusses the distribution of shear force from linear FE analyses of bridge structures. When the design is based on linear elastic FE analysis, it is desired to resemble the real behavior of reinforced concrete, such as redistribution of stresses due to cracking, by smearing out shear concentrations within larger parts of the structure. It is then assumed that this part of the structure carries the load. The two modes of failure in shear are discussed on the basis of design rules and recommendations given in Swedish codes and handbooks. The first expression of the width within which the shear force is distributed is given by BBK 94 as shown in equation (21). The expression applies only for cases where the slab is supported on line supports and for design in ultimate limit state. Davidson (2003) suggests a limitation of the distribution according to equation (22).

$$b_{eff} = \max(7d + b + t; 10d + 1{,}3x) \tag{21}$$

$$b_{eff} \leq 5h \tag{22}$$

d effective depth

b width of the load (*c in* Figure 21)

t thickness of paving

x distance from center of load to section which is considered to fail

The first part of the expression from BBK 94, $7d + b + t$, in equation (21), is originally based on some experiments that were carried out at Chalmers University of Technology in the 1970s, Hedman (1976). It was assumed that the capacity against concentrated shear force in slabs corresponds to the shear capacity of beams with a fictitious contributing width of b_{eff}. This width is dependent on conditions such as distance from load to support, boundary conditions and load configurations. The work of developing an expression for the contributing width is based on the approach that the capacity can be expressed as in equations (23) and (24).

$$V_p = b_{eff} \cdot d \cdot f_v, \text{ where} \tag{23}$$

$$f_v = k_\tau (1 + 50\rho)(1{,}6 - d)\sqrt{f_{ckub}} \cdot \frac{3d}{a'} \tag{24}$$

V_p is the capacity against concentrated shear force
k_τ is a factor based on experiments with other beams
ρ reinforcement ratio
a' shear span; distance between load and support in a beam

The experiments were performed on several slabs, some simply supported on two sides and some cantilever slabs on a line support. Based on the experiment results and theoretical considerations, Hedman (1976) concluded that the contributing width can

be expressed as in equation (25). See Figure 21 for explanation of the parameters x and c.

$$b_{eff} = K_d d + K_x x + c \tag{25}$$

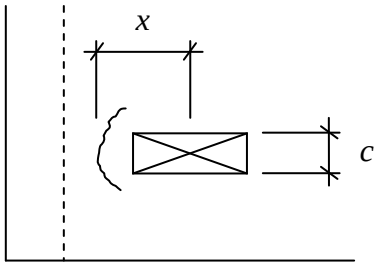

Figure 21. Concentrated load on slab where c is the width of the load parallel to the support and x is the distance from load center to the section where failure occurs. Adapted from Hedman (1976).

From the experiments, the value of K_x is decided to be equal to 1,0 and based on the assumption that the failure occurs in a section 0,5d from the edge of the load, K_d is decided to be equal to 6,0.

4 Non-linear FE analysis

To contribute to the understanding of how the cracking of reinforced concrete structures affect the shear flow, a non-linear FE model was established based on the specimens that were tested by Vaz Rodrigues *et al*. (2006), see Section 3.2. The main focus was put on the effects of flexural cracking on the shear force distribution. In addition, it was also of interest to review ultimate limit state effects such as yielding and plastic redistribution of flexural reinforcement.

4.1 General

Most commonly, a non-linear FE analysis is used when a detailed response of the structure is of interest. To perform such analysis, one must know all the dimensions, the exact amount of reinforcement and the reinforcement arrangement in beforehand. Consequently, it is not a practical method for design; rather it is useful for analysis of existing structures.

Generally in structural engineering, when a structure is to be modeled, certain idealization is necessary. This can concern simplifications when modeling loads and supports for instance, where a very detailed modeling might be unnecessary for the purpose of the analysis, while an incorrect modeling results in unrealistic behavior. Furthermore, the structural idealization concerns choice of material representations and element types. When the choices are made regarding structural idealization, the process goes on to modeling the structure (pre-processing), performing the analyses of interest and evaluating the obtained results (post-processing).

4.1.1 Structural idealization

Many choices must be made when creating a non-linear FE model, and they mainly depend on the purpose of the analysis. Some of the most important decisions before modeling the structure in a FE software consider element types, material models and boundary conditions. Here follows a description of how to make these decisions in order to set up an appropriate model.

Element types

Structural elements should be used for over-all behavior while continuum elements for detailed local effects. Examples of structural elements are shell elements which work well for describing failures of bending in slabs and to some extent also shear in walls. Another example is beam elements which are based on Bernoulli's beam theory, suiting for bending failure. Most structural elements are not designed to describe transverse shear failure correctly.

If behavior of transverse shear failure is of interest, continuum elements which are also called solid elements fit well for the purpose. Moreover, continuum elements must be used in cases when detailed simulations are desired. Examples of such situations are investigation of bond-slip behavior or effects of reinforcement corrosion on surrounding concrete. A fundamental difference between structural and continuum elements is that structural elements yield results in terms of sectional forces and mo-

ments, while continuum elements yield results in form of stresses. In contrast to continuum elements which only have translational degrees of freedom, structural elements also have rotational degrees of freedom. This allows for bending and torsional moments to be calculated directly. Otherwise, integration of the stresses over the cross-sections is necessary to get the moments.

Models of reinforcement

Until here, only elements for concrete have been described. There are three different ways of introducing reinforcement into the model, Plos (2000). The first and simplest is embedded reinforcement, which means that the concrete elements that surround the reinforcement are strengthened in the reinforcement direction. Structural elements can only be combined with embedded reinforcement. With this method, no additional elements or degrees of freedom are required. Results from elements with embedded reinforcement are usually given as the sum of the concrete and reinforcement contributions. The drawback of this method is that no interaction such as bond-slip can be included. If interaction has to be included, the reinforcement can be described as two-dimensional bars, which are structural elements, in combination with continuum concrete elements. For even more detailed analyses, both concrete and reinforcement can be modeled with 3D solid elements. This is the most advanced and time consuming method and is only used for very detailed analyses.

Material models

To decide about the failure of materials, the response for multi-axial stress states must be investigated. There are different three-dimensional material models that define the failure in a material, such as Von Mises yield criterion for steel. To use such a material model in a non-linear FE analysis, it is usually sufficient to choose a uni-axial stress-strain relationship as an input and the software can then use that information together with predefined relations and parameters to define the three-dimensional material response.

Since concrete has different properties in tension and compression, stress-strain relationships have to be chosen for both cases. Here follows some examples of material idealizations for concrete and reinforcement steel, see Figure 22. Simple linear material models can be used for concrete in compression and reinforcement if serviceability behavior is to be investigated. Concrete tension must be sufficiently accurate if cracking has to be described. For failure, it might be necessary to use more sophisticated material models to capture the real non-linear behavior.

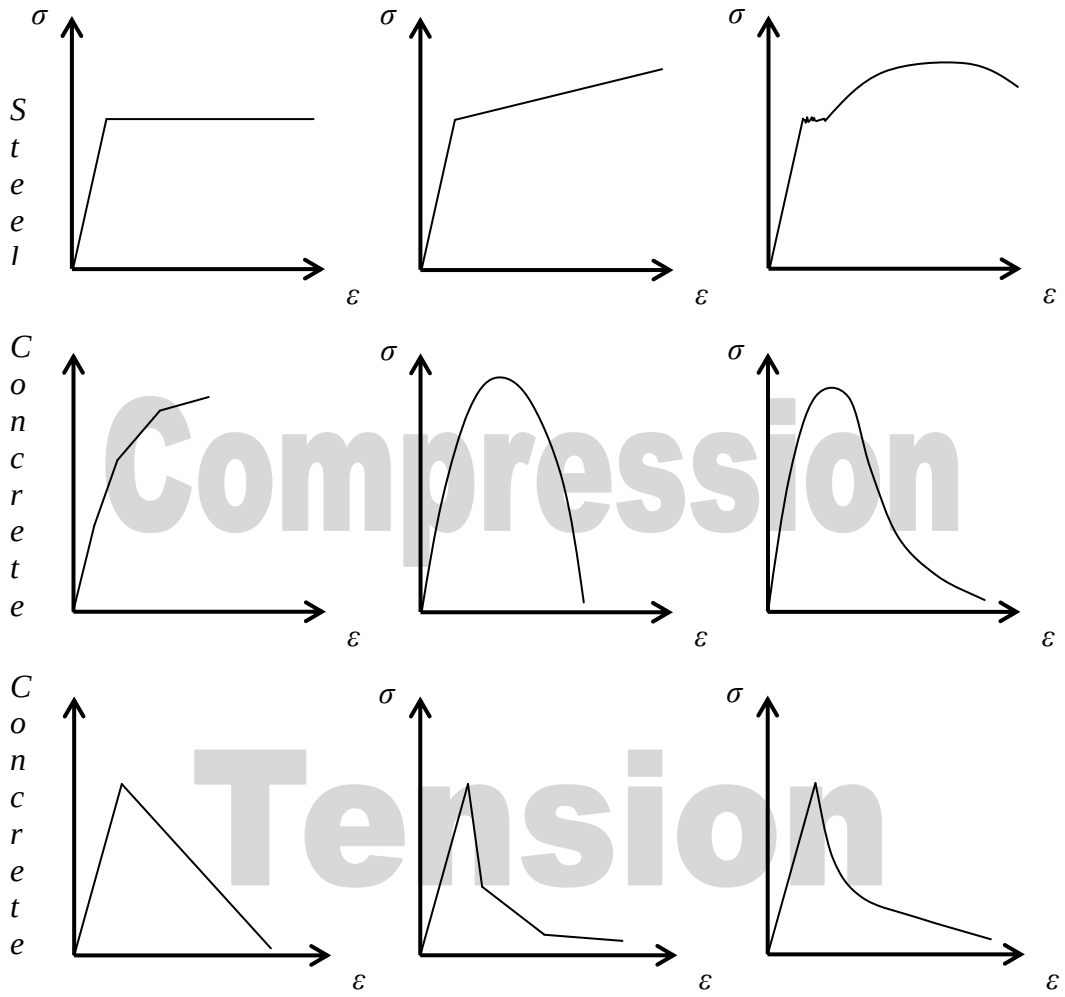

Figure 22. Stress-strain relations for steel and concrete. First row is for steel, second for concrete in compression and the last for concrete in tension. The level of accuracy increases to the right. The scales are not proportional. Adapted from lecture of Mario Plos.

In addition to the uni-axial material response, it is also necessary to describe concrete cracking. For this purpose, the concretes tensile behavior should be more carefully observed. To be able to show the principles of concrete cracking, a concrete specimen is illustrated in Figure 23. A characteristic feature of cracking in concrete under tension is that micro-cracks start to localize at a certain load level, point *a)*. For further load increase from point *a)*, the built-up strain will start to transform into crack openings. This means that for further elongation after point *a)*, the strains in-between the cracks will not increase, rather decrease as cracks form.

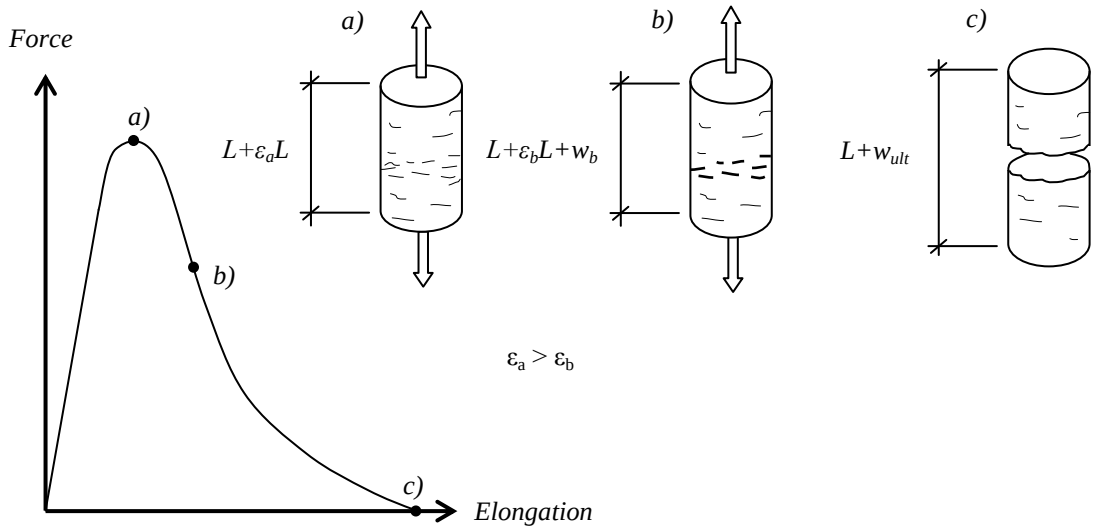

Figure 23. Tensile behavior of a plain concrete specimen. Adapted from Plos (2000).

The behavior and size of cracking cannot be described with strains alone. The length of the member is decisive. For elastic response, a longer specimen elongates more for the same amount of strain, than a shorter specimen. However, when a crack forms in the specimen, the material apart from the crack will unload and the elongation will turn into crack width. Thus, the longer specimen will get larger cracks for the same average strain in the specimen. This is the reason for why the cracking behavior must be described by a stress versus crack-opening relationship instead. The most important parameters that affect the fracture behavior are the tensile strength, the shape of the descending part of the graph and the area under the descending part, also referred to as the fracture energy. When modeling the concrete response in tension, two different curves are used, one stress-strain relationship for the un-cracked concrete and one stress versus crack-opening relationship for the cracked, see Figure 24.

Currently, there are three different approaches for modeling cracks with finite elements. They are called discrete, smeared and embedded crack approach. In the discrete crack approach, special purpose elements are used in places where cracks are expected. They can be non-linear springs and describe the cracks as localized entities, which is an advantage since it resembles the reality. A problem with this approach is the need of predicting the crack positions and directions. With smeared crack approach, cracks are represented as regions rather than individual units. The length of a cracked region is called crack band width. In this approach, it is assumed that a crack will localize within the crack band width and the deformation of the crack is smeared along that length. For plain concrete and for reinforced concrete with bond-slip, the crack band width should be set to one element length. For embedded reinforcement it should be set to the mean crack distance. With the smeared crack approach, the cracks can either be described with fixed/rotating cracks or with plasticity models. There are both benefits and drawbacks with these methods and a high competence is required for deciding which one to use. Embedded crack approach is the most advanced method of simulating cracks and it possesses all the advantages of the discrete

and smeared crack approach. However, it is not a wide spread method since commercial FE software have not implemented it yet.

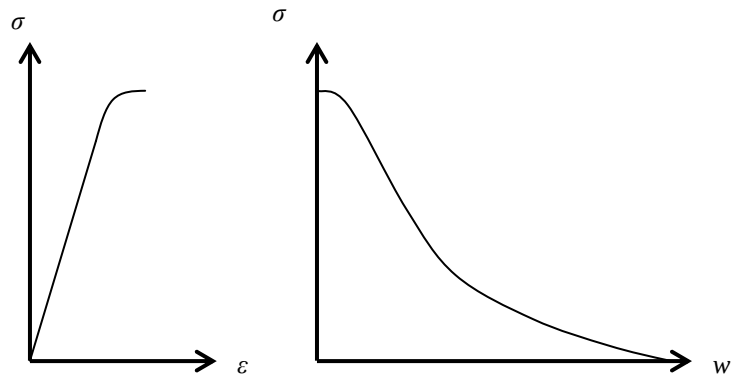

Figure 24. Stress-strain relation for un-cracked regions, to the left. Stress-crack opening for cracked regions within crack band width, to the right.

Boundary conditions

The results of a FE analysis are strongly dependent on the selected boundary conditions. Thus, it is important to make wise choices and strive to imitate the reality as accurately as possible. For instance, when a cantilever is designed, full rigidity is usually assumed for the fixed support. Depending on the surrounding structure or environment, such an assumption can be too strict since some degree of rotation might occur. Another typical situation is when designing flat slabs. The boundary conditions have to be different for a support column that is cast together with the slab and a steel column which acts more as a simple support. Also for these cases, an intermediate rigidity between fully fixed and simply supported boundary condition may be appropriate, depending on the purpose of the analysis.

4.1.2 Computation process

There are a number of important parameters that affect the computation process. Mesh density, element interpolation functions and integration schemes are some parameters that affect the accuracy of the solution. Furthermore, one must choose load-stepping method, iteration method and convergence criteria.

Mesh density

Before starting off with the analysis of the model, it must be verified that the numbers of elements or the density of the FE mesh is appropriate. A coarse mesh should be used for reduced computational demand if geometries and materials are homogenous. Where discontinuities are included, the stress flow in those regions will suddenly deviate from the rest of the structure. Therefore, the mesh must be denser to provide more accurate results. Such discontinuities can be sudden geometric deviations like a hole or a sharp corner in a slab. They can also be static discontinuities in form of concentrated loads. To ensure that the mesh gives correct results, a convergence study must always be performed. That means a gradual increase of numbers of elements until the results do not change significantly.

Element interpolation functions

In the most basic FE calculations, the results are obtained for nodes. To be able to represent the results outside a node, element interpolation functions are needed. When linear interpolation is used, the node results are averaged in between the nodes, i.e. the nodal values are weighed depending on the distance to the nodes from where the results should be represented. Linear interpolation functions are the least accurate ones but also require least amount of computation process. Higher order functions can be used if better accuracy is needed without increasing the number of elements in the FE mesh.

Integration schemes

When using quadrilateral finite elements, continuity problems can occur if the sides of the elements are not straight and parallel to the global coordinate axes. To overcome this, isoparametric mapping is required. This means that a quadrilateral element with arbitrary geometry can be represent in another coordinate system in such a way that a quadrat with parallel sides to that coordinate system is constructed. By doing so the problem of continuity is overcome, but the need of numerical integration arises, since the equations become too complex to calculate analytically, Ottosen and Petersson (1992). There are different methods for performing such integrations among which Gauss and Simpson integrations are commonly used methods. The results are now calculated in integration points instead of nodes and the position of the integration points can vary depending on method, not necessarily coinciding with the nodes. For a shell element, number of integration points can be chosen in the plane of the element and also over the height of the element in the thickness direction. The integration method together with the number of integration points compose the integration scheme, and highly affect the accuracy of the results.

Load stepping

The main difference of the computation process compared to a linear analysis is that in a non-linear analysis, the load is applied gradually on the model. This procedure is called load stepping or incrementation and allows for capturing the behavior for the whole loading history. After each step of load increase, the software searches for a solution that fulfills equilibrium. This requires two things. One is an iteration algorithm which tries different solutions until equilibrium is reached and the other is convergence criteria which sets a limit for and defines equilibrium.

The load stepping can be performed with three different methods. They are called load-controlled, displacement-controlled and arc-length incrementation. Which method that is the most appropriate depends on the behavior of the structure. When load-controlled incrementation is used, the actual load is increased and the program searches for a displacement field that corresponds to the applied load. The opposite process takes place when displacement-controlled incrementation is used. A certain node, or a set of nodes are displaced and the equilibrium is found by searching for the corresponding forces. One might ask why it is necessary to have anything else than load-controlled incrementations, since most problems in reality constitute application of loads on structures. This question is best answered with the help of a snap-through response, which is a special case of a very non-linear behavior, see Figure 25. The

disadvantage of the load-controlled incrementation in such a case is that a bifurcation point occurs. Bifurcation point is the point from which the next step will have multiple solutions to choose from. In reality, the state of equilibrium is the one which requires least potential energy to occur. Though, the software does not have the ability to perform such distinction. In a case with snap-through response, the displacement-controlled method will not encounter the same problem with bifurcation points.

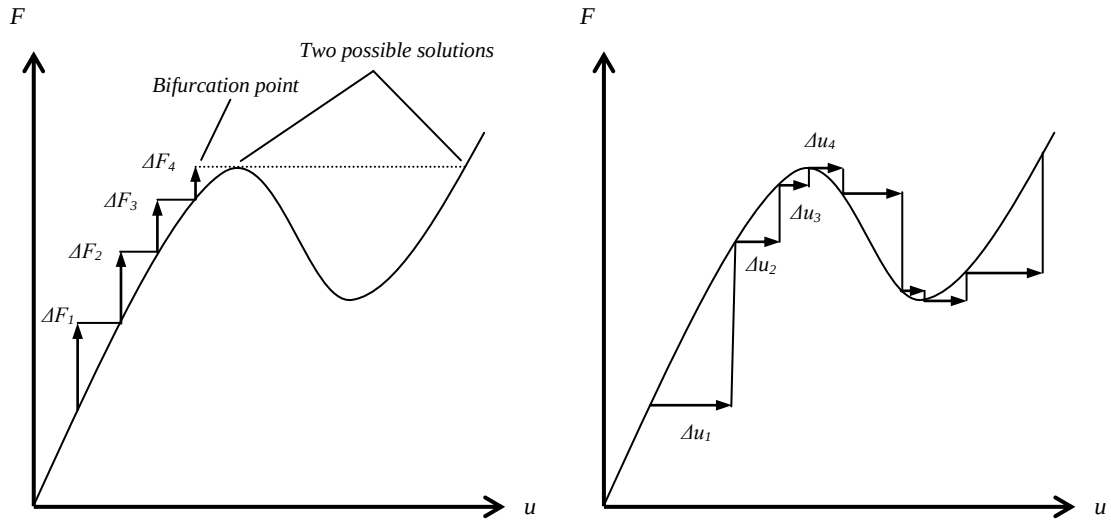

Figure 25. The difference between the load-controlled (left) and displacement-controlled methods (right) for a snap-through response.

A disadvantage of the displacement-controlled method is that the displacement of nodes can only represent concentrated loads on those nodes. Therefore, it can become troublesome when distributed loads are supposed to be modeled. Furthermore, the displacement-controlled method will encounter the same problem of bifurcation points for a snap-back response, see Figure 26.

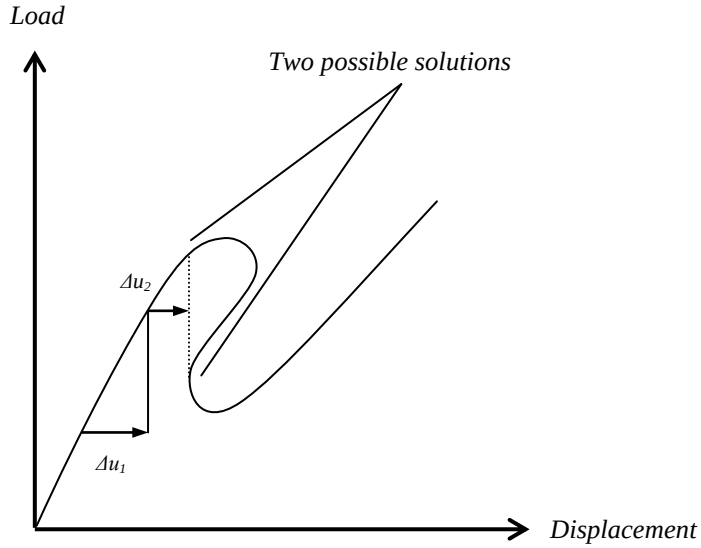

Figure 26. Bifurcation problem for the displacement-controlled method in combination with a snap-back response.

For such a case, the arc-length method must be used. This method is also referred to as a Riks analysis and the basics of it are shown in Figure 27. In few words, the goal is to find the intersection between the equilibrium path and a pre-defined arc, Bashir-Ahmed and Xiao-zu (2003). This way of finding the next solution makes this method advantageous for snap-back response.

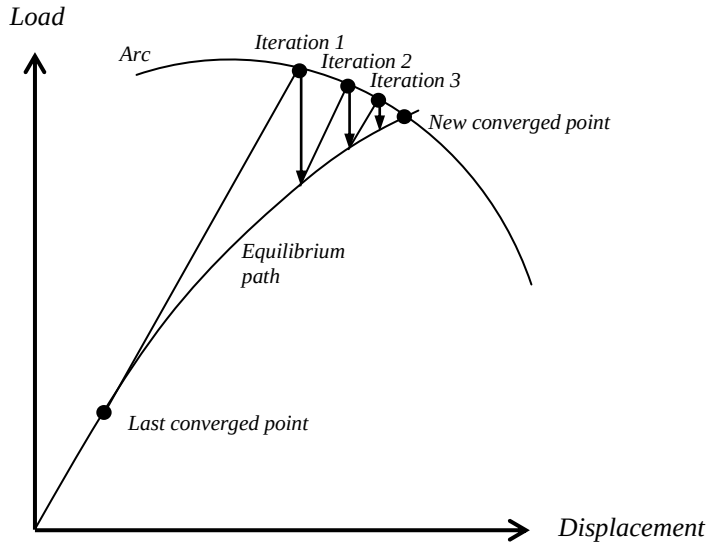

Figure 27. A principal illustration of the arc-length method. Adapted from Bashir-Ahmed and Xiao-zu (2003).

Iteration

The results of the iteration process are actually included in Figure 25 and Figure 26. It is the iteration method which finds the corresponding solution for each increment. That is the lines between the arrows. To achieve this, different numbers of iterations and computation capacity may be required depending on which iteration method that is used. Some common methods are Newton's method, modified Newton method and BFGS (Broyden–Fletcher–Goldfarb–Shanno) method.

Newton's method requires most computation capacity but least numbers of iterations. The reason is that the system matrix, which is the tangent stiffness, is updated for each iteration. Due to this fact, a better estimation is achieved and fewer repetitions required. The rate of convergence of this method is quadratic, Larsson (2010). The modified Newton method updates the system matrix once for each step, using the same stiffness matrix in all iterations. As a result, the rate of convergence becomes linear. The computations are less demanding but yield lower accuracy in each iteration, raising the numbers of iterations required as a consequence. The BFGS method is based on Newton's method but does not update the stiffness matrix in every iteration. Instead it uses information from the last converged step in order to make an approximation. BFGS method converges faster as it approaches the solution, giving a convergence rate in between linear and quadratic. This is one of the better methods when heavy models with many degrees of freedom have to be analyzed.

Convergence criteria

Since finite element method is an approximation, the analytical or exact solution will never be reached. Therefore a criterion is necessary to define equilibrium, and for each criterion, a tolerance is needed. The tolerance defines the accuracy by which the criterion is fulfilled. In the following cases, a value close to zero is needed for good approximation. A common way to express convergence is by stating that the out-of-balance force vector, which is the difference between internal and external forces in a system, approaches zero as the number of iterations goes towards infinity, see equation (26).

$$\mathbf{g} = \mathbf{f}_{int,i} - \mathbf{f}_{ext,i} \rightarrow \mathbf{0} \text{ as } i \rightarrow \infty \tag{26}$$

Other ways of expressing convergence can be with the ratio between the magnitude of the out-of-balance force vector in the current iteration and the first one in the increment, also called force norm, see equation (27).

$$\text{Force norm ratio } = \frac{\sqrt{\mathbf{g}_i^T \mathbf{g}_i}}{\sqrt{\mathbf{g}_0^T \mathbf{g}_0}} \tag{27}$$

Similarly, the displacement norm can be used, as the ratio between the magnitude of displacement in current iteration and the one performed in the beginning of the increment, see equation (28).

$$\text{Displacement norm ratio} = \frac{\sqrt{\delta\mathbf{u}_i^T \delta\mathbf{u}_i}}{\sqrt{\Delta\mathbf{u}_0^T \Delta\mathbf{u}_0}} \tag{28}$$

Alternatively, the energy norm ratio can be used. It is based on the internal energy, which is the area under the load-displacement curve. The criterion is the ratio between the internal energy in the current iteration and the internal energy form the first iteration in the increment, see equation (29). A description of the internal energy norm ratio is shown in Figure 28.

$$\text{Energy norm ratio } = \left| \frac{\delta\mathbf{u}_i^T (\mathbf{f}_{int,i+1} + \mathbf{f}_{int,i})}{\Delta\mathbf{u}_0^T (\mathbf{f}_{int,1} + \mathbf{f}_{int,0})} \right| = \frac{\delta E_1}{\Delta E_0} \tag{29}$$

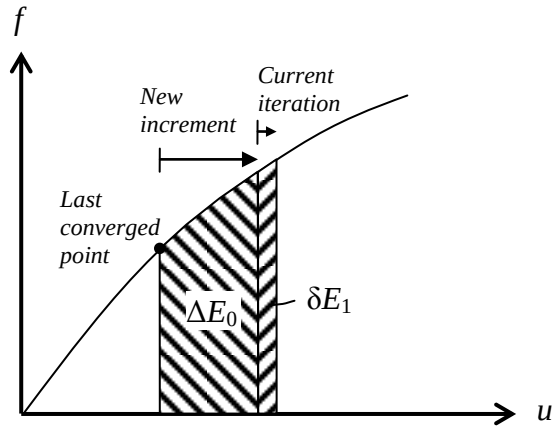

Figure 28. Internal energy from the first iteration of the increment ΔE_0, and the internal energy in the current iteration δE_1.

4.1.3 Post-processing

The stage of post-processing mainly involves evaluation of the results and verification of FE model and software. Evaluation mainly regards extraction and presentation of relevant results with graphs and tables for critical sections, without having to present results from the whole model. For heavy models with many degrees of freedom, presenting results for all nodes can be very time consuming and un-practical, not to mention un-necessary. Nevertheless, results can be presented graphically with contour plots to give an illustration of the over-all behavior. A suiting method to present the structural response is with a graph of the load-displacement relation, which preferably should always be included.

Verification of the FE model can be done by investigating whether some basic results are reasonable or not. A comparison of the maximum deflection can be made with a linear case, where the results from the non-linear analysis should have given larger deflections if cracking has occurred. Alternatively, a more accurate and complicated non-linear hand-calculation can be made for simpler structures, based on the curvature distribution, to achieve a more realistic deflection. Furthermore, equilibrium can be checked by comparing the reaction forces with the applied loads. To verify the FE software, it might be necessary to more thoroughly investigate the background of the calculations to detect possible errors.

For the ultimate limit state, results can give information about the ultimate load carrying capacity and the mode of failure. Safety aspects should be considered such as variation of material properties and loads, when deciding the load carrying capacities. For serviceability limit state, deformation, stress redistribution, crack widths and material stresses/strains can be found.

4.2 Bridge deck cantilever

The redistribution of shear flow after flexural cracking was simulated for a bridge deck cantilever subjected to four concentrated wheel loads, similar to the test DR1a, performed by Vaz Rodrigues *et al*. (2006), see section 3.2. Results of interest are mainly the change of shear flow distribution along a control section for successive load increase with effects from events such as cracking, stress redistributions, yielding in flexural reinforcement and plastic redistributions.

The main reason for choosing to model the DR1a load configuration was that the capacity of this test came closest to the theoretical flexural capacity. With the type of non-linear analysis performed, only flexural behavior and failure can be simulated. Thus, it will be possible to follow the behavior of test DR1a farthest, before the behaviors stop to agree. In addition, DR1a was the only test where the reinforcement started to yield, which is of interest for the redistribution of the shear flow.

4.2.1 Finite Element model

The software used to perform the FE analyses is Midas FX+ *v.3.1.0* for pre-processing and TNO Diana *v.9.4.4* for computation and post-processing. The cantilever was modeled with a length of 2,78 m, from the support edge to the free end, and a length of 10,0 m along the support, see Figure 19. The thickness varied from 380 mm at the support to 190 mm at the free end and the system line of the slab was placed in the mid-plane of the thickness. Since structural elements work well for describing bending and thus also flexural cracking, shell elements were chosen for this analysis.

It was detected that the FE software produced incorrect results of shear forces when continuously varying shell thickness was used. Also, using reinforcements that were inclined in relation to the system line of the concrete, lead to incorrect results. The reason is that when shell elements with continuously varying thickness are used in this software, the results are calculated based on the local coordinate system of each integration point. Besides the coordinate systems of the integration points in the level of the system line, all other local coordinate systems are inclined in relation to the global coordinate system. This leads to an underestimation of the shear forces since only the normal components of the shear forces will be included instead of the vertical component, see Figure 29.

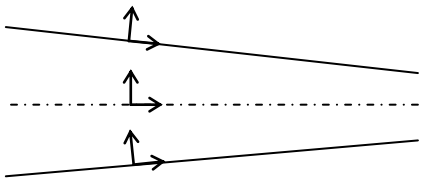

Figure 29. Continuously varying shell thickness results in integration points with local coordinate axes that deviate from the global one.

When reinforcement that is inclined in relation to the shell elements is used, the stress in the longitudinal direction of the reinforcement will get two components, one vertical and one horizontal. The vertical component will help carry some of the shear force. However, this was not included in the calculated shear force. Therefore, the

software presents lower values for the shear, representing the concretes contribution only.

To come around these problems, the concrete was modeled as 14 separate longitudinal segments, each having its own, constant thickness and the top and bottom reinforcement parallel to the system line, see Figure 30. With this solution, both problems are solved.

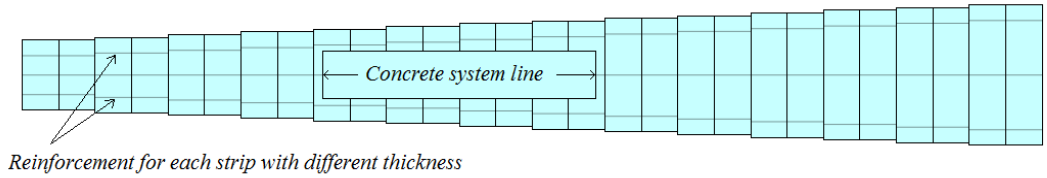

Figure 30. Division of the slab into longitudinal strips with different thicknesses.

Reinforcement layout

The reinforcement layout that had to be modeled consists of 12 mm bars with a spacing of 150 mm in both directions in the bottom, and in longitudinal direction in the top. The reinforcement in transversal direction in the top consists of 16 mm bars with a spacing of 75 mm, where every second bar is curtailed, see Figure 31.

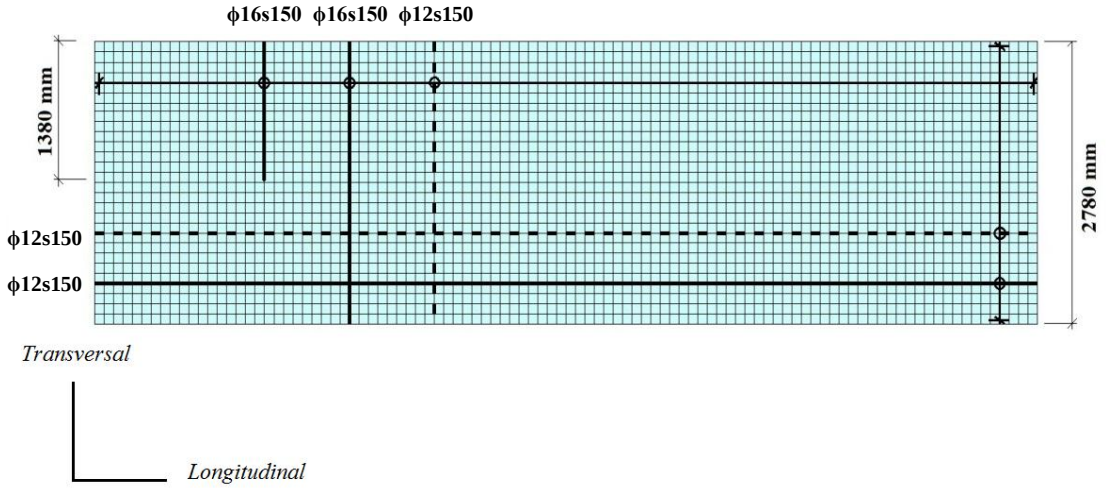

Figure 31. Flexural reinforcement layout in FE model.

The reinforcement was modeled as embedded with planes of reinforcement grids, each representing reinforcement in both x- and y-direction.

Boundary conditions

The slab was modeled with two different boundary conditions, one fully fixed at the support edge and one modeling the real support geometry, taking into account the flexibility of the support more realistically. This was done to investigate the differences in behavior and to make a comparison between the load-displacement curves from the FE models and the real test. The support conditions of the tested slab can be seen in Figure 32.

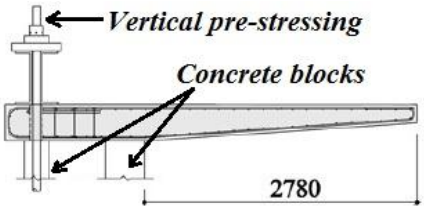

Figure 32. Support conditions of the laboratory testing. Adapted from Vaz Rodrigues et al. (2008).

In figure Figure 33, the modelled boundary condition is shown for the case where all degrees of freedom along the supporting edge were restrained. The result of the analysis is compared to the real test, by means of load-displacement curves.

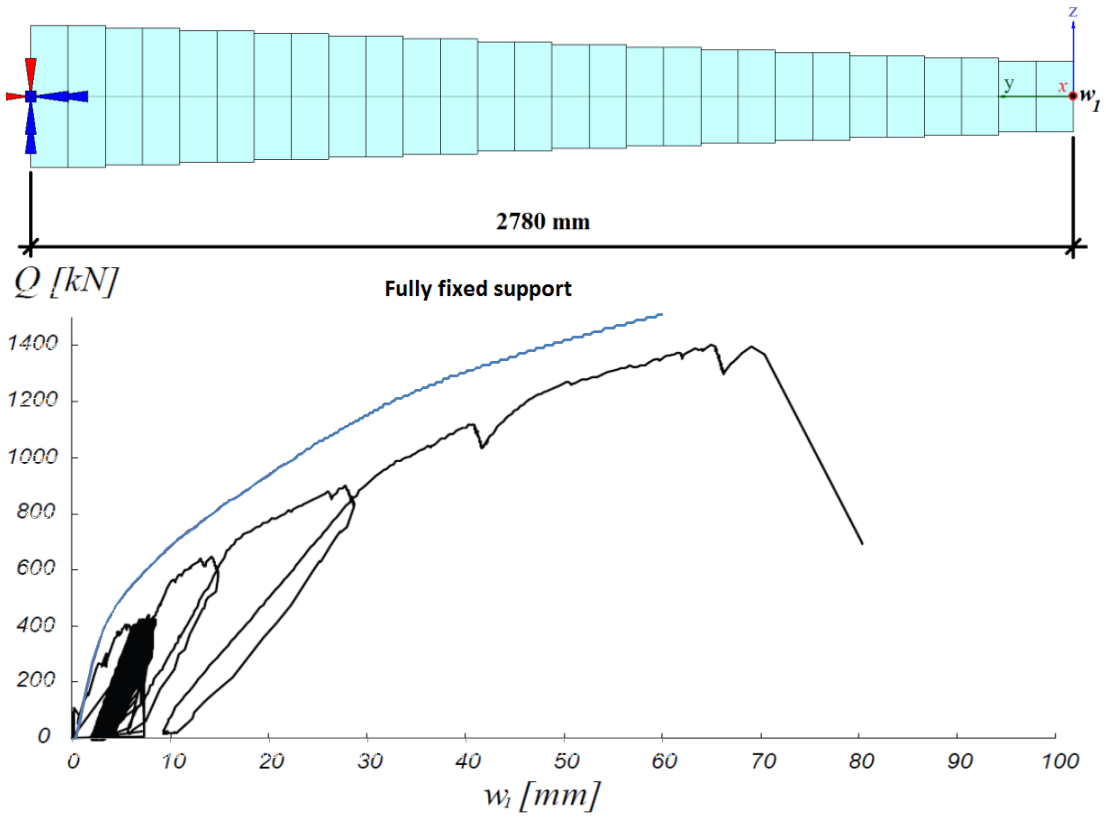

Figure 33. Illustration of the modeled support and load-displacement results compared to the real measurements, for fixed boundary conditions. Displacements are taken from a point in the middle of the slabs length, at the tip of the free end. Adapted from Vaz Rodrigues (2007).

It is important to mention that the slab was initially subjected to cyclic loading, and was also un-loaded several times at higher load levels. To some extent, this resulted in larger deformations. It was observed that the FE model had a considerably more stiff response than the test, certainly due to the unrealistic boundary conditions.

In the next model, the additional part of the slab apart from the cantilever was included in order to model the flexibility more correctly, see Figure 34. The supporting concrete blocks were modeled as non-linear springs, representing the stiffness of the concrete in compression and having very low stiffness in tension to allow uplifting where it occurs. The ends of the springs were prescribed for translation in all directions. The region where the pre-stressing bars were present was modeled by prescribing translations in z and y-directions.

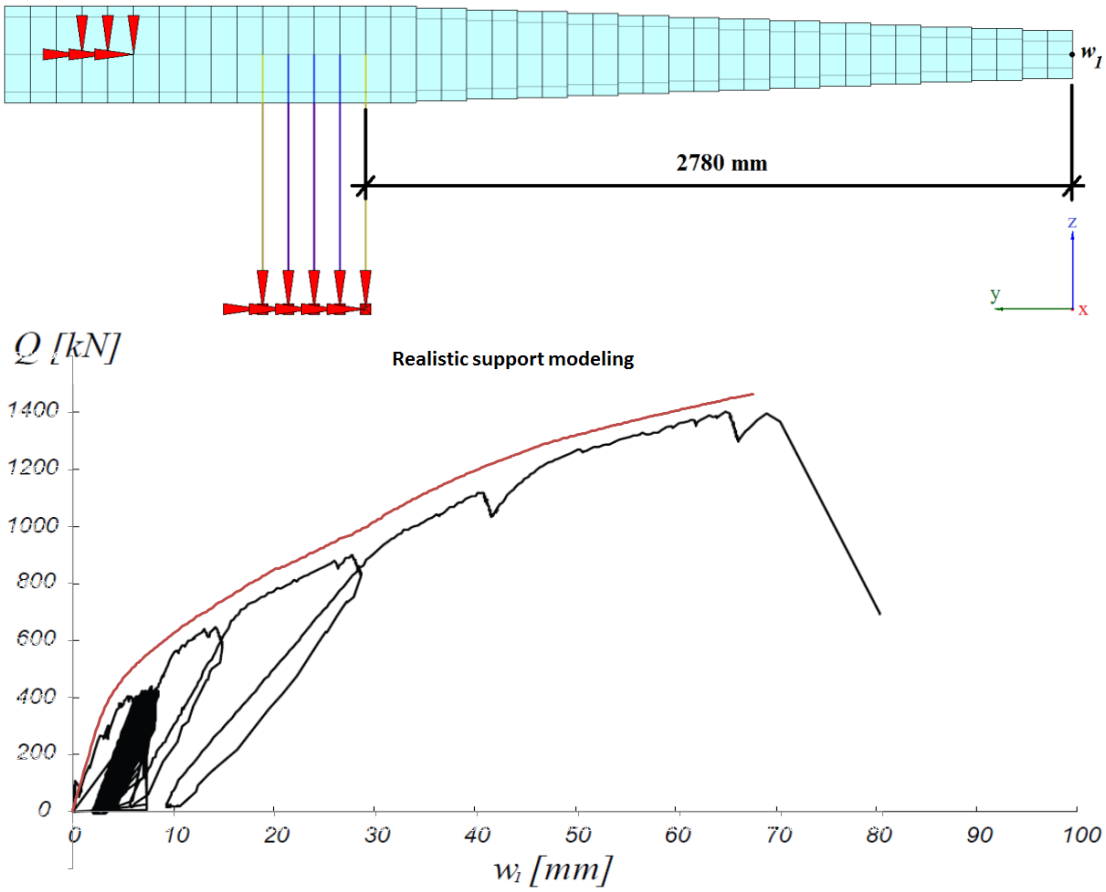

Figure 34. Illustration of the modeled support and load-displacement results compared to the real measurements, for realistic boundary conditions. Displacements are taken from a point in the middle of the slabs length, at the tip of the free end. Adapted from Vaz Rodrigues (2007).

This way of modeling the support resulted in a more realistic load-displacement curve and was chosen for further analyses. Since the slab could not fail in shear in the FE analysis, as the case was for the tested slab in the laboratory, all FE results beyond the real load-bearing capacity were disregarded.

Loads

The self-weight was modeled as gravity to properly account for the variation of thickness. This load was determined based on the acceleration of 9,82 m/s^2 and the density of 2500 kg/m^3 for concrete, including the weight of the reinforcement. The concentrated loads were modeled using prescribed displacement in order to appropriately capture the snap-through response of structural concrete. To model the distribution of the wheel loads, acting on an area of 0,4 x 0,4 m, nine nodes were displaced gradually at the same time and with the same load magnitude on each node, see the left part of Figure 35. The eligibility of this somewhat simplified load modeling was investigated and compared to a more accurate modeling. It was shown that the results did not deviate significantly, see Appendix A.

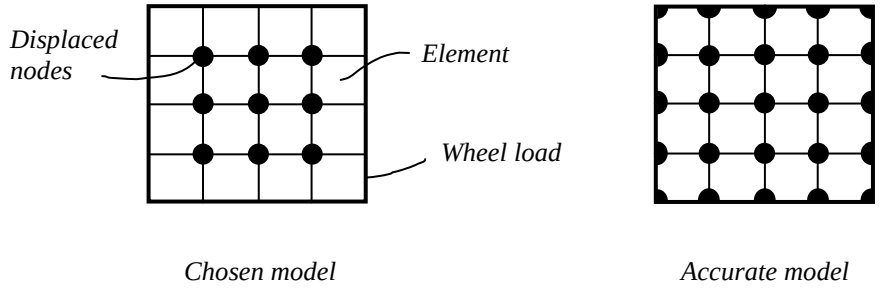

Figure 35. Displaced nodes to represent a 0,4 x 0,4 m wheel load (left). Alternative accurate load modeling (right).

In order to displace several nodes simultaneously, with equal load on each node, a loading sub-structure is necessary for each wheel load, see Figure 36. The loading sub-structures were modeled with very stiff beams (corresponding to steel with cross-sectional areas of 1 x 1 m^2), constructed to be statically determinate. The stiff beams were connected with tying elements, dashed lines in Figure 36, which only have one degree of freedom at each node, the translation in z-direction. This makes it possible to give any desired shape to the loading sub-structure. As long as the ties are assigned to correct nodes on the concrete deck, the displacement of the concrete nodes will be equal to the displacement of each corresponding tie node.

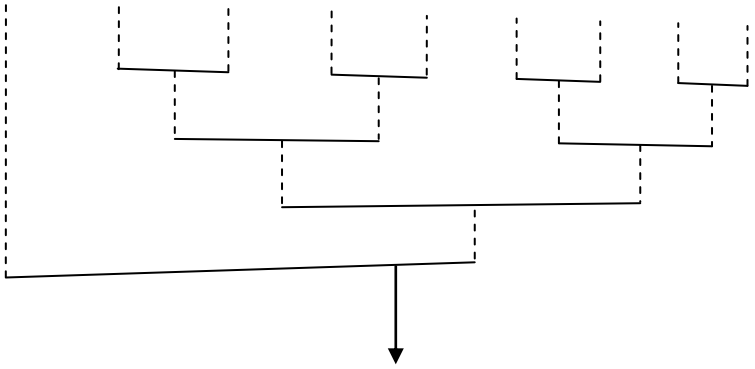

Figure 36. Loading sub-structure for displacement of nodes. Solid lines are beams and dashed lines are ties.

The loading sub-structures for each wheel load were then connected to form a large loading structure, see Figure 37. The boundary conditions on the loading structure are prescribed translation in y-direction for all nodes, prescribed rotation around the x and z-axes for all nodes and prescribed translation in x-direction for one end-node on each beam element. To combine the distributed loading for the self-weight with the displacement-controlled wheel load, a spring was used with negligible stiffness (1000 N/m) in compression and "infinite" stiffness ($10^{\wedge 10}$ N/m) in tension (for the case where the load is pulled from below as in Figure 37). The reason to have this non-linear spring is that the node which is displaced needs to be modeled as a support in the FE software Diana. Thus, when the self-weight is applied, the loading structure would prevent the concrete deck from moving down, if this spring was not used.

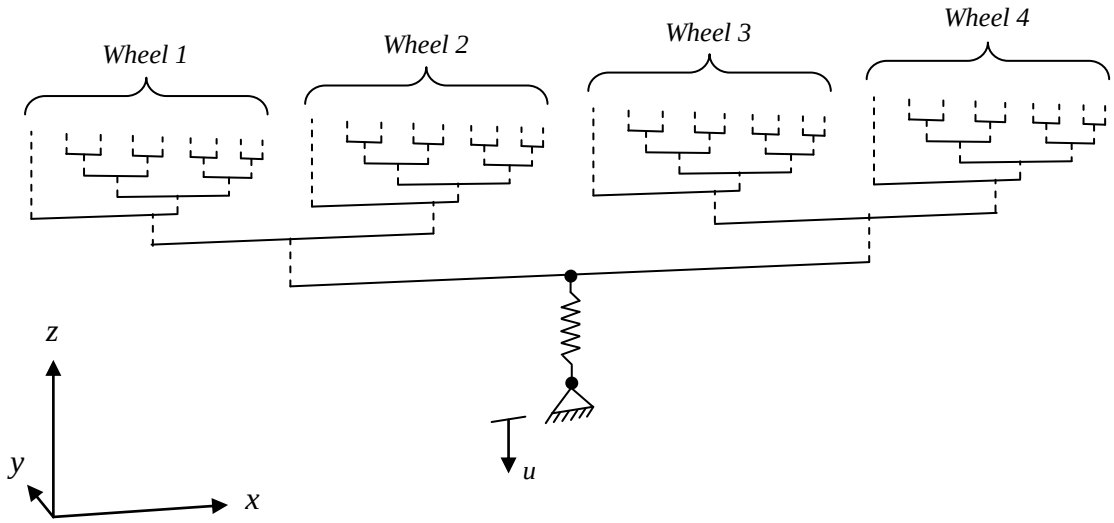

Figure 37. Loading structure for all wheel loads.

Finite element mesh

Quadrilateral curved shell elements of size 0,1 x 0,1 m were used with linear element interpolation functions. Gauss integration was used in the plane of the elements with 2 x 2 integration points. In the thickness direction, Simpson integration with nine integration points was used, resulting in total 2 x 2 x 9 = 36 integration points per element.

A convergence study was carried out where the number of elements was increased from 2800 to 4375 for a linear elastic analysis and only for the self-weight. The out-comes were not significantly different compared to the coarser mesh so the model with 2800 elements was considered to have converged, see Appendix B.

4.2.2 Material models

Concrete

For the cracking, the material model used for concrete was based on the smeared crack approach with a rotating crack model. The material properties were chosen to match the concrete in the tested cantilever, see section 3.2. In Vaz Rodrigues *et al.* (2006), the measured compressive strength, f_{cc}, and Young's modulus, E_c, were given. The tensile strength was chosen for a C40/50 concrete, since it matches the compressive strength. The fracture energy G_f, was set to 90 Nm/m^2 according to Model code 90 (1993), for the given concrete strength and the aggregate size used, 16 mm. The crack band width was set to 88 mm, which is equal to the calculated mean crack distance, see Appendix C. The properties of the concrete modeled in the FE analysis are presented in Table 2 below.

Table 2. Material properties of modeled concreted.

Tension model	Compression model	f_{cc} [MPa]	f_{ct} [MPa]	E_c [GPa]	ν [-]	ρ [kg/m^3]
According to Hordijk (1991)	According to Thorenfeldt *et al.* (1987)	40	3	36	0,2	2500

The uni-axial stress-strain relation in tension was chosen according to Hordijk (1991). The uni-axial response in compression was chosen according to Thorenfeldt *et al.* (1987). The chosen models are illustrated schematically in Figure 38.

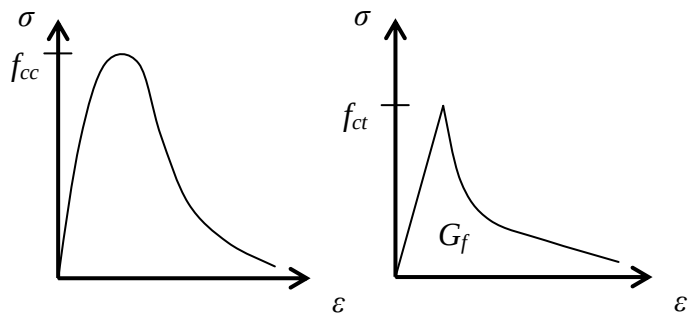

Figure 38. Compression model to the left and tension model to the right.

Reinforcement

All reinforcement was assigned the same yield strength of 515 MPa, Young's modulus 200 GPa and an elastic-ideally plastic uni-axial response, see Figure 39. The three-dimensional yield criterion is chosen according to Von Mises.

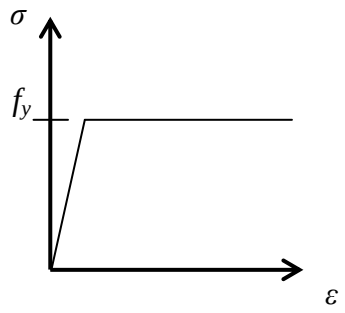

Figure 39. Elastic-ideally plastic stress-strain relationship for reinforcement.

4.2.3 Computation

As mentioned before, displacement-controlled load stepping was performed when the wheel loads were applied, and successively increased. However, for the self-weight, a gravity force was applied. The load application of the self-weight was made in 10 steps. By the time that the complete self-weight had been applied, the spring was compressed by a certain amount. The goal was then to displace the spring to its original, un-stressed state with as few steps as possible. The default displacement per step was set to 0,025 mm. Though, it was possible to multiply that displacement with different factors to enable the ability to customize each step size to the desired magnitude. The first displacement of the spring was made by 0,25 mm (10*0,025) to try to reach its un-loaded length quickly. After this step, the spring was still compressed but very close to its un-stressed length. The ten upcoming steps had a factor of 1 (0,025mm / step). This is because convergence difficulties can occur if the step size is too large at the transition from compression to tension, since the stiffness changes abruptly. After this, when the spring was tensioned, the rest of the load (step 12 and beyond) was applied with a displacement of 0,125 mm per step, a factor of 5.

The iteration method, BFGS, was chosen with the option of starting with the tangential stiffness in the beginning of each step. Two convergence criteria were chosen, using force and displacement norm, respectively. Both must be fulfilled in order to gain convergence. The tolerance was set to 0,001 for both criteria.

5 Results

In this chapter, the achieved results will be presented by firstly presenting the overall results for the purpose of validation and evaluation of the reasonability of the model. Afterwards the results of interest for the aim of this thesis will be presented, specifically the shear redistribution.

5.1 Overall results

The layout of the whole model can be seen in Figure 40. As was shown in part 4.2.1, the way of modeling the support conditions indicated in the figure resulted in a behavior that resembles the real slabs response in the best way.

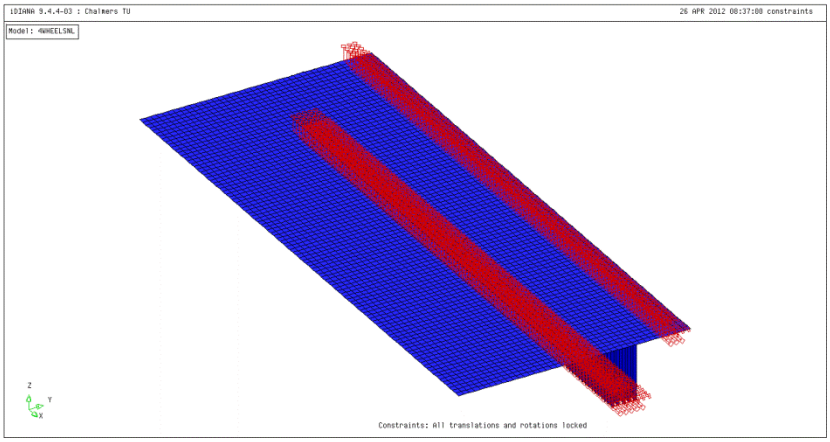

Figure 40. The layout of the un-deformed model with support and boundary conditions indicated.

The deformed shape after application of full self-weight is illustrated in Figure 41 and Figure 42.

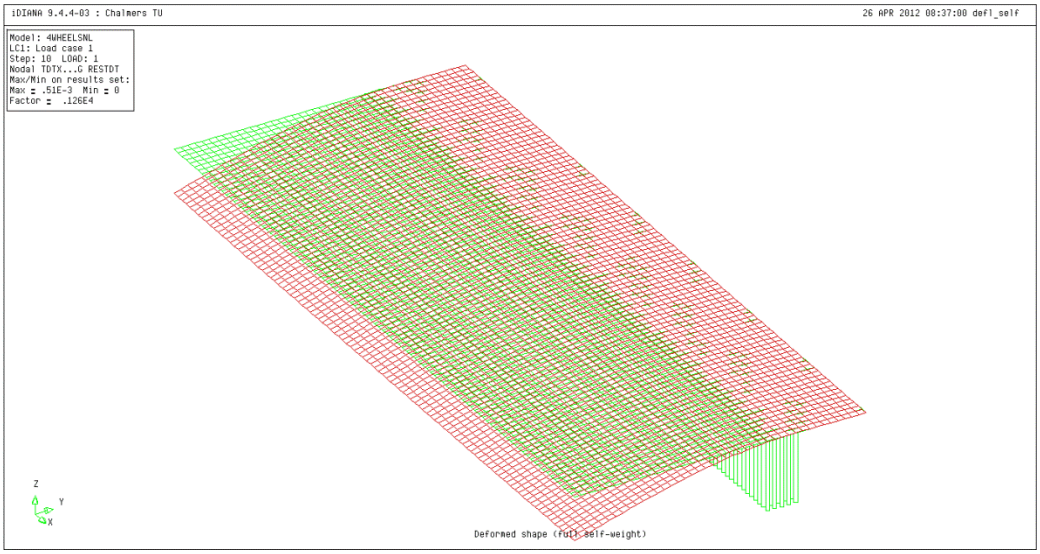

Figure 41. Deformation due to self-weight, in perspective view.

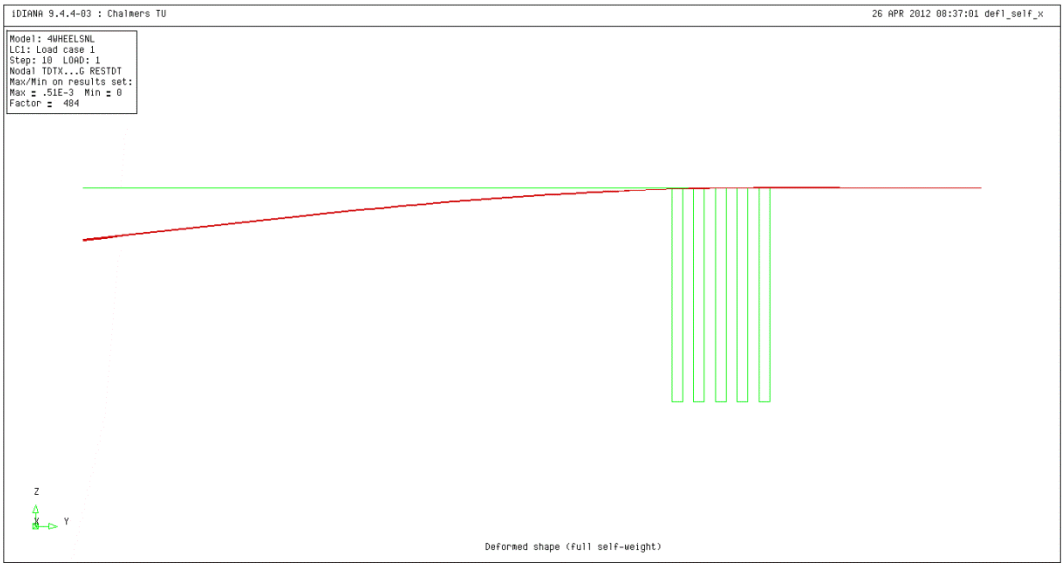

Figure 42. Deformation due to self-weight, view in x-direction.

The positions of the wheel loads and the deformations caused by application of the wheel loads can be seen in Figure 43 and Figure 44. The distances between the wheel loads do not agree fully with the actual distances from the testings (900 and 1440 mm respectively). Due to that the loads were modeled acting in nodes, their positions must be adjusted to the FE mesh.

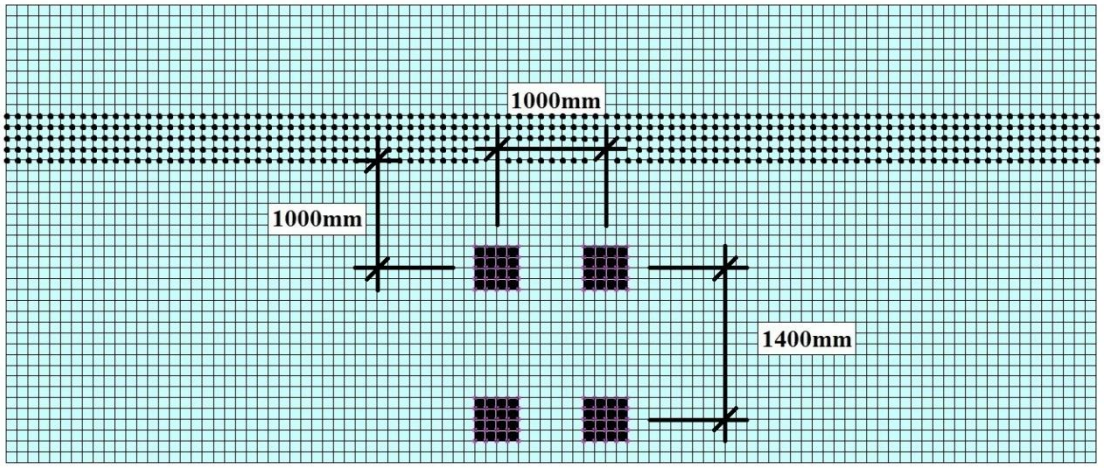

Figure 43. Positions of the wheel loads, placed centrically along the length of the slab. Dotted nodes represent support springs.

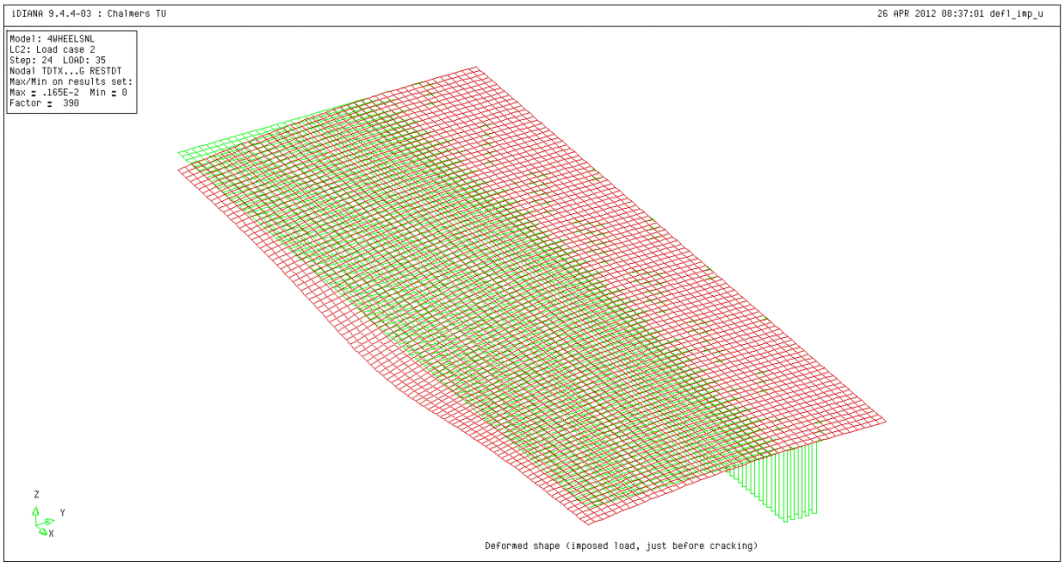

Figure 44. Deformation due to application of wheel loads, in perspective view.

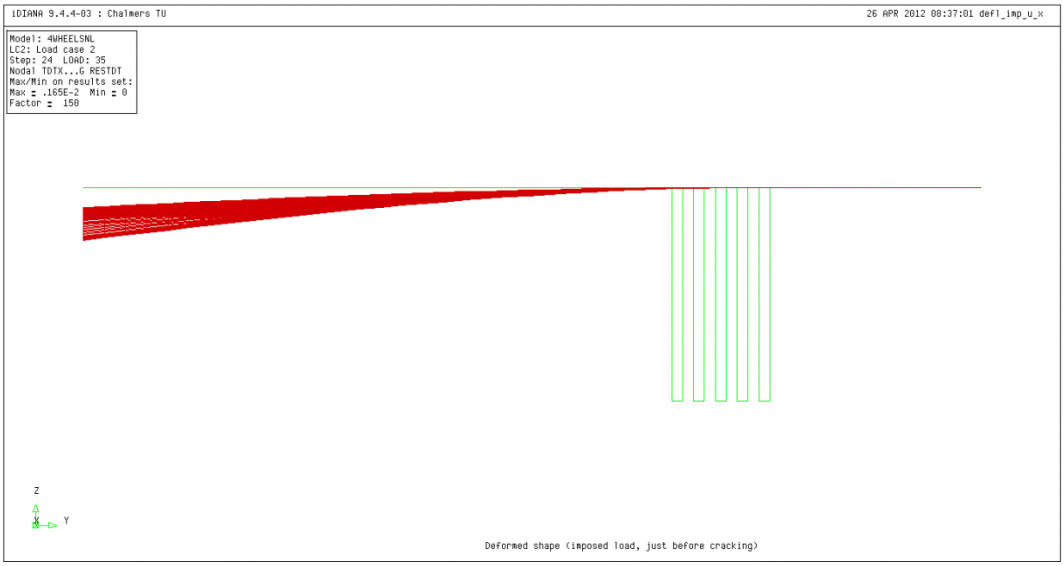

Figure 45. Deformation due to application of wheel loads, view in x-direction.

A graph, describing the reaction force in the loading spring on the y-axis, and a load factor on the x-axis, is shown in Figure 46. The load factor (l.f) should be multiplied with the default displacement of 0,025 mm, to achieve the total displacement of the spring. As was shown in Figure 37, the reaction force represents the total load, i.e. the sum of all wheel loads.

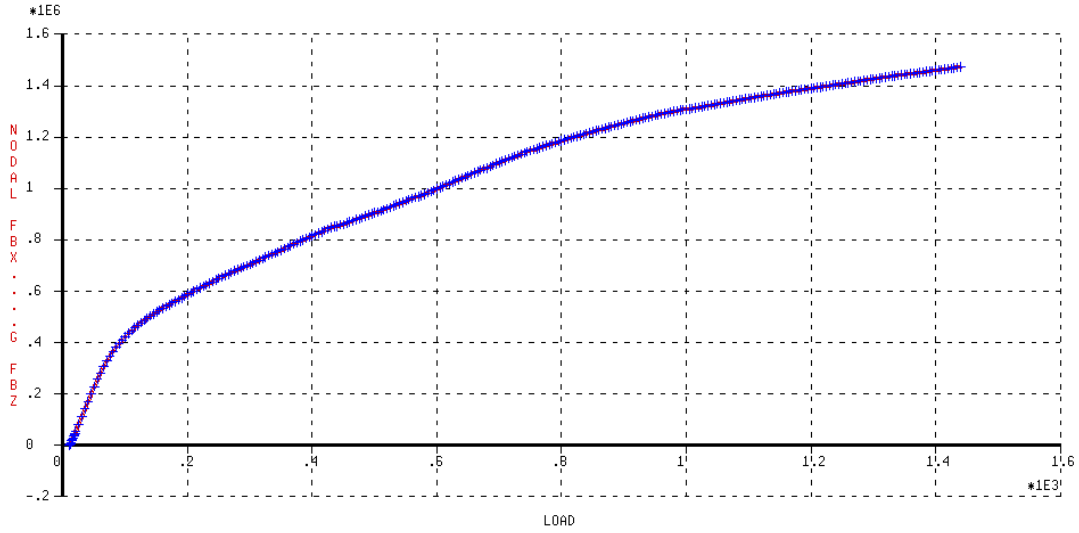

Figure 46. Load-displacement curve for the spring node.

In order to make a comparison to the tested slab, the load-displacement curve above was modified to show the displacement of a node at the free end, along the middle of the cantilevers length, since that was the point measured in the testing, see Figure 47.

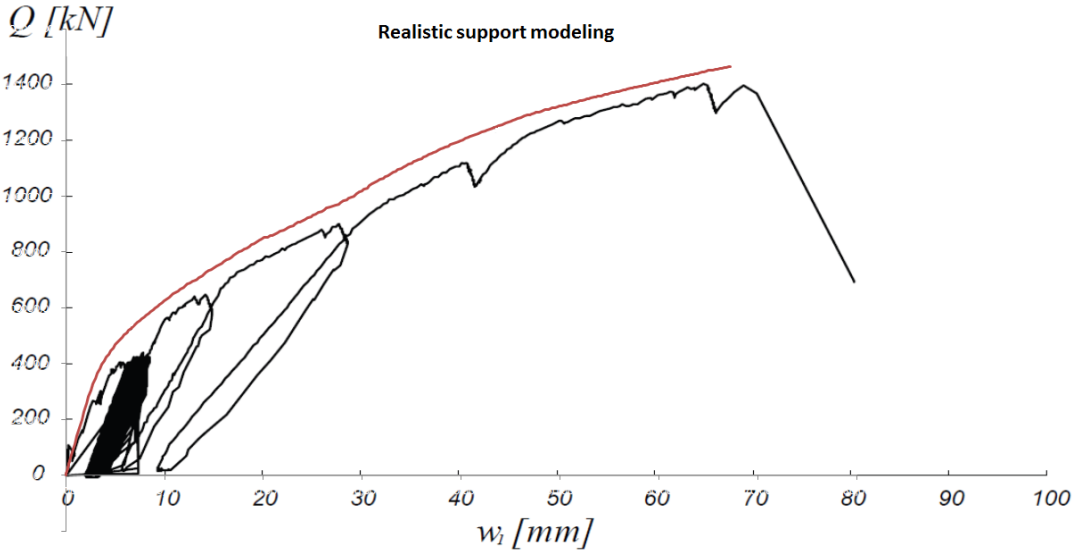

Figure 47. Load-displacement curve of a node at the free end, placed in the middle of the length of the slab. Adapted from Vaz Rodrigues (2007).

5.1.1 Critical events

The first cracks occurred at a total load of Q = 172 kN. They occurred close to the supporting springs, in the middle of the length of the slab. Yielding in the top transversal reinforcement was the next major event and occurred at a load of Q = 1115 kN. The position of the first yielding in the top transversal reinforcement was in the same place as the first cracks that occurred. Plastic redistribution occurred in the top transversal reinforcement close to, and along the support. The bottom longitudinal reinforcement started to yield at a load of Q = 1284 kN.

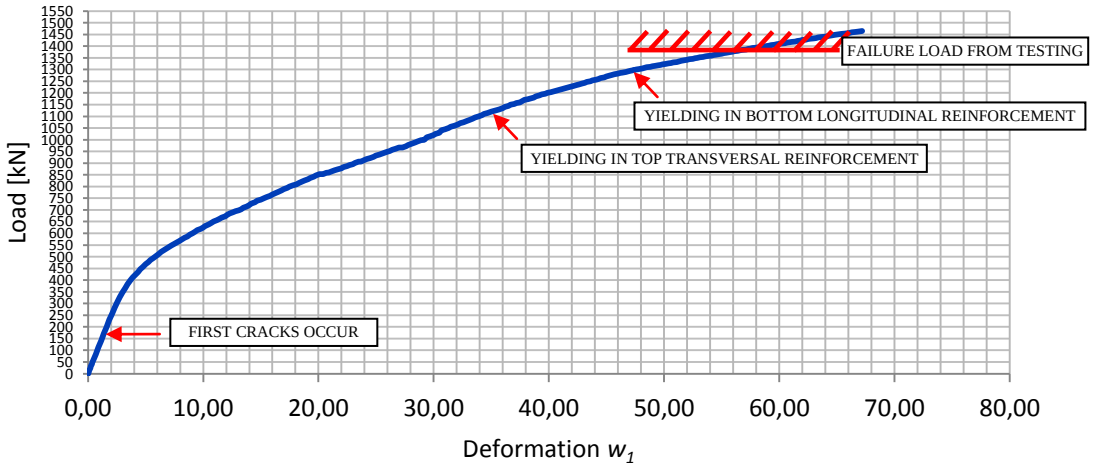

Figure 48. Critical events shown in the load-deformation curve.

5.1.2 Crack development

In the following, the development of cracks in the top and bottom surfaces is illustrated, see Figure 51 to Figure 57. It can be seen that the FE model achieved a crack pattern that is similar to the mechanism which can be expected with the yield-line method, see Figure 49.

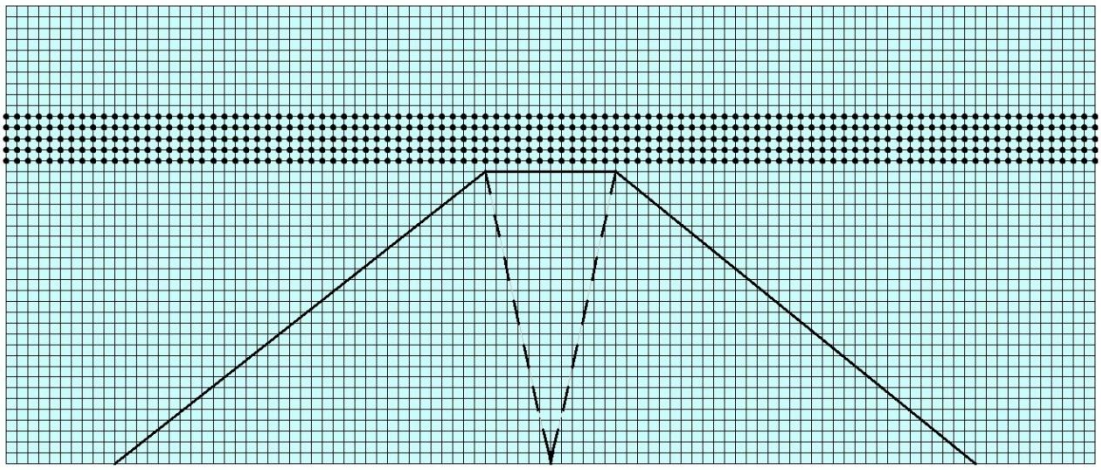

Figure 49. Schematic illustration of the expected mechanism with the yield-line method. Solid lines represent yield-lines for the top surface and dashed lines for the bottom surface.

The steps from which the contour plots for the top strains were extracted are put into the load-displacement diagram to relate to the global behavior, see Figure 50. For the contour plots for the bottom strains and the shear forces, other steps have been used, but they are not shown in the figure below. The step numbers vary proportionally along the displacement axis (all steps above 20) making it possible to interpolate between the indicated values.

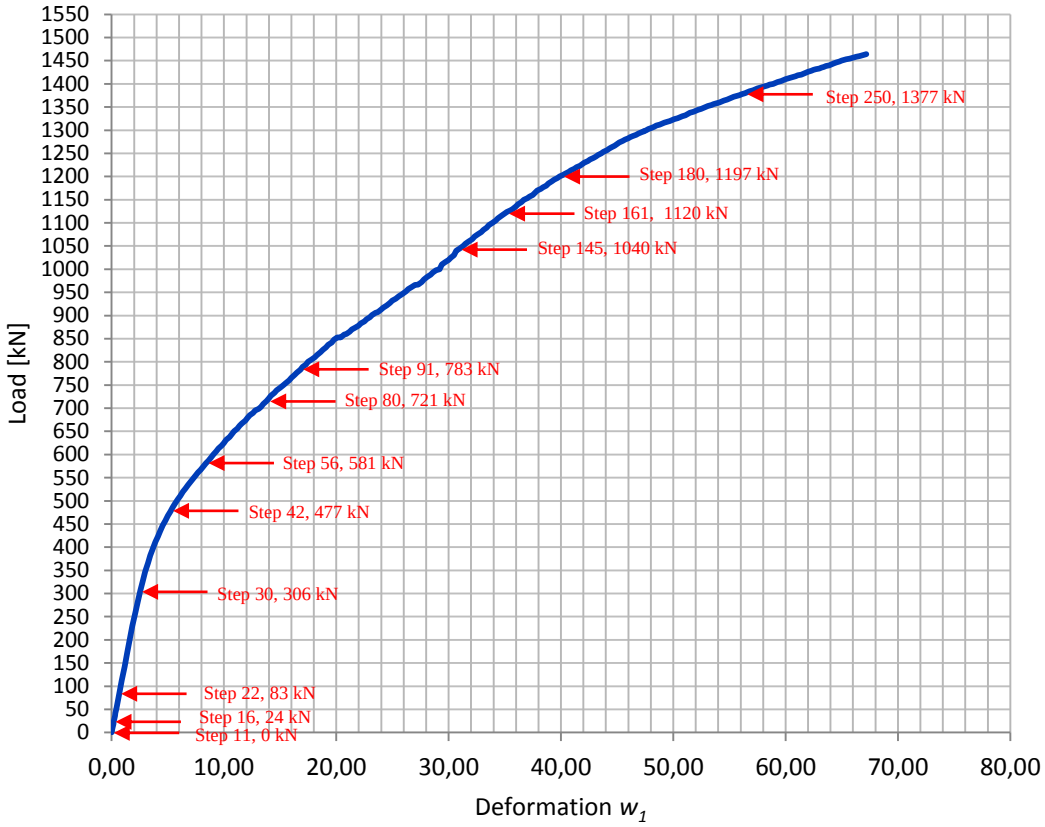

Figure 50. The steps for which the top tensile strains are presented, put into the load-displacement curve.

In the following figures, the development of the principal tensile strains at the top surface is shown, see Figure 51 to Figure 54. Concentrations of strain can be interpreted as cracked regions. In between step 22 and 30, significant strain concentrations occurred at the middle part of the support due to cracking, and it continued to spread with an angle of about 45° degrees towards the free end. A second line of strain concentration parallel to the support could be seen in the middle of the slab in step 145. It occurred at the position where half of the top reinforcement was curtailed. The concentration of strains in step 250 shows that the cracks near the support grew much larger than the rest of the cracks. This confirms that the yielding of the top reinforcement mainly occurred here.

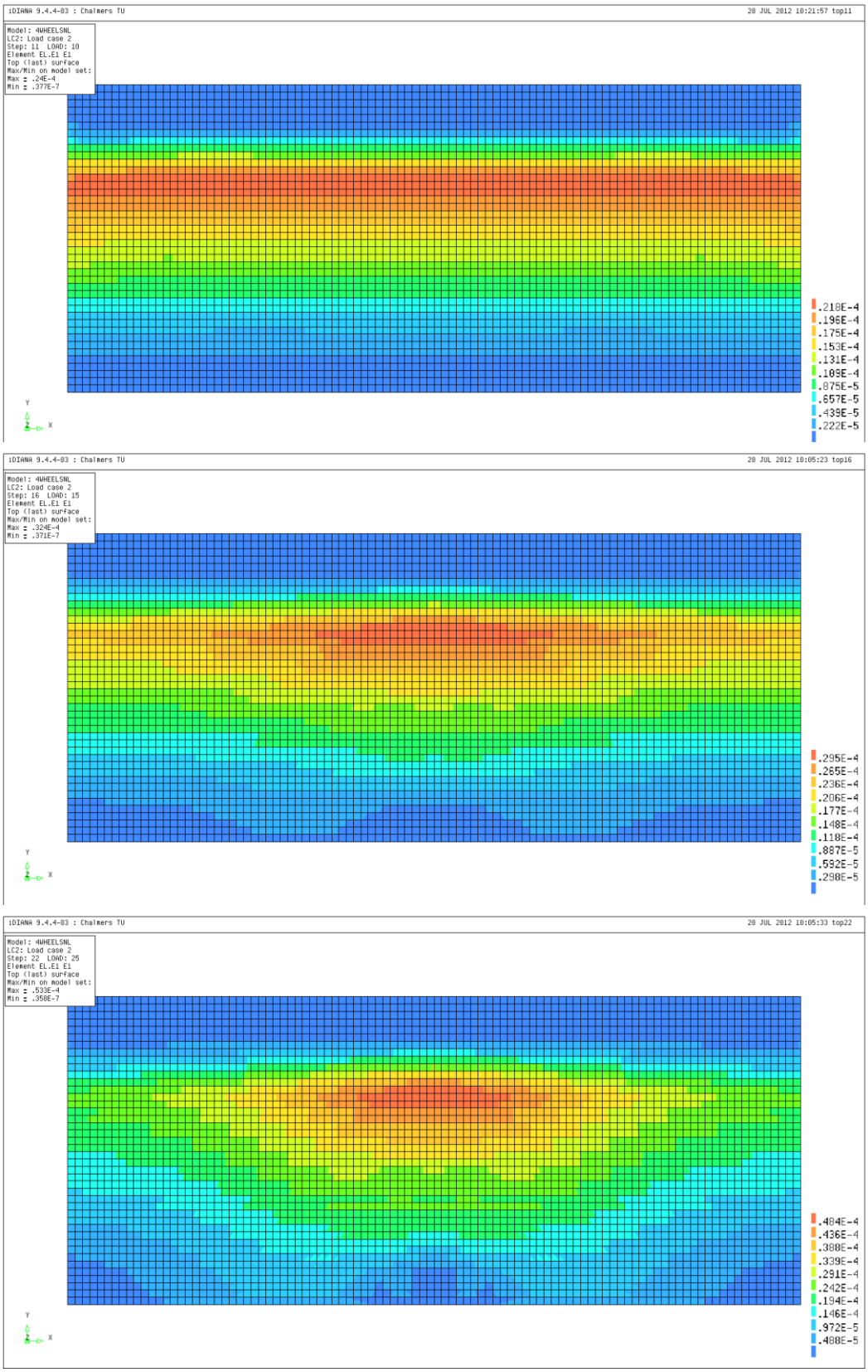

Figure 51. Top tensile strains for steps 11, 16 and 22.

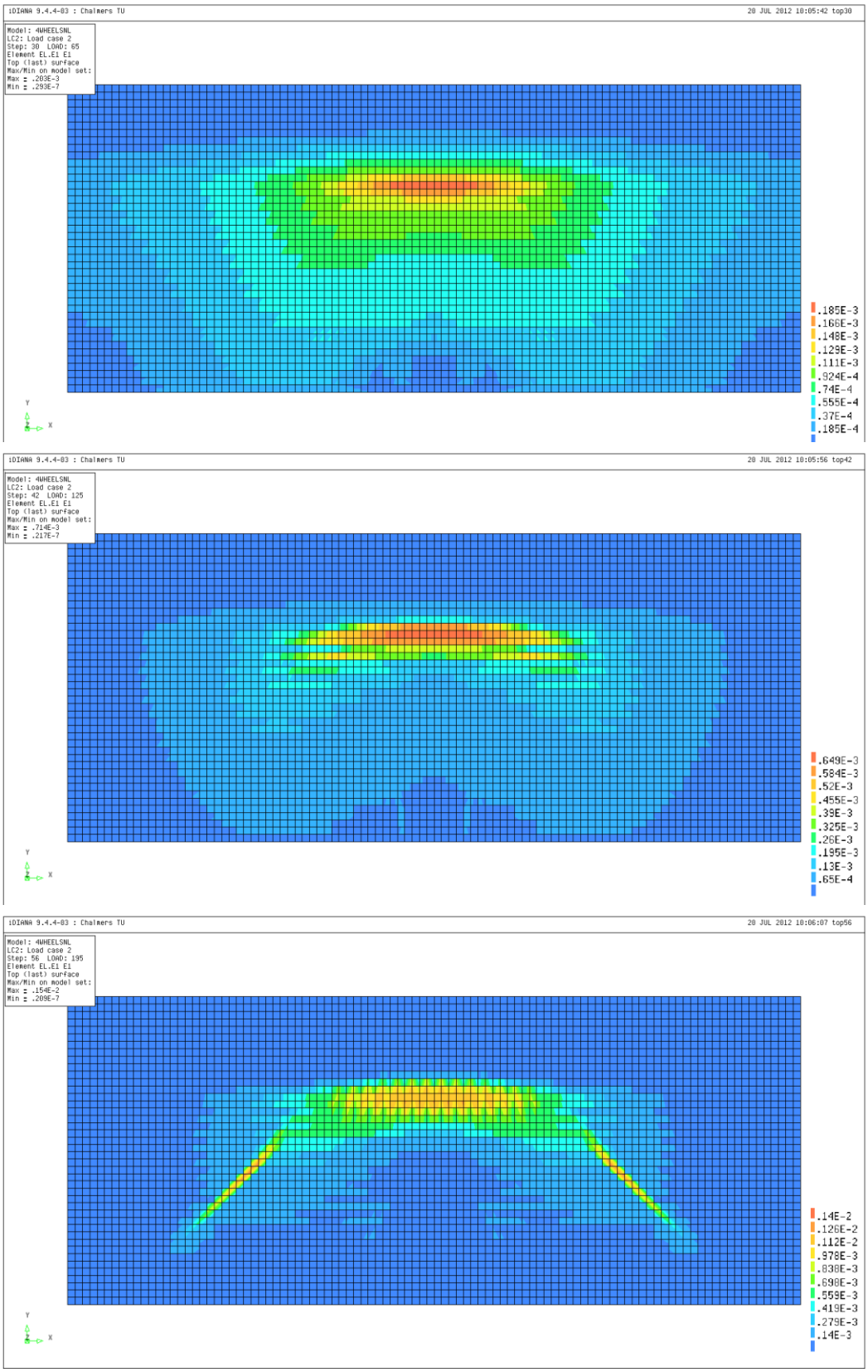

Figure 52. Top tensile strains for steps 30, 42 and 56.

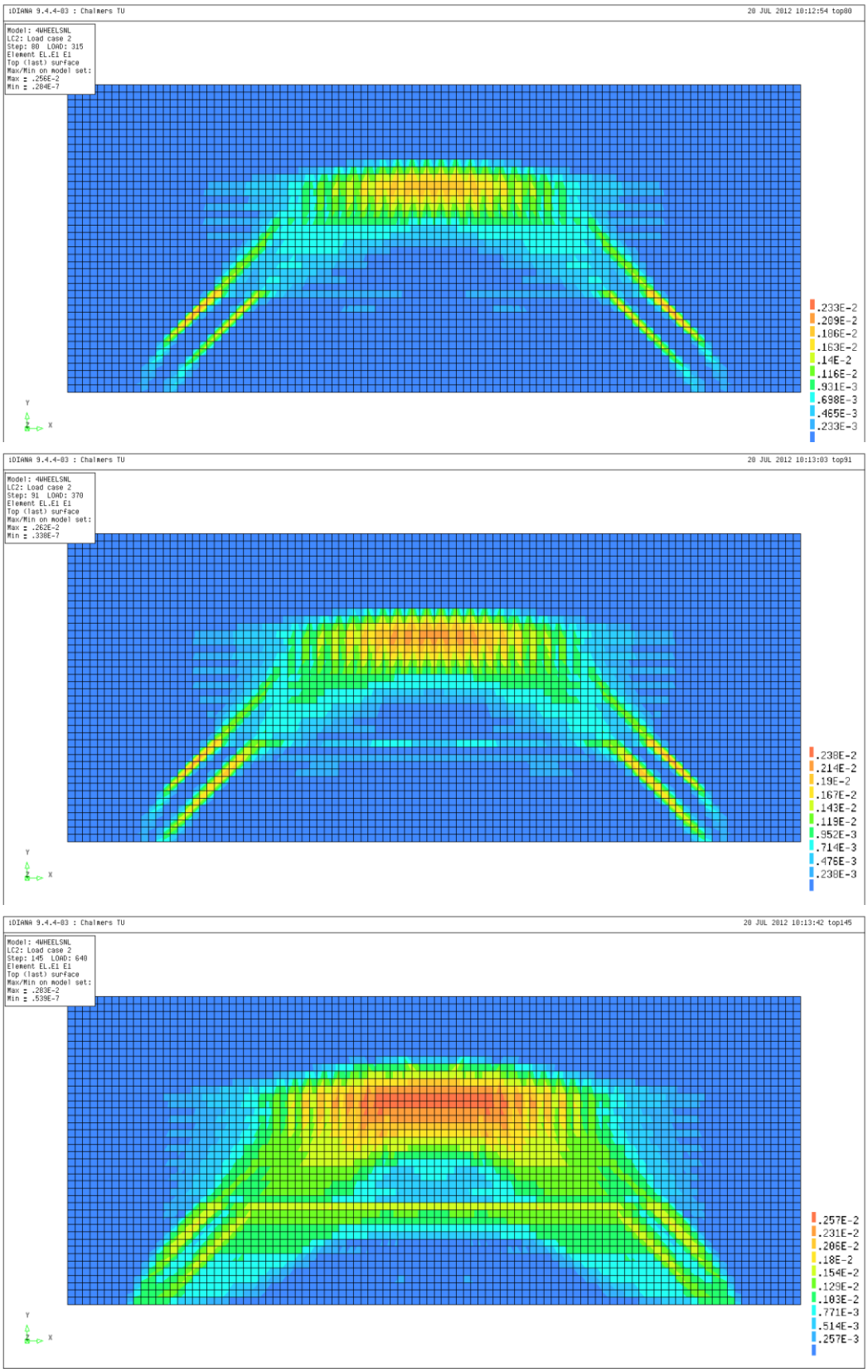

Figure 53. Top tensile strains for steps 80, 91 and 145.

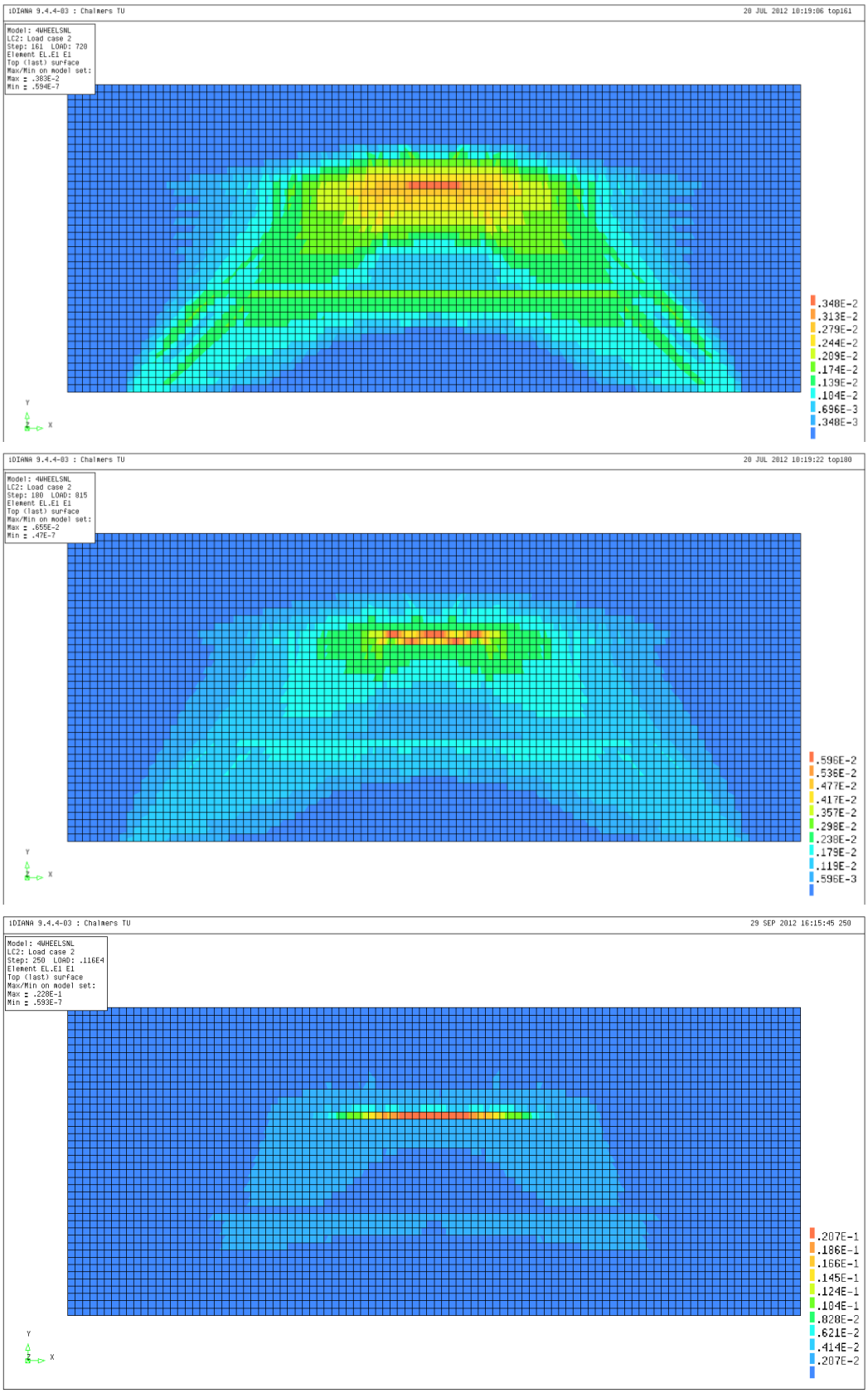

Figure 54. Top tensile strains for steps 161, 180 and 250.

In Figure 55 to Figure 57, the development of the principal tensile strains for the bottom surface is illustrated. It can be seen that the strain right beneath the outermost load pair dominated throughout the whole loading. The propagation of the cracks occurred towards the support in a V-shape.

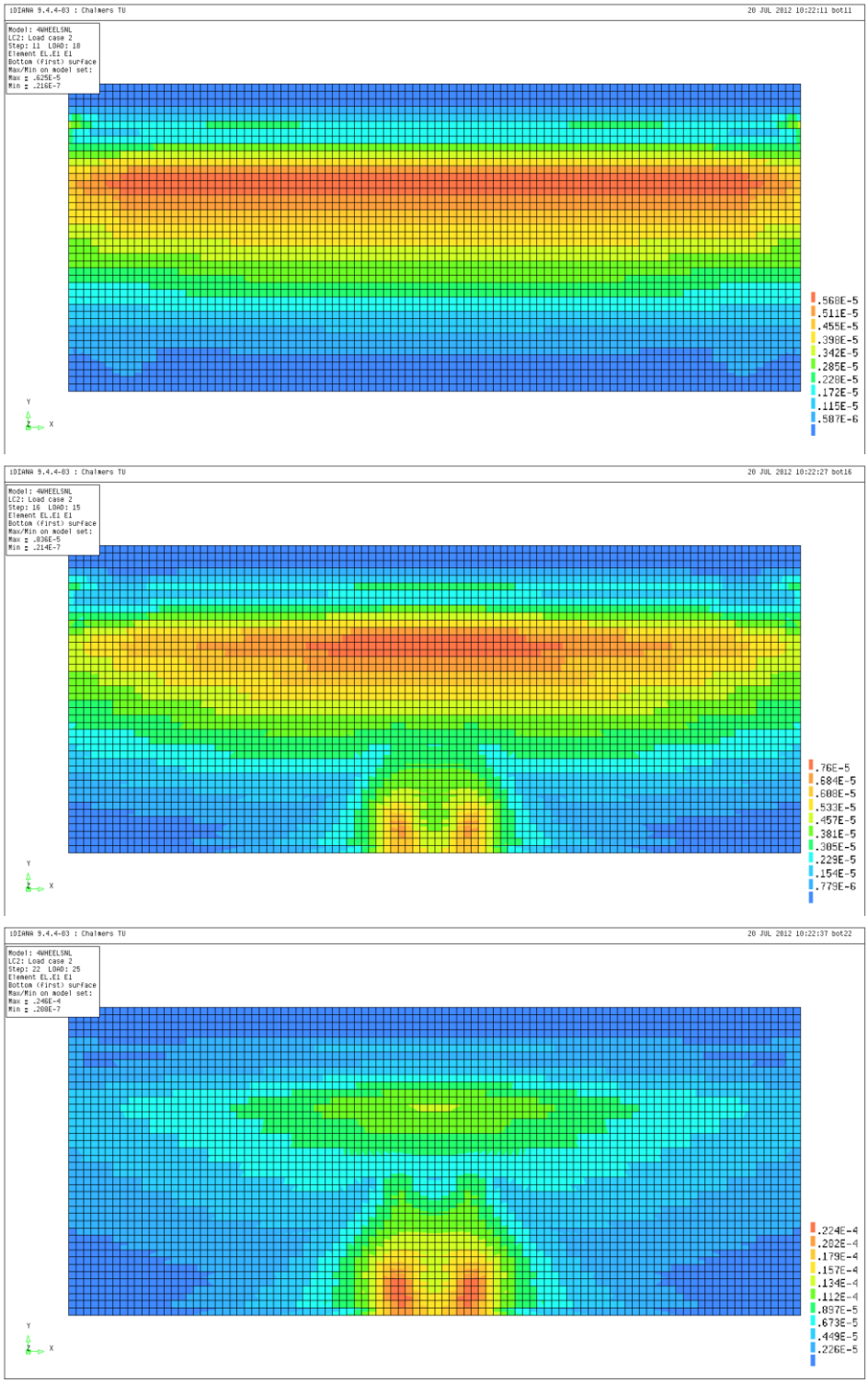

Figure 55. Bottom tensile strains for steps 11, 16 and 22.

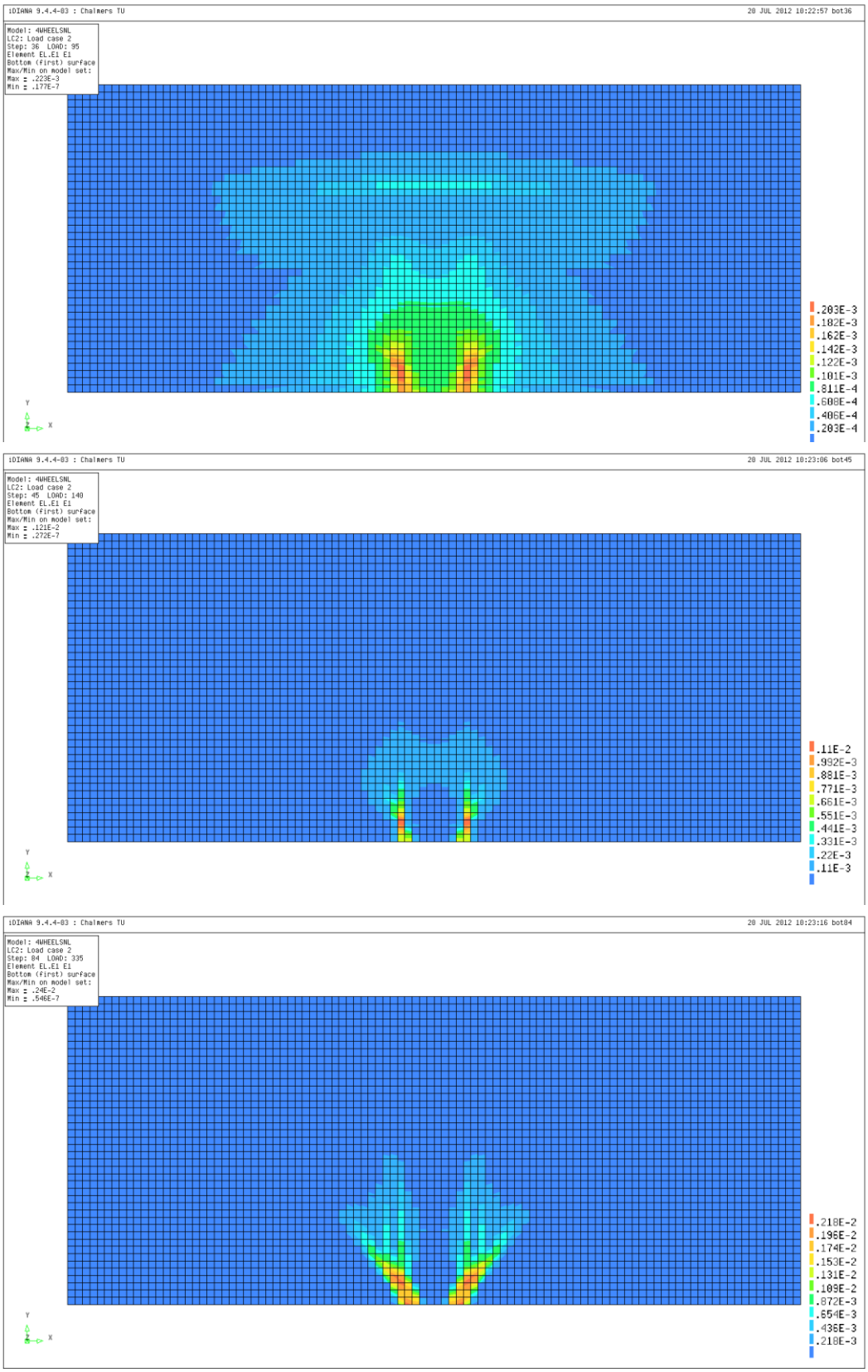

Figure 56. Bottom tensile strains for steps 36, 45 and 84.

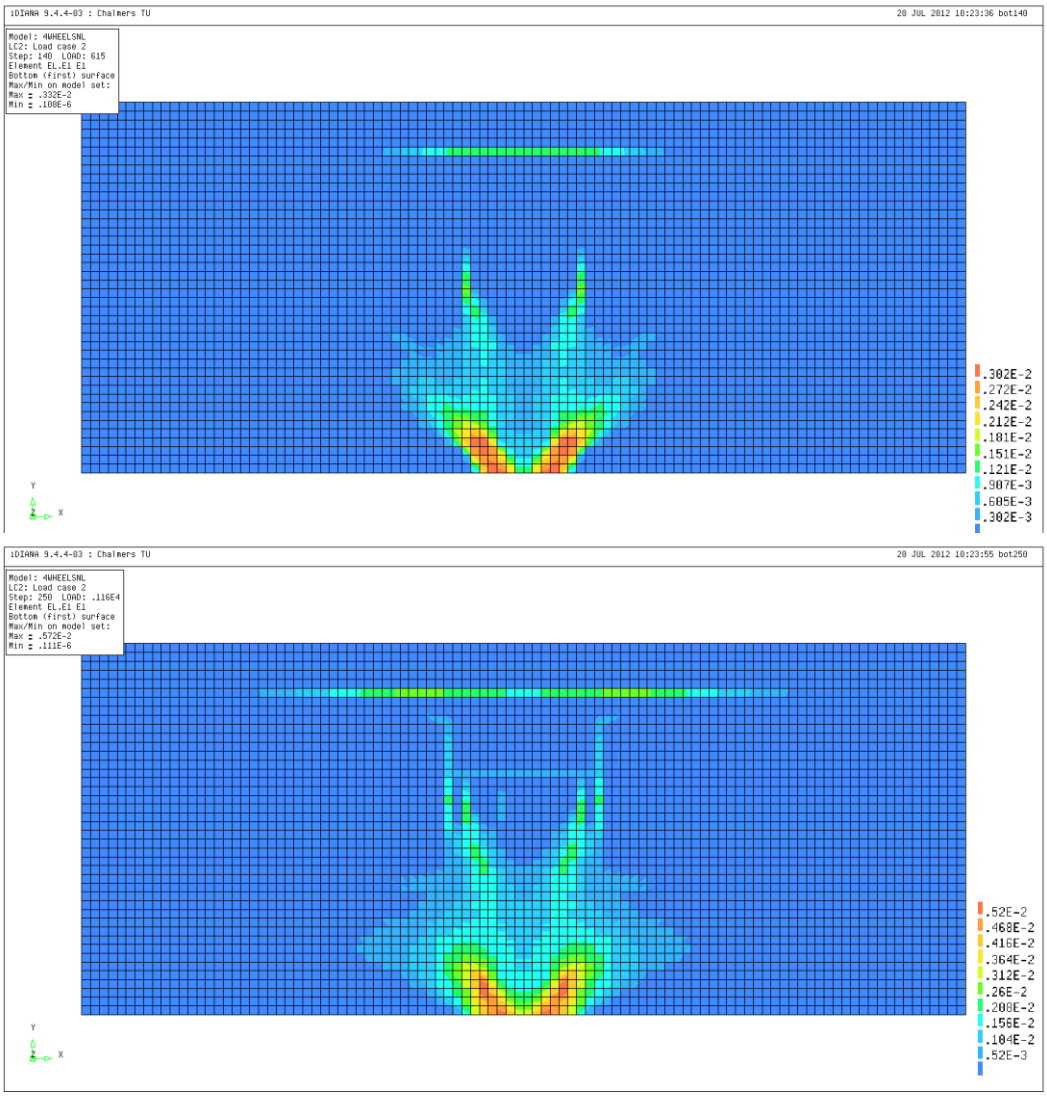

Figure 57. Bottom tensile strains for steps 140, 250.

5.2 Shear distribution

The results regarding the shear distribution are presented both with contour plots and with diagrams of the shear component perpendicular to the support line (y-direction). In Figure 58 to Figure 63, the distribution in the slab of the shear force component in transversal direction is shown.

5.2.1 Transversal shear force distribution in the slab

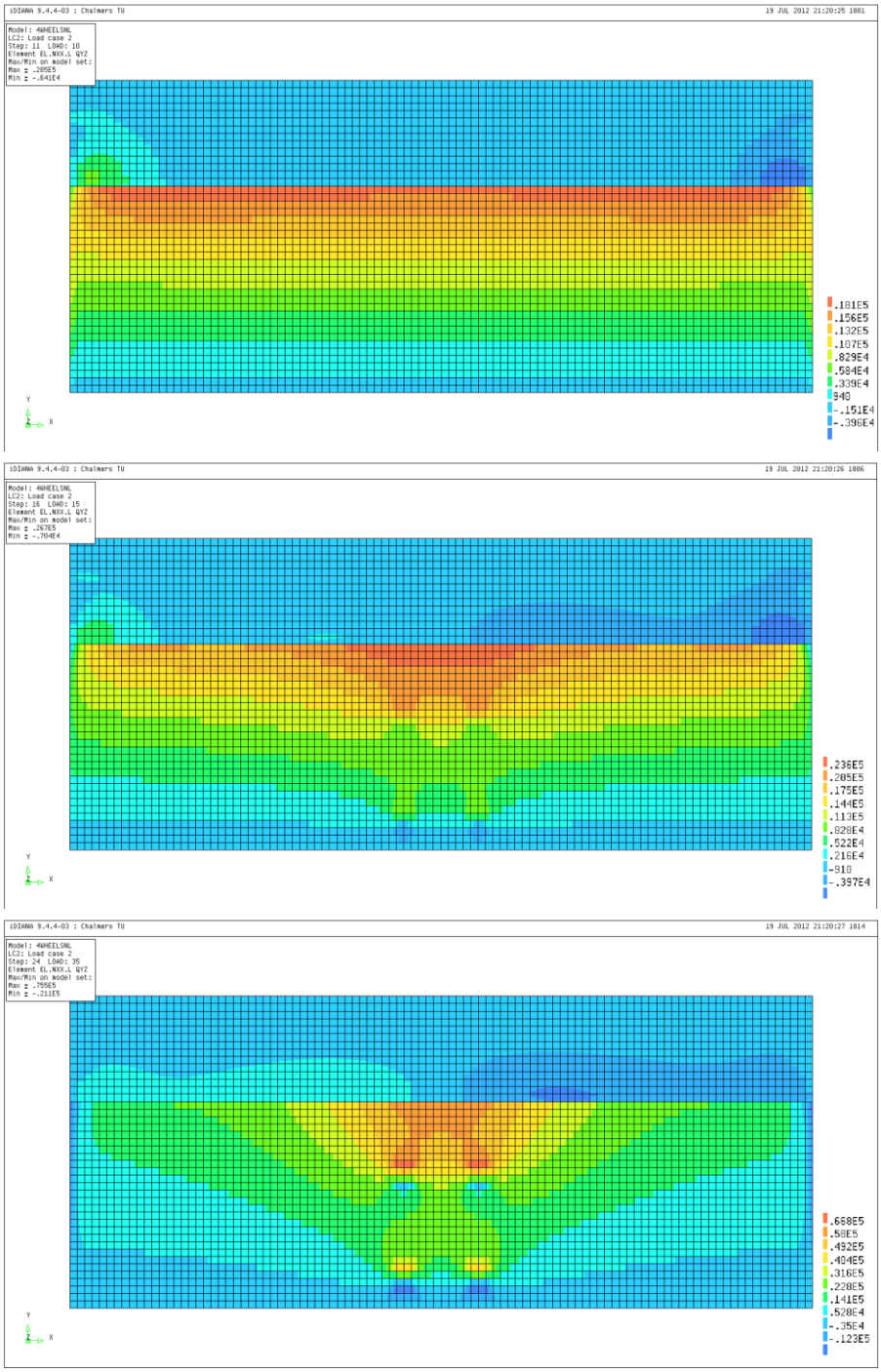

Figure 58. Shear force per unit width [N/m] in y-direction for steps 11, 16 and 24.

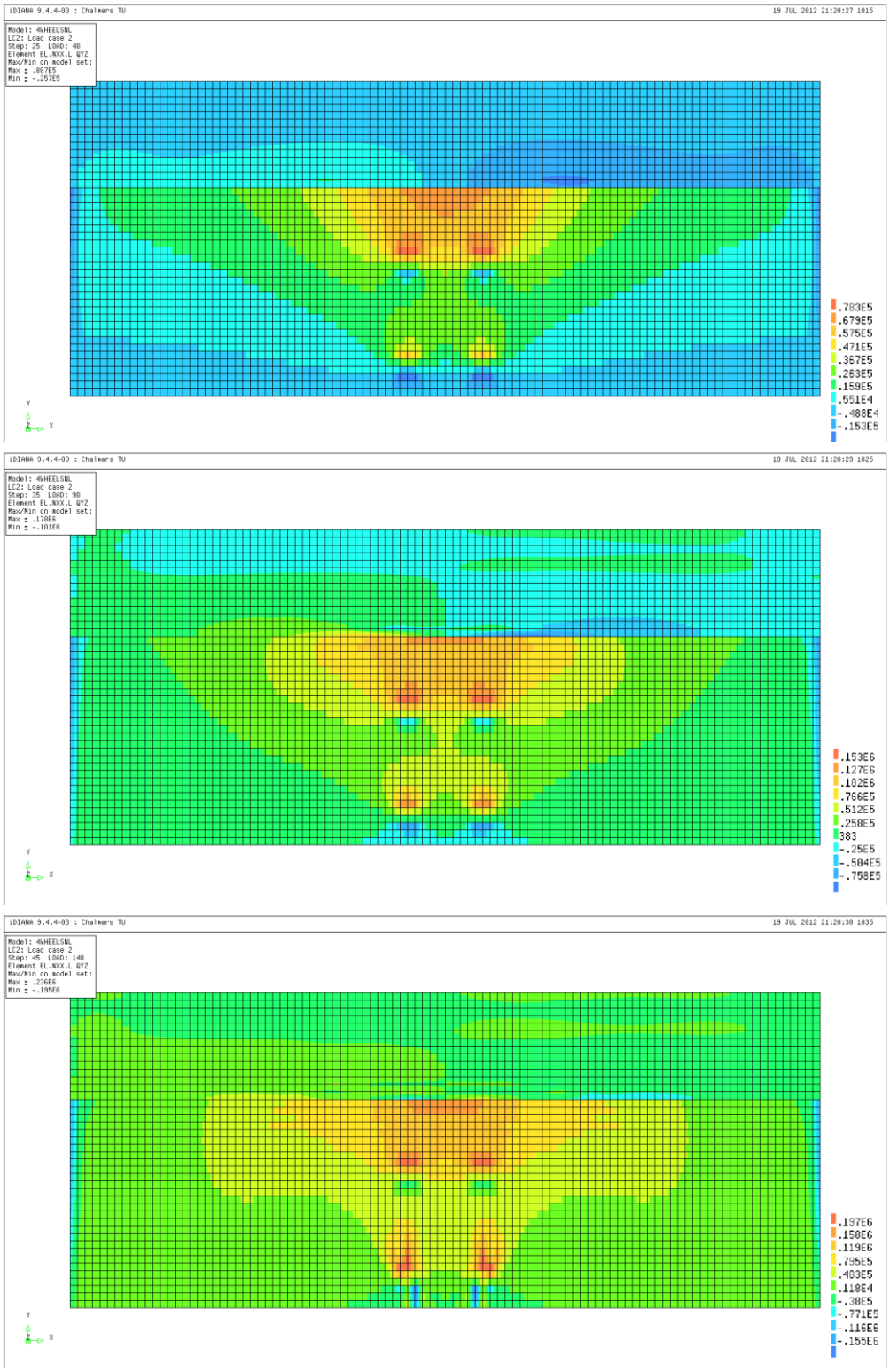

Figure 59. Shear force per unit width [N/m] in y-direction for steps 25, 35 and 45.

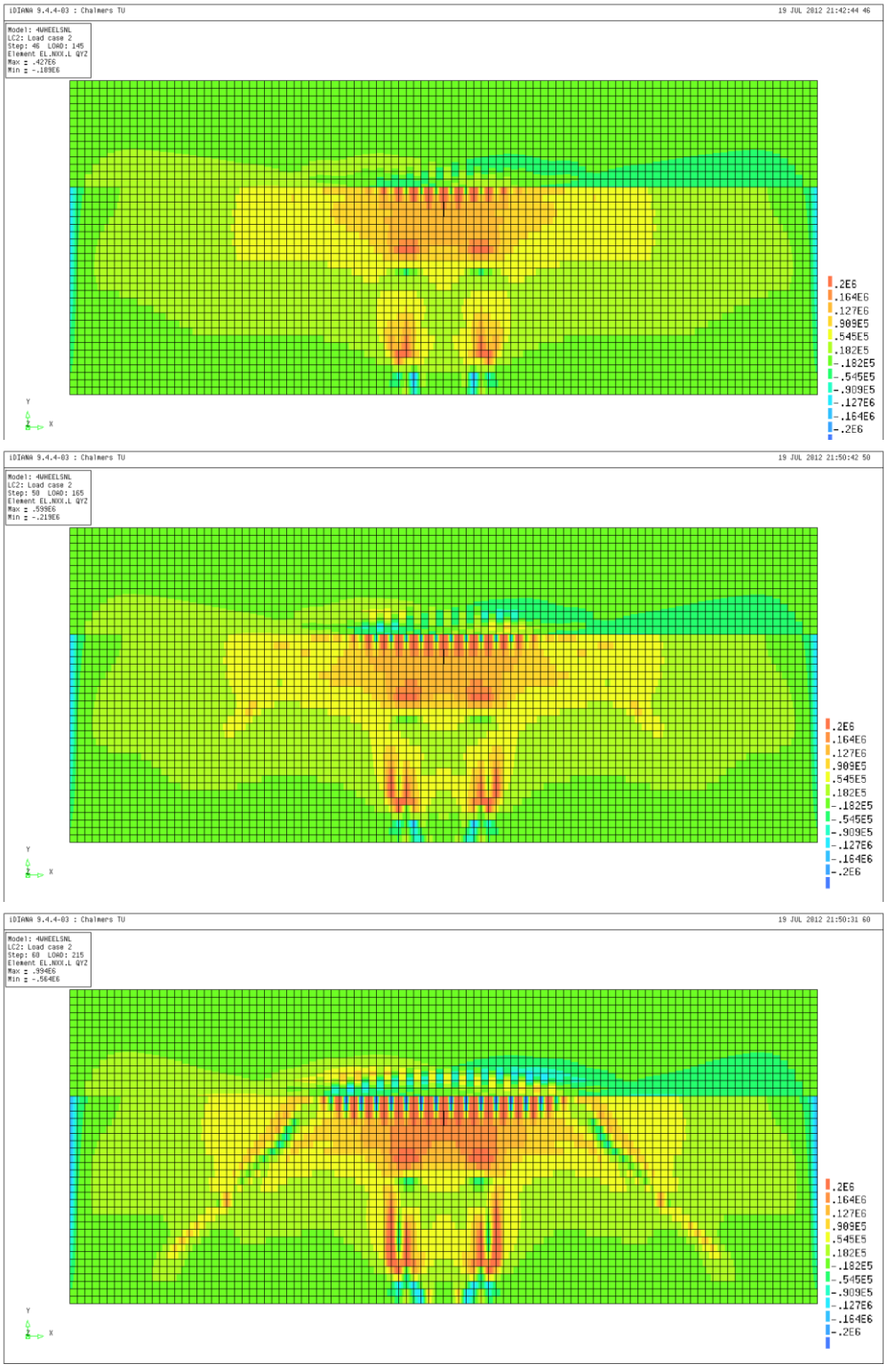

Figure 60. Shear force per unit width [N/m] in y-direction for steps 46, 50 and 60.

Fluctuations in the shear field, that were not there for the lower loads, started to occur at step 46, see Figure 60. They can be distinguished by the varying colors in the plots, altering between blue and red.

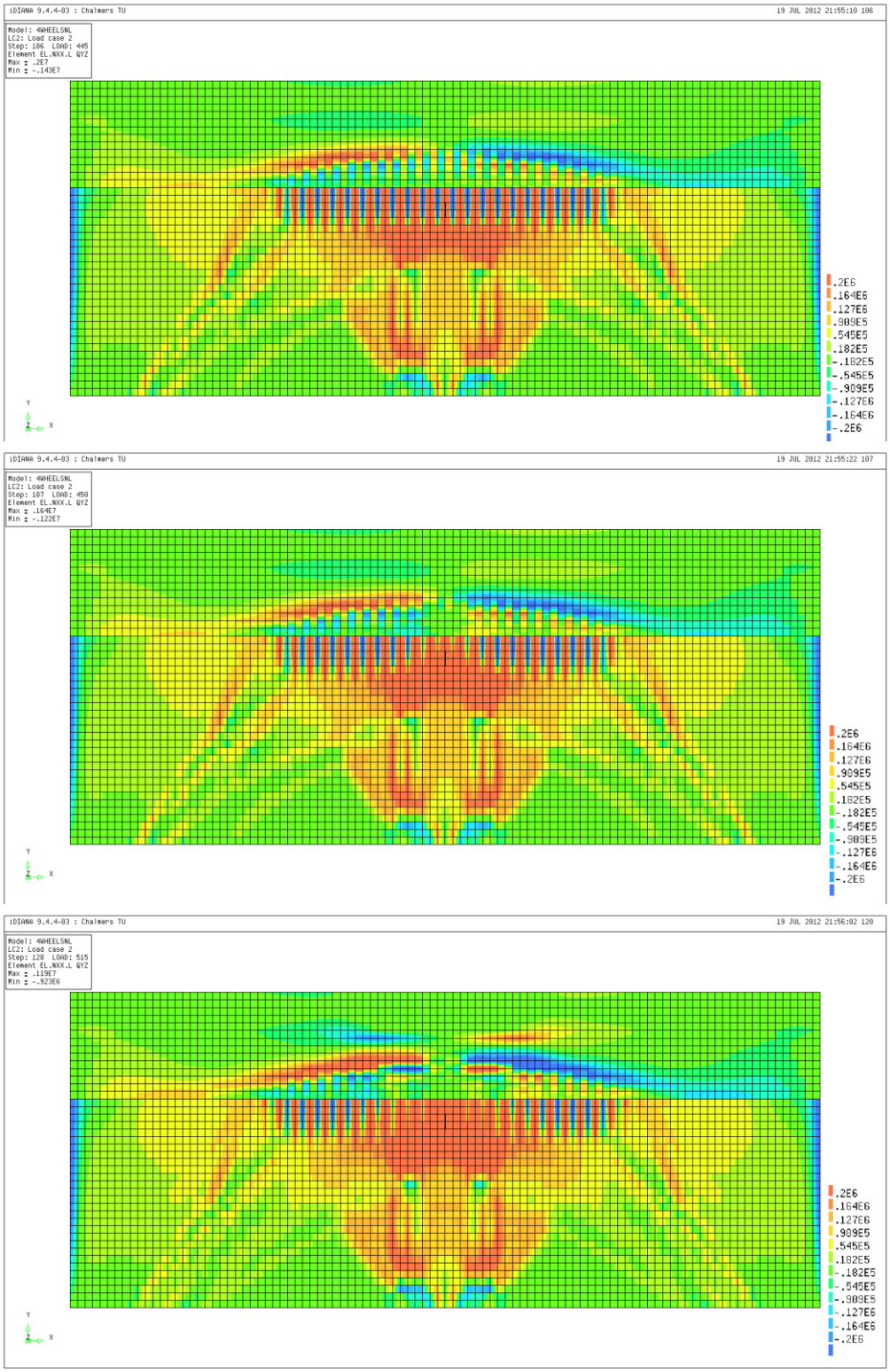

Figure 61. Shear force per unit width [N/m] in y-direction for steps 106, 107 and 120.

In Figure 61, after step 106, the fluctuations started to move apart from each other. The maximum shear was still carried in the middle of the support.

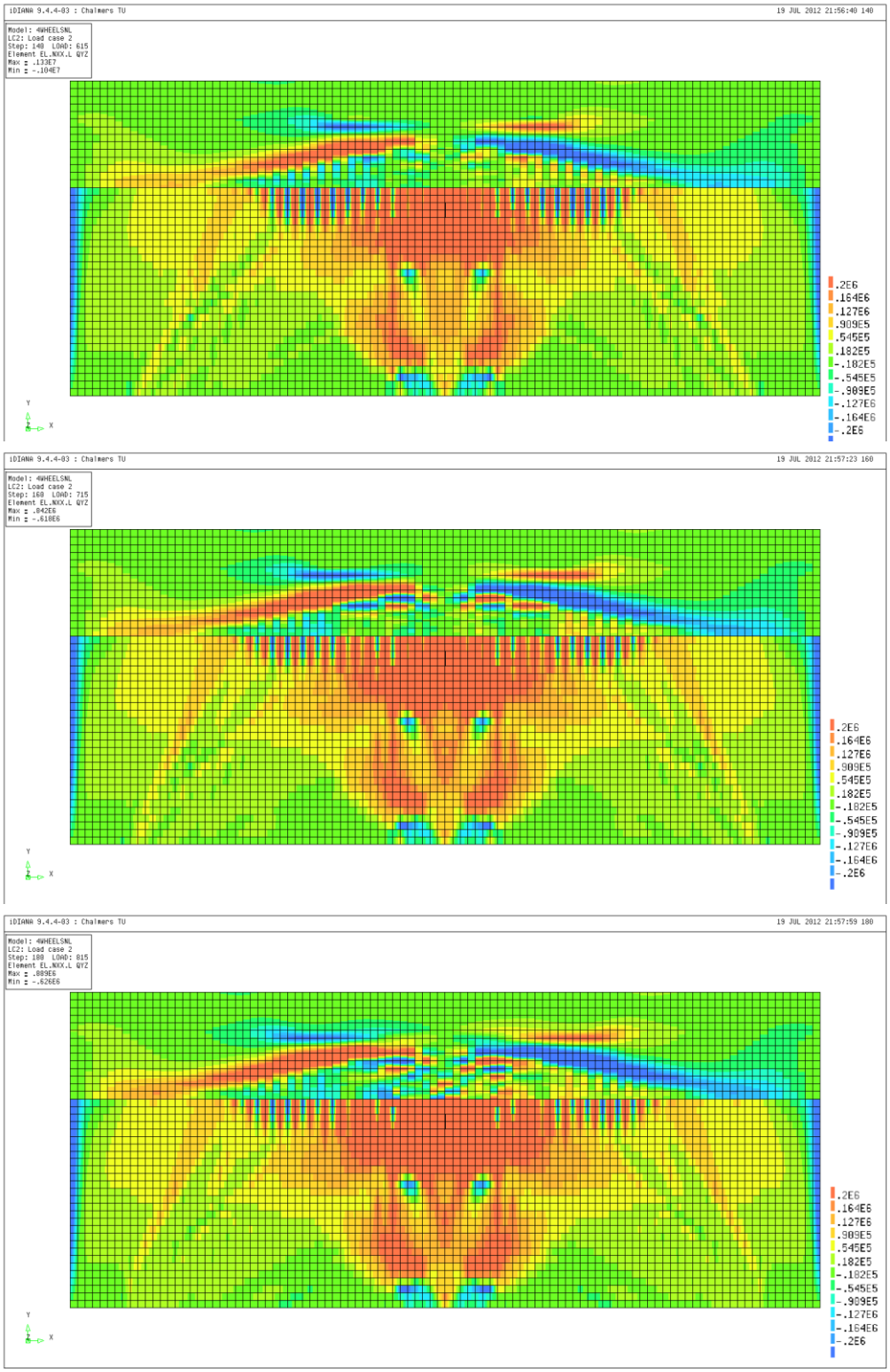

Figure 62. Shear force per unit width [N/m] in y-direction for steps 140, 160 and 180.

In Figure 62, it can be seen how the fluctuations at the support continued to move apart from each other. After yielding in the top transversal reinforcement, the shear started to spread to larger parts of the support. This continued until about step 240.

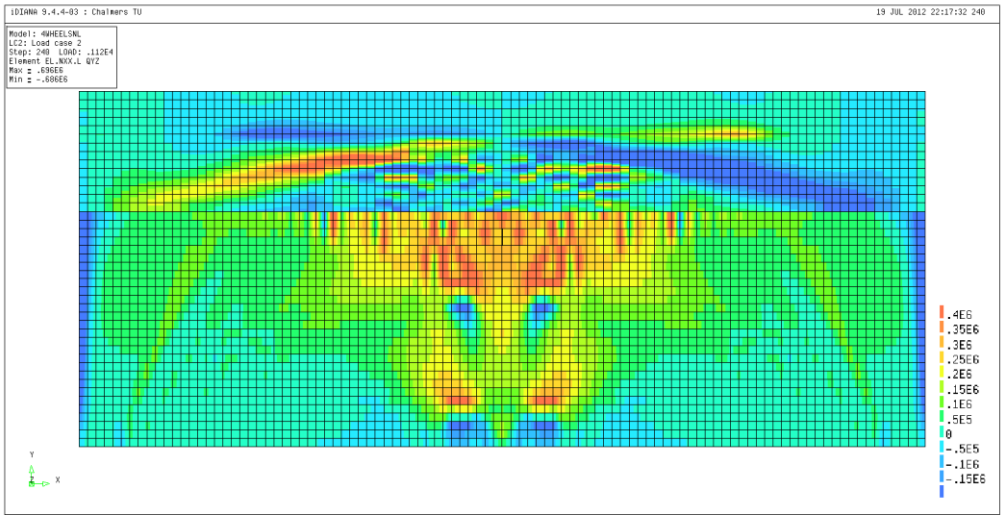

Figure 63. Shear force per unit width [N/m] in y-direction for steps 240.

Nothing apparent happened with the shear distribution from step 240 to 305, beside very small changes. This indicates that most of the plastic redistribution already happened before step 240 and that the model is reaching a plateau in the load-displacement curve, i.e. a mechanism. The fluctuations are more discussed in Section 5.2.3 and Chapter 6.

5.2.2 Transversal shear force distribution along the support

The distribution of shear force in transversal direction was studied along a control line parallel to the support, at a distance of 278 mm from it. An example of the fluctuating shear force results is shown for step 50 in Figure 64. It is obvious that there is an average shear force distribution around which the results fluctuate. If it is assumed that the fluctuations only are local effects, and thus not affecting the behavior of shear distribution globally, trend lines can be used to represent the average values along the parts of the control line where the fluctuations occur, in order to determine the overall shear distribution. The averaging makes the trend lines become a bit offset from the original graph, since they represent the mean values in the middle point of the original result values. An alternative way to make trend lines is to use polynomials adapted to the curve with the least square method.

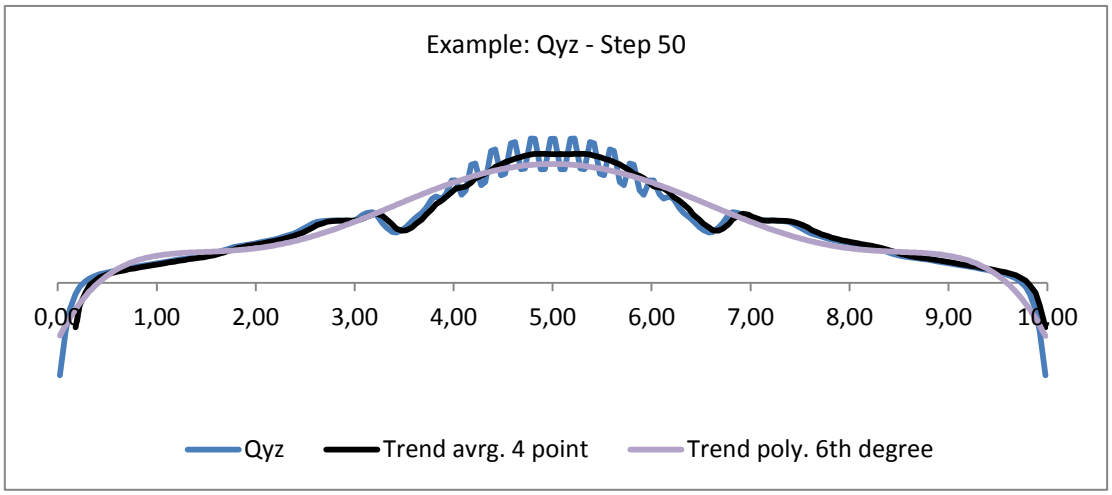

Figure 64. An example of fluctuating shear results (step 50).

Since the fluctuations take overhand for larger loads, only the trend lines of the shear are presented in the following. In addition, the shear force diagrams are normalized with respect to the applied load, so that the effect of magnitude should not influence the shape of the curve. In Figure 65 to Figure 67, the trend lines are calculated as "moving averages", meaning that a specific number of values are averaged, in these cases 4 values. As can be seen, also the averages fluctuate. Nevertheless, the behavior of shear distribution can be distinguished. To facilitate the distinction of the distribution behavior, the same results are presented again in Figure 68 to Figure 70, this time with 6^{th} degree polynomial trend lines. These lines become very approximate and undetailed, though the distribution is easier to distinguish.

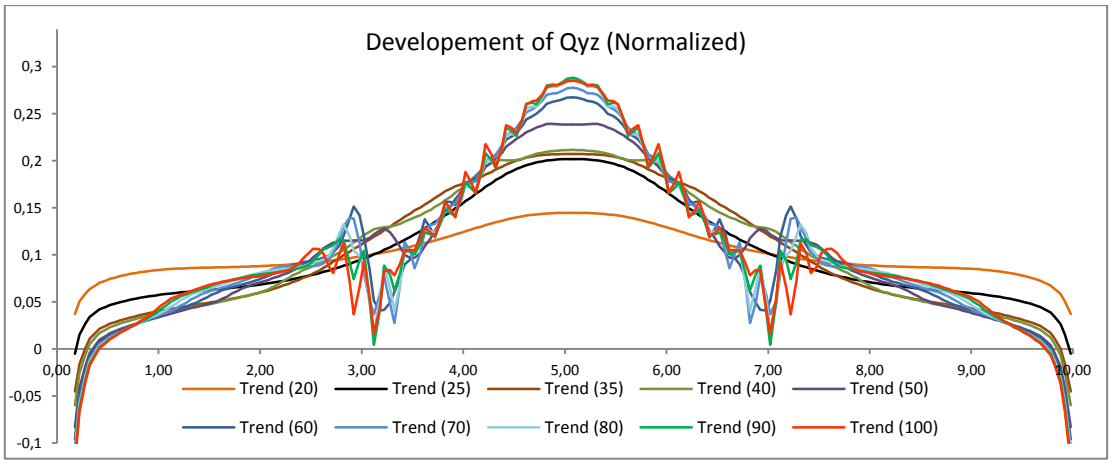

Figure 65. Average trend lines for shear in y-direction for steps 20, 25, 35, 40, 50, 60, 70, 80, 90 and 100.

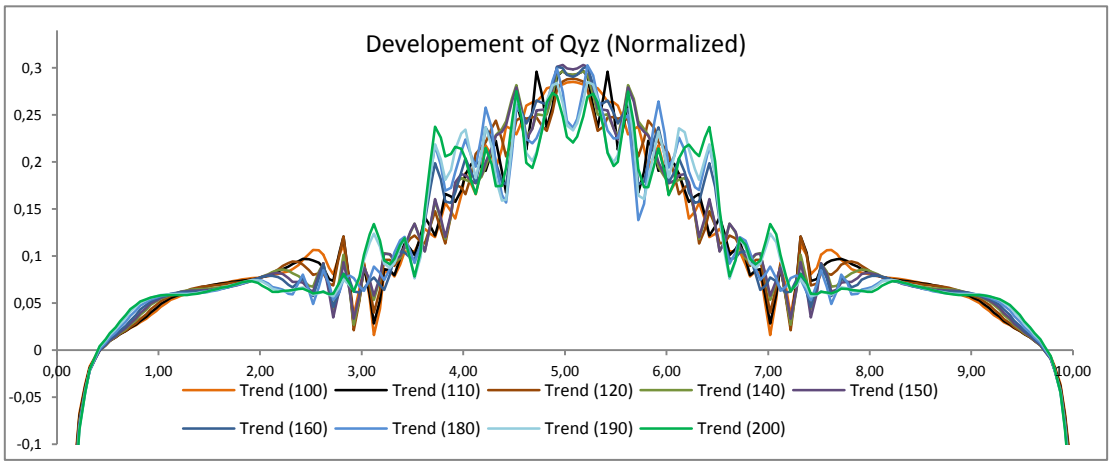

Figure 66. Average trend lines for shear in y-direction for steps 100, 110, 120, 140, 150, 160, 180, 190 and 200.

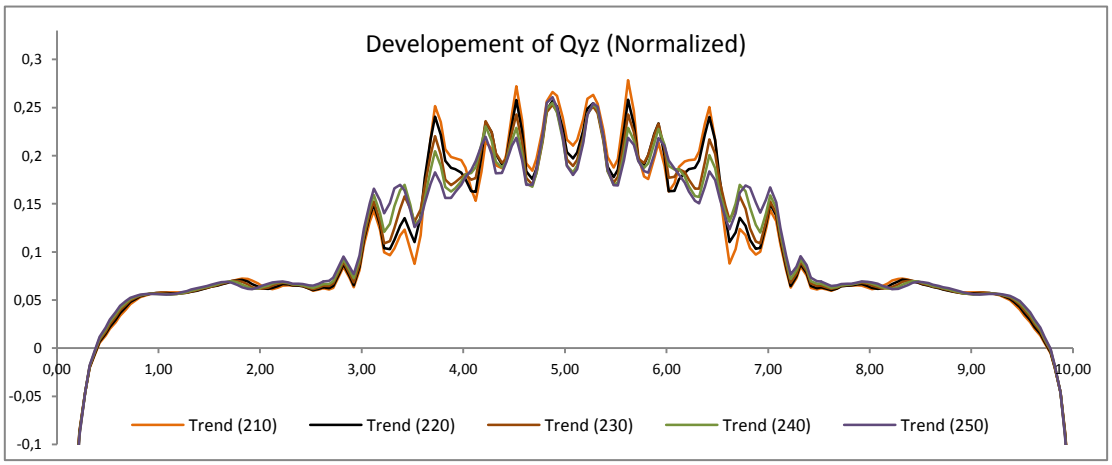

Figure 67. Average trend lines for shear in y-direction for steps 210, 220, 230, 240, 250.

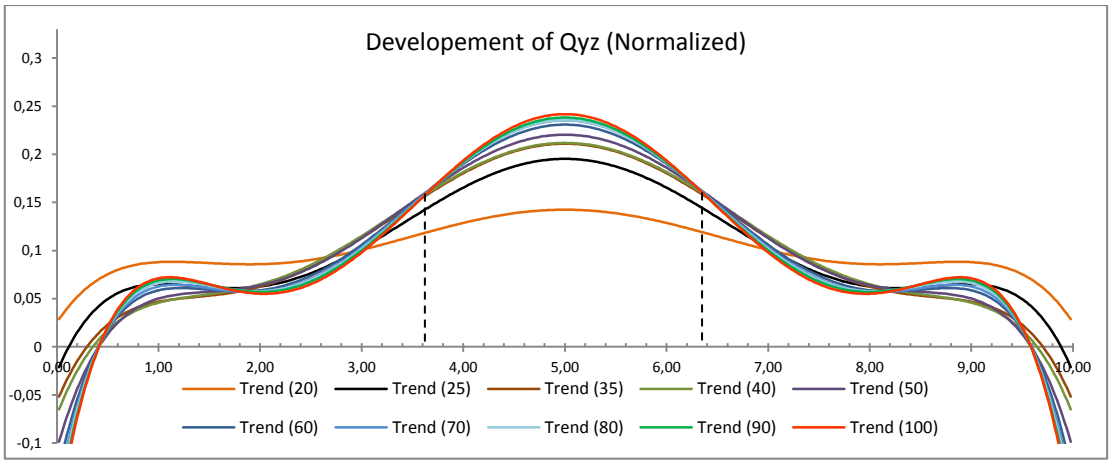

Figure 68. Polynomial trend lines for shear in y-direction for steps 20, 25, 35, 40, 50, 60, 70, 80, 90 and 100. Dashed lines indicate points at which the results are constant with load increase.

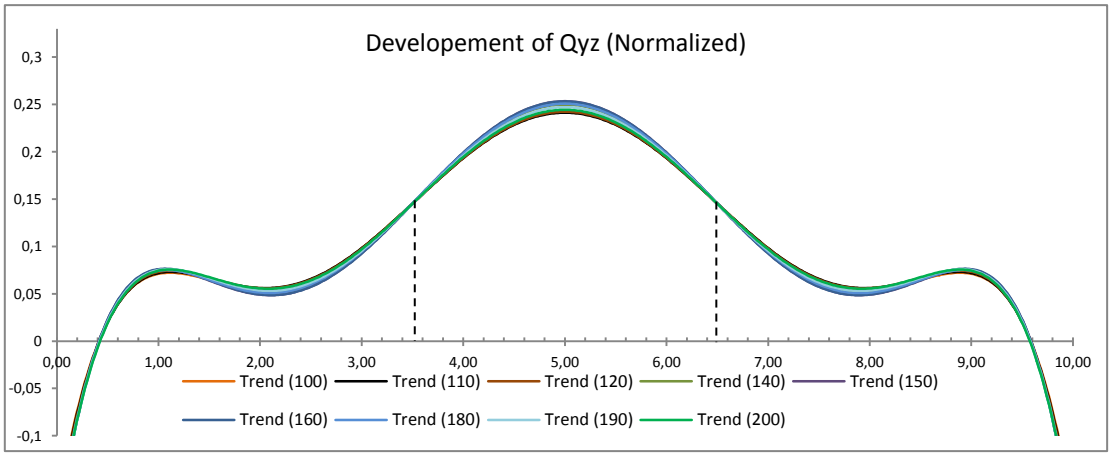

Figure 69. Polynomial trend lines for shear in y-direction for steps 100, 110, 120, 140, 150, 160, 180, 190 and 200. Dashed lines indicate points at which the results are constant with load increase.

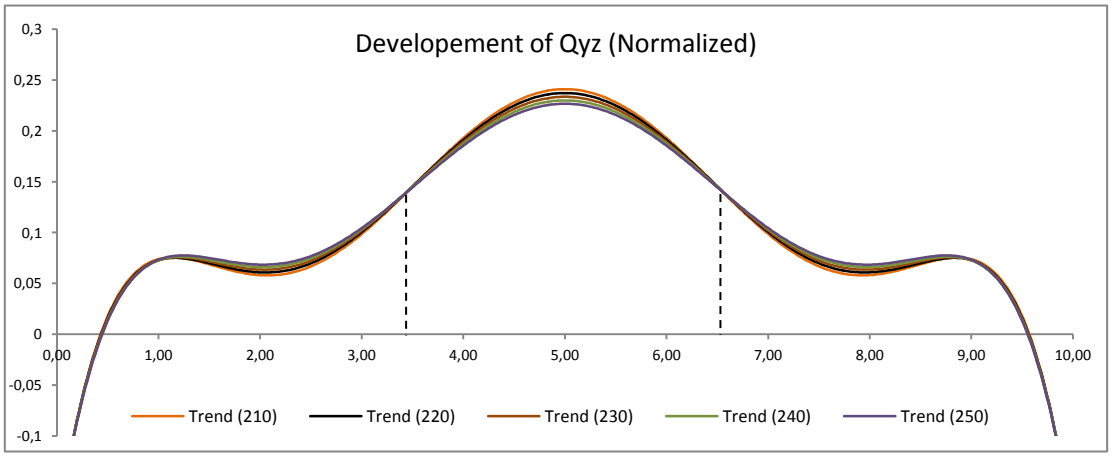

Figure 70. Polynomial trend lines for shear in y-direction for steps 210, 220, 230, 240, 250. Dashed lines indicate points at which the results are constant with load increase.

As can be seen in Figure 65 and Figure 68, after cracking (step 25), the normalized transversal shear force started to increase in the middle and decrease outside about x = 3 and 7m. Furthermore, it can be observed that the shear also increased and distributed to the outermost parts, between about x = 1 to 2,5m and x = 7,5 to 9m (Figure 65). A schematic description of this redistribution process is made in Figure 71a. The red dots indicate that the relative shear force in these points does not change as the load increases.

In Figure 66 and Figure 69, the same process is seen up to the step when yielding started in the top reinforcement (step 160). After that step, the redistribution process became reversed; the normalized shear force in the middle started to decrease due to loss of stiffness and redistributed to the sides. It can be observed that the positions with constant normalized shear force moved slightly apart from each other, see Figure 71b.

The effects of plastic redistribution can be distinguished as the shear clearly redistributed from the middle towards the sides of the control line, see Figure 67, Figure 70 and Figure 71c. The movement of the positions with constant normalized shear force apart from each other is now apparent.

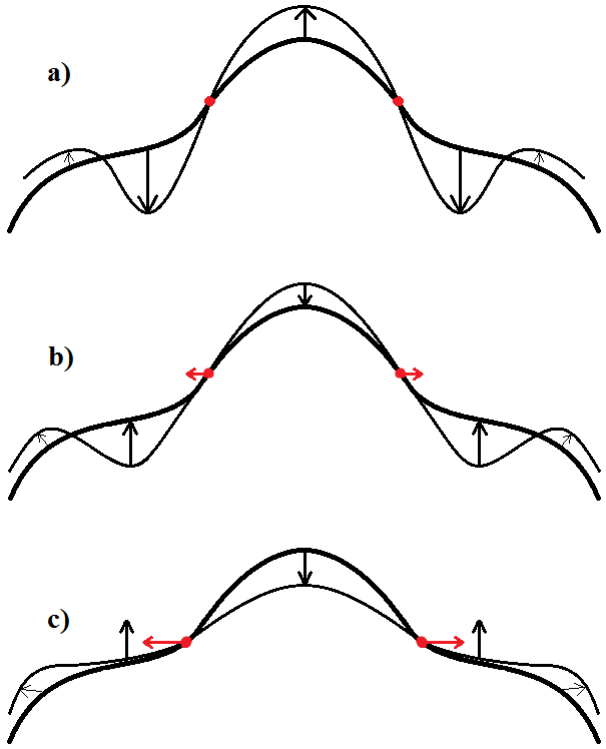

Figure 71. Behaviour of shear distribution after cracking (a), yielding (b) and plastic redistribution (c).

5.2.3 Observation of shear force fluctuations

In the beginning of the analysis, it was observed that no shear force fluctuations occurred at all, before step 46. Furthermore, it was seen that the fluctuations of shear results increased in magnitude around the mean value, for increasing load. This tendency died out when the applied load approached the load of yielding. Instead the fluctuations got less and also decrease in magnitude. When creating averaging trend lines, it was obvious that also the trend lines started to fluctuate for higher loads.

Some plots are shown in the following figures, showing what happens between step 45 and 46, right when the fluctuations start. The areas shown in the plots are a smaller part in the middle of the slab along to the support, approximately 2.5 x 1.2 m, i.e. where the strains are the largest, see Figure 72.

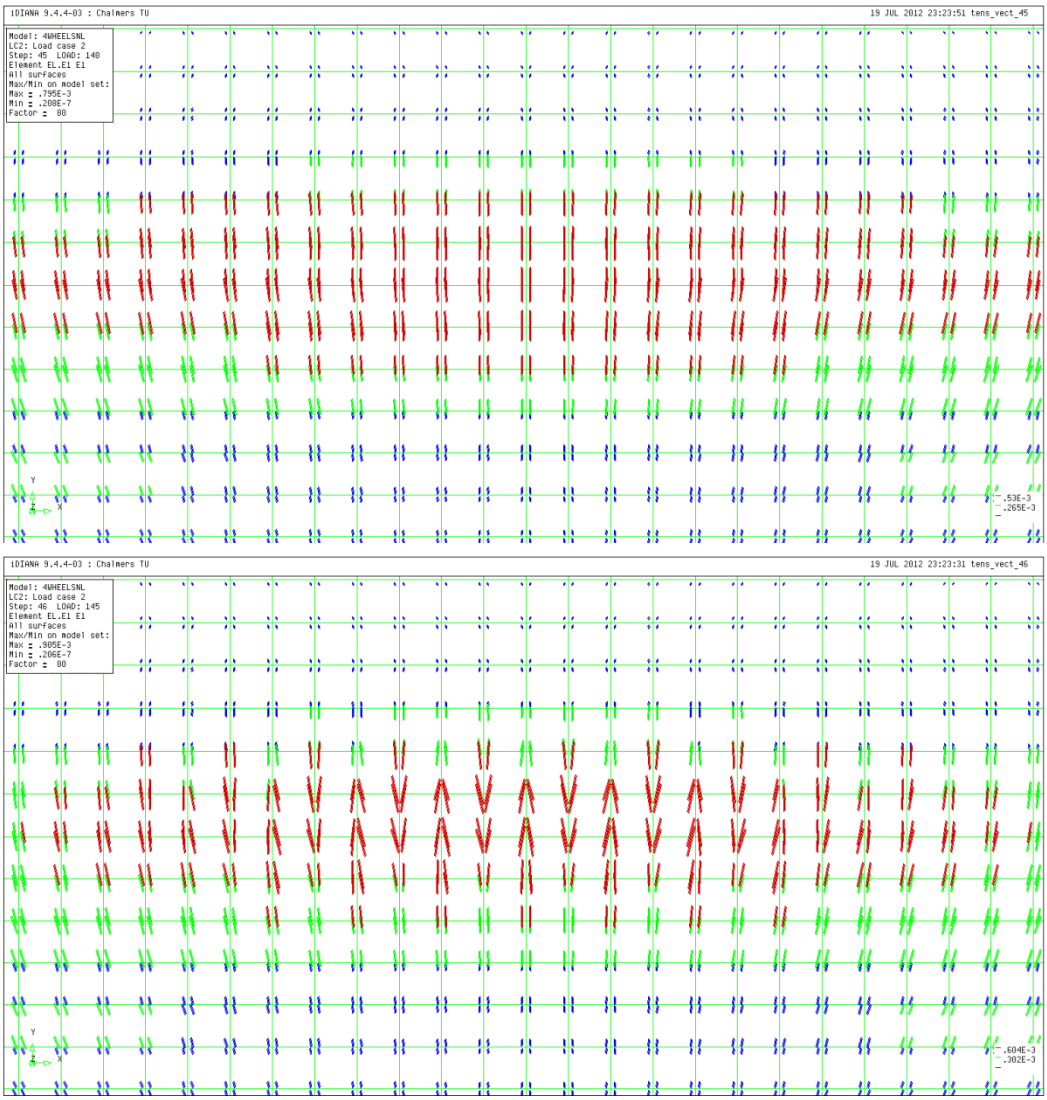

Figure 72. Fluctuating principal tensile strain vectors. The vectors are shown for each integration point. Step 45 above and 46 below.

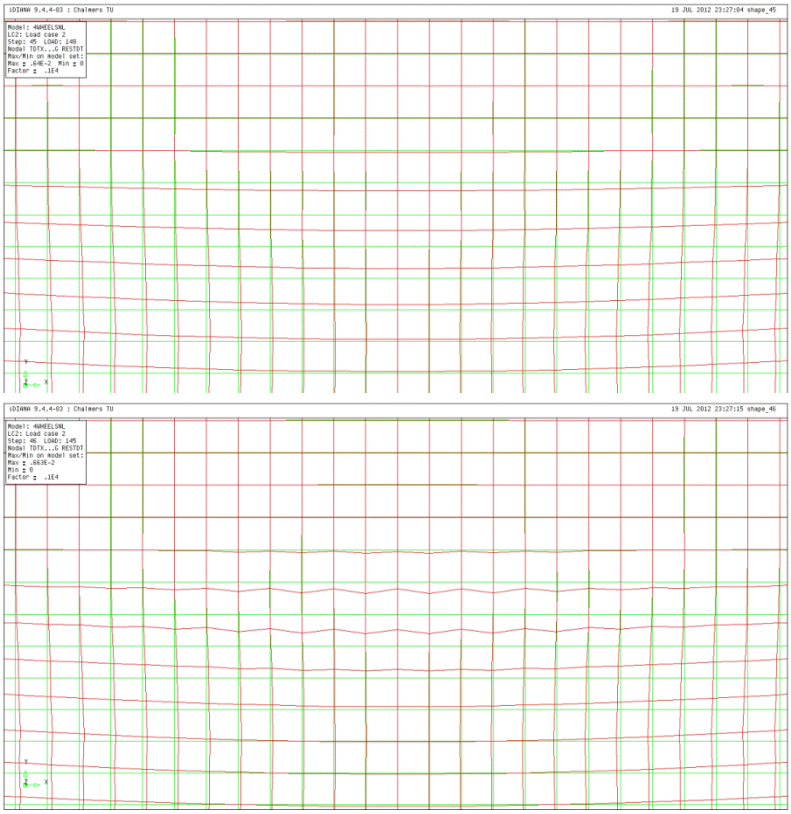

Figure 73. Fluctuating nodal deformations, magnified to clarify. Step 45 above and 46 below.

The finite element software TNO Diana, categorizes the crack into six different statuses, see Figure 74. With high probability, the fluctuations are due to alternation between different crack statuses within neighboring elements or integration points.

1. The status is *no crack* if there is no crack yet.
2. The status is *open* for cracks on the fully open loading branch.
3. The status is *closed* for fully closed cracks, the material is elastic again in compression.
4. The status is *active* for cracks on the partially open loading branch.
5. The status is *inactive* for cracks on the fully open unloading branch.
6. The status is *partial* for cracks on the partially open (secant) unloading branch.

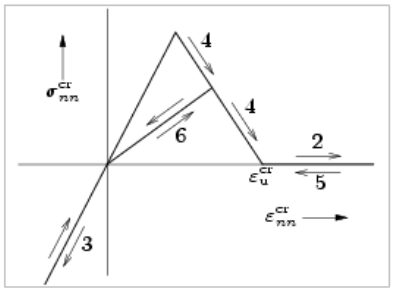

Figure 74. Crack status - linear tension softening. Adapted from TNO Diana Manual (2010).

5.2.4 Comparison to linear elastic results

In order to help understanding what differences there are between the linear analysis and the non-linear analysis, a comparison between the shear in transversal direction (y-direction) of step 232 was made with a linear elastic case, see Figure 75. The applied load at that step is 1340 kN. Step 232 was chosen because the load level lies in between the load of yield initiation in the bottom reinforcement (1284 kN) and the load at which the specimen failure occurred in the laboratory testing (1380 kN). It is desired that the load level studied is well below the failure load but still take into account ULS behavior, since the closer the FE results get to the failure load the more unreliable they get due to the fact that shear failure cannot be described in this model. Since shear failure is brittle and occurs very abruptly, the real slabs behavior is considered not to be influenced by shear cracks much before the failure occurs.

In design, it is usually only of interest to consider the part of the results with maximum shear, since the whole slab is designed for the maximum value. Thus, the behavior of the sides is disregarded. It is considered that there is certain ability of further plastic redistribution left after step 232, so a design regarding shear based on this comparison would be on the safe side. For this case, the maximum shear from linear analysis decreased by a factor of 0,815 because of the non-linear effects. The width of the area within which the results of the linear analysis exceed the trend line is equal to 3,2m, which is 3,2 times larger than the mid-point distance between the wheel loads.

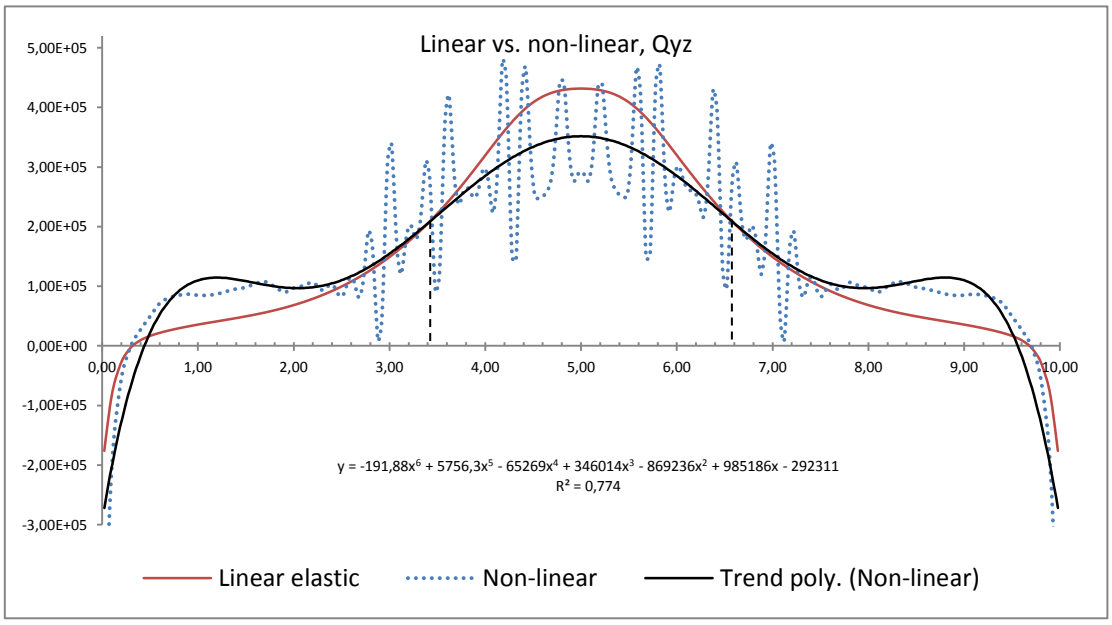

Figure 75. The 6th degree polynomial trend of the shear in y-direction of step 232 is compared to a linear elastic case. The total load is 1340 kN.

Based on these results, a distribution of the shear for the purpose of design could look something like the illustration in Figure 76.

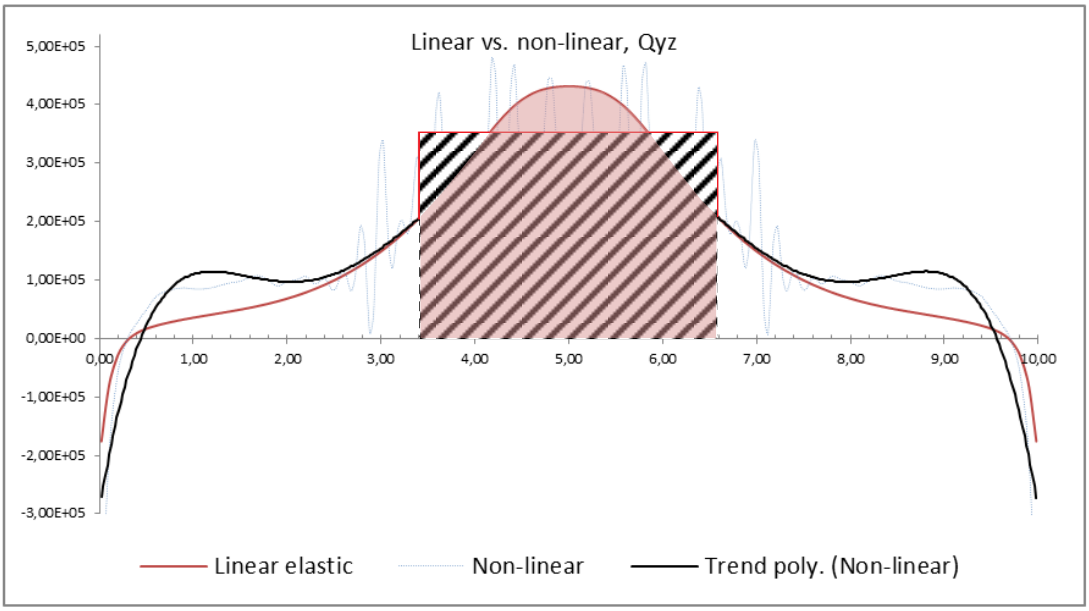

Figure 76. Distribution of linear elastic results.

In this case, the slab can be designed for 81.5% of the maximum linear shear, and the linear shear can be distributed within 3 – 3.15m. This is the length which gives the same area under the shear distribution from the linear analysis as the area of a rectangle with the height equal to the maximum shear from the non-linear analysis.

6 Discussion

When it comes to the reliability of the results from the non-linear analysis in this thesis, it is dependent on whether the role of the fluctuations is of importance for the overall behavior or not. All discussions and conclusions are based on the assumption that the fluctuations only are local events, unimportant for the global structural behavior. Even though this is not proven, the load-displacement behavior of the model is very similar to the specimen tested in laboratory. Also the crack patterns point toward that the model correctly describes the reality, since it resembles the mechanism from a yield-line method. These facts are arguments for that the fluctuations are insignificant for the purpose of this thesis.

It is also assumed that the shear failure mode of the specimen does not change its behavior before the shear failure occurs. Even though a secondary shear crack occurs, presumably at the load of 1100 kN (w_1 =42mm), the load displacement-curves continue to agree. This indicates that at least the global response of the structure was unaffected by the shear crack, see Figure 47.

It is observed that the shear redistribute to the middle of the support due to propagation of cracking, see Figure 65 and Figure 68. This may be because of the inclined cracks that surround and enclose the loads, forcing the load to be transferred directly to the middle of the support, instead of crossing the inclined cracks and spread outwards.

It may be confusing that the shear seems to spread outwards from the middle and redistribute according to the contour plots, contradicting the following diagrams. However, it is important to remember that the results in the contour plots are not normalized, so the increased shear in some regions is not necessarily the same as redistribution of shear to those regions.

It can be discussed whether the distribution of shear force that was performed in Section 5.2.4 can be used in a design case or not. Firstly, the shear is extracted from a distance of 278 mm from the support (approx. 0.75h), which probably is on the safe side. Usually the shear acting closer than the effective height is larger and considered to be carried directly by the support. Secondly, the linear case is compared to a polynomial trend line of degree 6. The "goodness of fit" which is the R^2-value is equal to 0,77 for step 232. This means that the fit is acceptable but still not perfect (which would be $R^2 = 1,0$).

Good capacity of plastic redistribution is observed since the model could carry increasing loads long after the yielding in top reinforcement occurred. Since it is mainly the plastic redistribution that reduces the shear compared to the linear analysis, large efficiency benefits can be achieved if such structures are designed correctly.

Regarding recommendations, it is necessary to perform many more non-linear analyses with parameter studies to become certain of geometric effects, effects of boundary conditions and different types of loadings. It is probably also needed to consider safety aspects regarding different uncertainties that may occur, resulting in somewhat more conservative recommendations.

7 Conclusions

- The study shows that the shear stress along the support of a cantilevering concrete slab becomes more evenly distributed when the non-linear flexural response is taken into account in the structural analysis through a non-linear finite element analysis.

- Sufficiently long cantilever decks have good capacity of plastic redistribution. Plastic redistribution caused the shear to redistribute away from the plasticized regions.

- To be able to simulate the behavior of the tested slab correctly, it was realized that the support could not be modeled as fully fixed

- The shear was redistributed towards the middle part of the support even though that part had cracked. This was probably due to the formation of the inclined cracks, see Figure 52. This resulted in that the straight way to the support became a more effective path than crossing the inclined cracks in order to redistribute outwards.

- The maximum shear from the linear analysis was reduced to 81.5% after cracking and plastic redistribution.

- The shear in the edge regions of the slab becomes higher when taking the non-linear flexural response into account, compared to a linear elastic analysis, which can be important to bear in mind.

- The secondary shear crack from the laboratory testing did not affect the overall behavior of the slab.

8 Future work

- For further analyses of this kind it is important to find out the reason for the fluctuations in shear force, and how to avoid this kind of response. Important things to investigate are the influence of the element type and integration and the material model for concrete cracking.

- As an alternative, non-linear analyses with solid elements could be made to capture shear behavior. What events or behaviors were not captured by shell elements?

- For a general recommendation, parameter studies are of importance and effects of load configurations, boundary conditions and structure geometries need to be investigated.

9 References

Engström B., Al-Emrani M., Johansson M., Johansson P. (2008): *Bärande konstruktioner Del 1*. Chalmers University of Technology, Göteborg, 2008.

Engström B. (2011): *Design and analysis of continuous beams and columns.* Chalmers University of Technology, Göteborg, 2011.

Eurocode 2 (2008): *Design of concrete structures - Part 1-1: General rules and rules for buildings.* Swedish Standards Institute, 2008.

Muttoni A., Fernández Ruiz M. (2008): *Shear Strength of Members without Transverse Reinforcement as Function of Critical Shear Crack Width*. ACI Structural Journal, 2008, title no. 105-S17.

Blaauwendraad J. (2010): *Plates and FEM – Surprises and Pitfalls.* Springer, Ede, The Netherlands.

Vaz Rodrigues R. (2007): *Shear strength of reinforced concrete bridge deck slabs.* Ph.D. Thesis, EPFL, N° 3739, Lausanne, 2007.

Muttoni A., Thürlimann B. (1986): *Shear Tests on Beams and Slabs Without Shear Reinforcement.* Institut für Baustatik und Konstruktion, Zürich, 1986, 12pp.

Muttoni A. (2008): *Punching Shear Strength of Reinforced Concrete Slabs without Transverse Reinforcement*. ACI Structural Journal, 2008, title no. 105-S42.

Vaz Rodrigues R., Muttoni A., Burdet O. (2006): *Large Scale Tests on Bridge Slabs Cantilevers Subjected to traffic Loads.* Proceedings of the 2nd fib Congress, vol.1, Naples, 2006, 232 p.

Miller R. A., Aktan A. E., Shahrooz B. M. (1994): *Destructive Testingo f Decomissioned Concrete Slab Bridge.* Journal of Structural Engineering, Vol. 120, No. 7, 1994.

Vaz Rodrigues R., Fernández Ruiz M., Muttoni A. (2008): *Punching shear strength of R/C bridge cantilever slabs.* Engineering structures, Vol. 30, Netherlands, 2008, pp. 3024-3033.

Vaz Rodrigues R. (2006): *Shear Strength of RC Bridge Deck Cantilevers*. 6th International PhD Symposium in Civil Engineering, IBK Publikation SP-015, 2006, pp. 160-161.

Hedman (1976): *Skjuvhållfasthet hos tunna betongplattor belastade med rörliga punktlaster*. Preliminary intermediate report.

Plos M. (2000): *Finite element analyses of reinforced concrete structures.* Chalmers University of Technology, Göteborg, 2000.

Ottosen N., Petersson H. (1992): *Introduction to the Finite Element Method*. Prentice Hall, New York, 1992.

Bashir-Ahmed, M., Xiao-zu, S. (2003): *Arc-length technique for nonlinear finite element analysis*. Tongji University, Shanghai.

Larsson, F. (2010): *Non-linear finite element analysis VSM014 – A short introduction*. Chalmers University of Technology, Göteborg, 2010.

Model code 90 (1993): *CEB-FIP model code 1990: Design Code*. Thomas Telford Publishing, 1993.

Hordijk, D.A. (1991): *Local Approach to Fatigue of Concrete*. PhD thesis, Delft University of Technology, 1991.

Thorenfeldt, E., Tomaszewicz, A., Jensen, J.J. (1987): Mechanical properties of high-strength concrete and applications in design. In Proc. Symp. Utilization of High-Strength Concrete (Stavanger, Norway), (Trondheim, 1987), Tapir.

TNO Diana Manual (2010): *Diana – Finite element analysis – User's Manual – Analysis Procedures – Release 9.4.2*. TNO DIANA BV. Schoemakerstraat 97, 2628 VK Delft, The Netherlands.

Appendix A – Support modeling

The study is made on a rectangular cantilever deck fully fixed at one of the long sides and subjected to two wheel loads. To represent the distribution of the wheel loads with displacement controlled loading, somehow the nodes within the wheel distribution had to be displaced. Therefore, three load models with varying accuracy were tested in a linear elastic analysis and the shear distribution in y-direction along a line in between the loads and the support line were compared to each other. In the simplest model, 4 point loads of the same magnitude were placed within the wheel. For the intermediate model, nine equal point loads were used, and in the most accurate model, all nodes within the wheel were subjected to point loads. Though, in this case, edge nodes were subject to loads with half of the magnitude of the inner loads. In the same manner, the corner nodes got loads with a quarter of the magnitude of the inner loads.

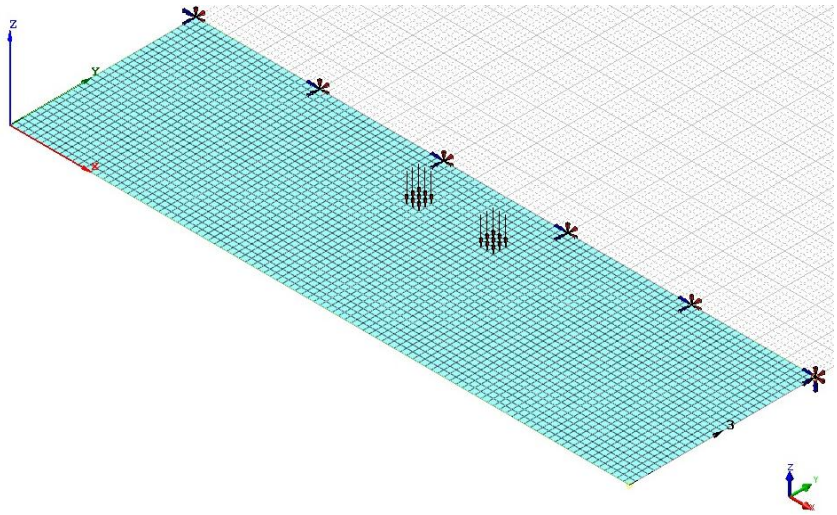

Simplest:

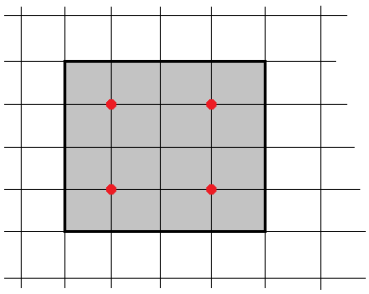

Intermediate:

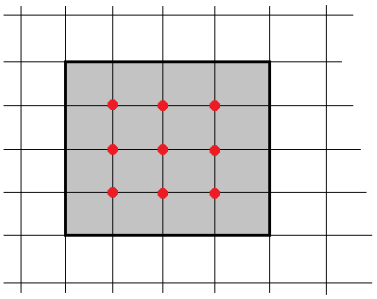

Fully detailed:

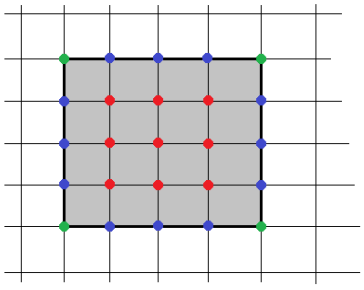

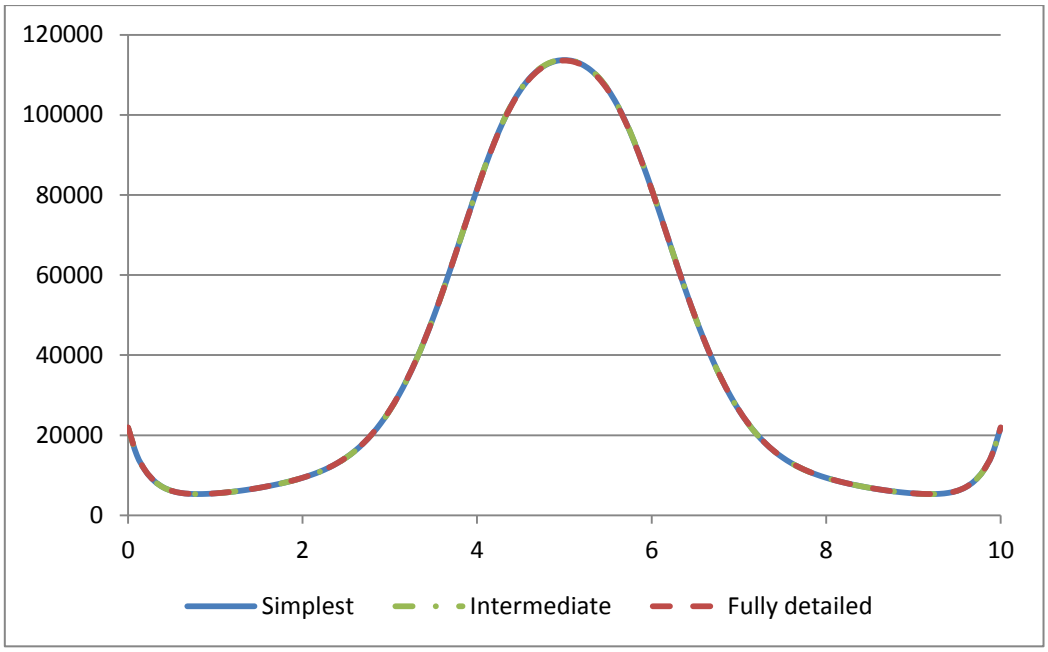

It was shown that minimal differences were achieved in the shear distribution with the different load models.

Appendix B – Convergence study and verification

Regular – 100x28 = 2800 elements

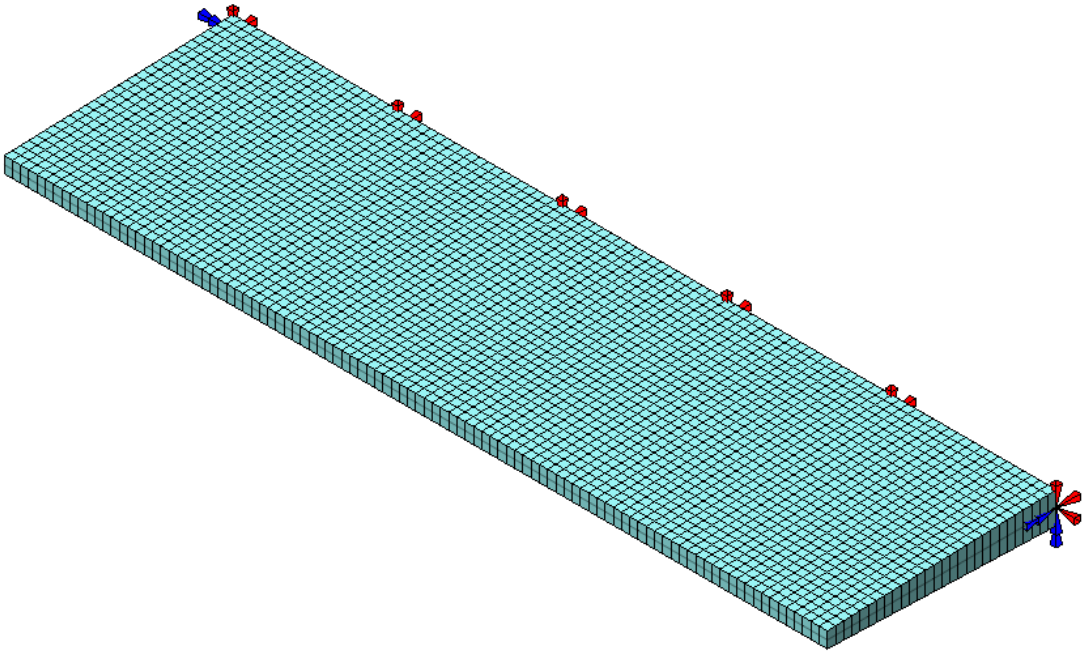

Regular - deflection

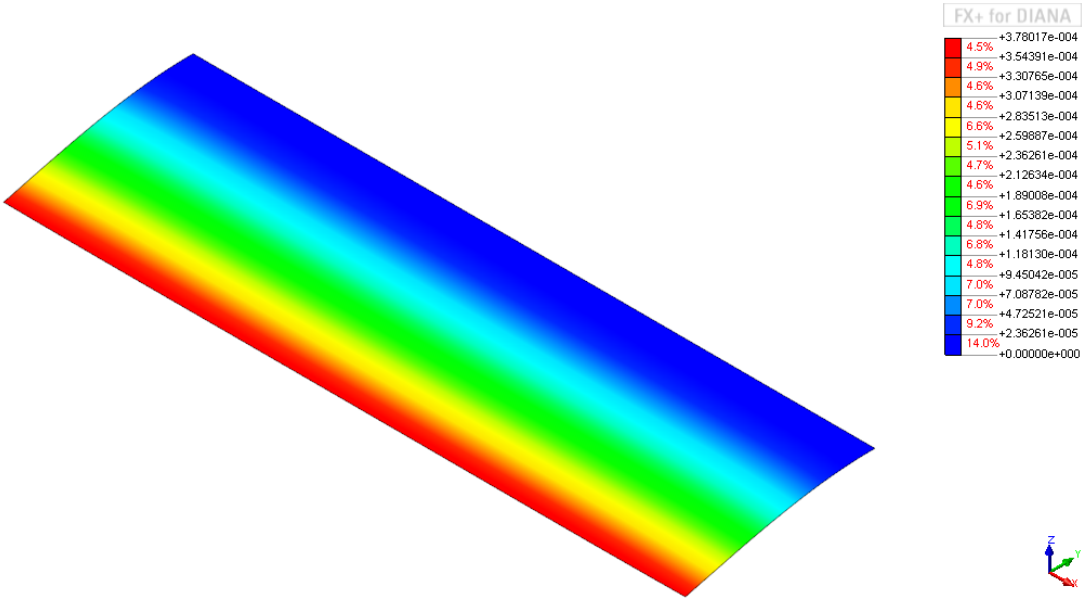

Denser – 125x35 = 4375 elements

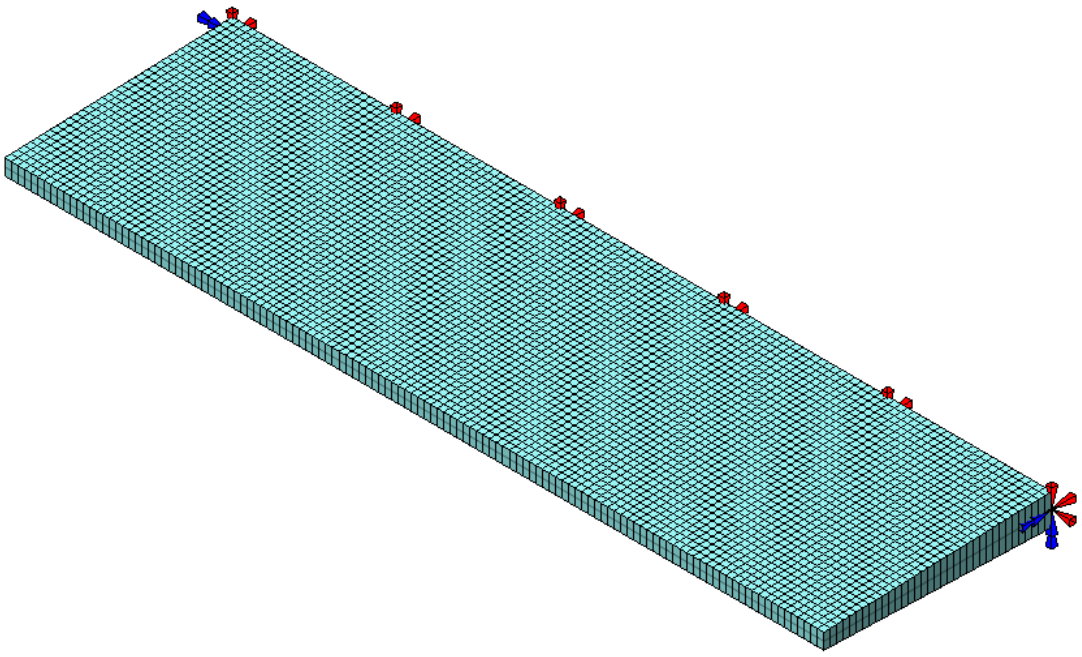

Denser – deflection

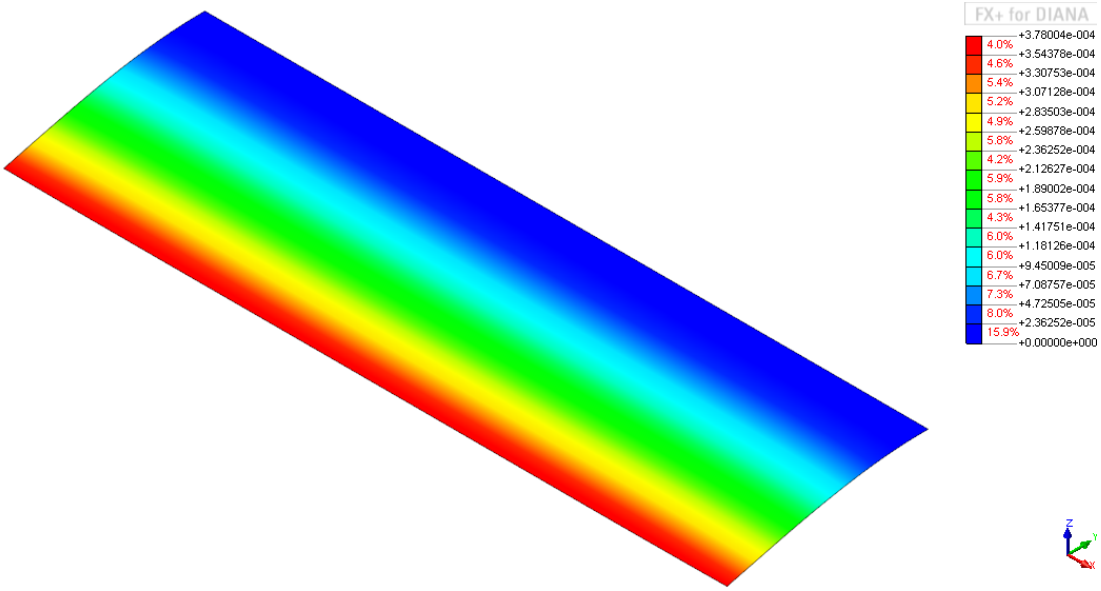

Maximum deflection for 1 m wide cantilever, self-weight

$\gamma_{btg} := 25\frac{kN}{m^3}$ $b := 1.0m$ $l := 2.78m$ $E := 36GPa$

Average thickness

$t_m := \frac{(0.38 + 0.19)m}{2} = 0.285\,m$ $g := \gamma_{btg} \cdot t_m \cdot b = 7.125 \cdot \frac{kN}{m}$

$I_m := \frac{b \cdot t_m^{\,3}}{12} = 1.929 \times 10^{-3}\,m^4$

$\delta_{max} := \frac{g \cdot l^4}{8 \cdot E \cdot I_m} = 0.766 \cdot mm$

Varying thickness

$t_1 := 0.38m$ $t_2 := 0.19m$ $t_{onethird} := t_1 - \frac{(t_1 - t_2)}{1} \cdot \frac{1}{3} = 0.317\,m$

$I_{max} := \frac{b \cdot t_1^{\,3}}{12} = 4.573 \times 10^{-3}\,m^4$

$I_{onethird} := \frac{b \cdot t_{onethird}^{\,3}}{12} = 2.646 \times 10^{-3}\,m^4$

$\delta_{max1} := \frac{b \cdot t_2 \cdot \gamma_{btg} \cdot l^4}{8 \cdot E \cdot I_{max}} + \frac{b \cdot t_2 \cdot \gamma_{btg} \cdot l^4}{30 \cdot E \cdot I_{max}} = 0.273 \cdot mm$

$\delta_{max2} := \frac{b \cdot t_2 \cdot \gamma_{btg} \cdot l^4}{8 \cdot E \cdot I_{onethird}} + \frac{b \cdot t_2 \cdot \gamma_{btg} \cdot l^4}{30 \cdot E \cdot I_{onethird}} = 0.472 \cdot mm$

$\delta_{max3} := \frac{b \cdot t_2 \cdot \gamma_{btg} \cdot l^4}{8 \cdot E \cdot I_m} + \frac{b \cdot t_2 \cdot \gamma_{btg} \cdot l^4}{30 \cdot E \cdot I_m} = 0.647 \cdot mm$

The FEM deflection lies in between δ_{max1} and δ_{max2}, which is considered reasonbale.

Appendix C – Mean crack distance

Mean crack distance

x-direction (ϕ12s150)

The main cracking perpendicular to x-direction occurs in bottom surface. Thus, bottom reinforcement is considered. Moreover, the level of the neutral layer will be in the middle of the cross-section since the reinfrocement amount is the same for bottom and top reinforcement in x-direciton.

$\phi_x := 12mm \quad c := 30mm \quad k_1 := 0.8 \quad k_2 := 0.5 \quad k_3 := 3.4 \quad k_4 := 0.425$

$d := t_m - (30 + 12 + 6)mm = 0.237\,m \quad xx := \frac{t_m}{2}$

$h_{cefx} := \min\left[2.5\cdot(t_m - d), \frac{(t_m - xx)}{3}, \frac{t_m}{2}\right] = 0.048\,m$

$A_{ceffx} := b\cdot h_{cefx} = 0.048\,m^2 \quad A_{sx} := \frac{1000}{150}\frac{\pi\cdot\phi_x^2}{4} = 7.54\times10^{-4}\,m^2 \quad \rho_{eff.x} := \frac{A_{sx}}{A_{ceffx}} = 0.016$

$S_{rmax.x} := k_3\cdot c + k_1\cdot k_2\cdot k_4\cdot\frac{\phi_x}{\rho_{eff.x}} = 0.231\,m$

y-direction (ϕ16s75)

$\phi_y := 16mm$

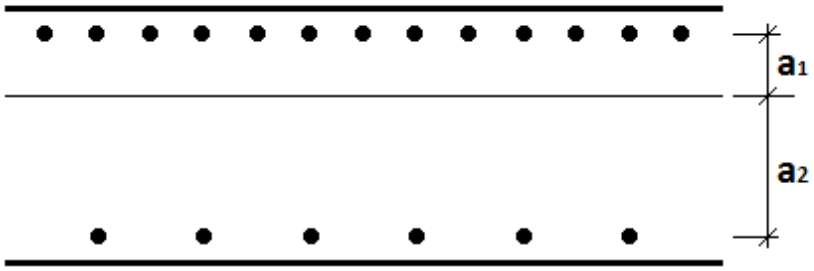

$a_1\cdot\phi_y\frac{1000}{75} = a_2\cdot\phi_x\cdot\frac{1000}{150} \quad a_1 + a_2 = t_m - 2\cdot30 - \frac{16}{2} - \frac{12}{2}$

$a_1 := \left(\frac{211\cdot\phi_x\cdot\frac{1000}{150}}{\phi_y\cdot\frac{1000}{75} + \phi_x\cdot\frac{1000}{150}}\right)mm = 0.058\,m$

$x_y := t_m - a_1 - 30mm - \frac{16}{2}mm = 0.189\,m$

$$h_{cefy} := \min\left[2.5\cdot(t_m - d), \frac{(t_m - x_y)}{3}, \frac{t_m}{2}\right] = 0.032\,m$$

$$A_{ceffy} := b\cdot h_{cefx} = 0.048\,m^2 \qquad A_{sy} := \frac{1000}{75}\,\frac{\pi\cdot\phi_y^{\,2}}{4} = 2.681\times10^{-3}\,m^2 \qquad \rho_{eff.y} := \frac{A_{sy}}{A_{ceffy}} = 0.056$$

$$S_{rmax.y} := k_3\cdot c + k_1\cdot k_2\cdot k_4\cdot\frac{\phi_y}{\rho_{eff.y}} = 0.15\,m$$

Max / Mean distance

$$S_{rmax} := \frac{1}{\frac{\cos(0)}{S_{rmax.y}} + \frac{\sin(0)}{S_{rmax.x}}} = 0.15\,m$$

$$S_{rmean} := \frac{S_{rmax}}{1.7} = 0.088\,m \qquad \text{BBK 04?}$$